Antarctic climate of the past 200 years from an integration of instrumental, satellite, and ice core proxy data

David P. Schneider

A dissertation
submitted in partial fulfillment of the
requirements for the degree of

Doctor of Philosophy

University of Washington

2005

Program Authorized to Offer Degree:
Department of Earth and Space Sciences

University of Washington
Graduate School

This is to certify that I have examined this copy of a doctoral dissertation by

David P. Schneider

and have found that it is complete and satisfactory in all respects,
and that any and all revisions required by the final
examining committee have been made.

Chair of Supervisory Committee:

_____
Eric J. Steig

Reading Committee:

_____
Eric J. Steig

_____
Stephen G. Warren

_____
John M. Wallace

Date: _____

University of Washington

Abstract

Antarctic climate of the past 200 years from an integration of instrumental, satellite, and ice core proxy data

David P. Schneider

Chair of the Supervisory Committee:
Associate Professor Eric J. Steig
Department of Earth and Space Sciences

Ice core records are the only direct means of extending Antarctic climate records into the past, before observations began in the late 1950s. Before proxy records are used with confidence, their relationship to climate parameters of interest (e.g. temperature, geopotential height, precipitation) must be clearly demonstrated. I assess the dominant patterns of variance in climate parameters over the Antarctic through an analysis of passive microwave and thermal infrared data from instruments on polar-orbiting satellites. Differences between the two data sets are largely due to near-surface snow properties. The most important mode of the Southern Hemisphere (SH) atmospheric circulation, the Southern Annular Mode (SAM), is associated with the leading empirical orthogonal functions of the satellite temperature data sets. Stable isotope ratios of water (δD and $\delta^{18}O$) were measured in nearly two dozen, sub-annually resolved, ~200-year-long ice cores that were obtained during traverses across West Antarctica. I use data from twelve of the cores in a compositing analysis to asses whether atmospheric modes have an expression in the isotopic composition of the firn. The SAM has a distinct spatial expression in δ; δ anomalies have the same sign as temperature anomalies at several of the sites. All of the δ records strongly correlate with the seasonal cycle of temperature. However, neither the coefficients from the seasonal regressions nor the compositing analysis are reliable as a calibration for reconstruction of temperature. I show that an important target for ice core calibrations is the average of the annual mean temperature records from Antarctic weather stations. This index has a strong correlation with the first mode of the infrared temperature data. Stacked ice core records have good skill in explaining its variance. A 200-year reconstruction of this index is presented, based on scaling a stack of five ice core records. During the period of overlap (1856-1999) with the observed SH mean temperature record, the reconstruction suggests that Antarctic temperatures (excluding the Peninsula) have had a relatively stable mean, though have slightly increased, at

about half the rate of the SH mean. Deviation of Antarctic temperature trends from the SH warming can in part be explained by the positive trend in the SAM since the mid-1970s.

TABLE OF CONTENTS

Page

LIST OF FIGURES

Figure Number Page

LIST OF TABLES

ACKNOWLEDGEMTS

This dissertation is the culmination of my graduate school studies. It seems hardly representative, however, of all of the advice, support, and adventure that I have had as a graduate student over the years. The name on the title page is not representative of all of the people who have contributed to my work. Furthermore, while this document highlights scientific research accomplishments, it does not do justice to the types of things that have really kept me in school—Cookie Fridays in the office, Christmas spent on the West Antarctic Ice Sheet, christening a Norwegian fjord after a conference, beers at Big Time and at Oktoberfest in Munich, invigorating political debate on climate change issues, running a marathon with friends from school and climbing Mt. Rainier, to name a few.

For all of the scientific work and perks of this trade, I have many people to thank. I will leave too many people out, but this list will be a start. First and foremost, Eric Steig has been a fabulous advisor. I cannot thank him enough for all of the hours he has spent advising me, securing funding, reading and editing all drafts of my papers and abstracts, gently making me do more work, writing letters, signing forms, taking me from Philadelphia to Seattle, and setting a perfect example of balance between research, teaching, family, and fun. I know we will be collaborating more in the future.

The rest of my committee, Mike Wallace, Steve Warren, and Dale Winebrenner have been very helpful and supportive over the years. I would also like to point out that the depth and scope of knowledge related to my work at the University of Washington is staggering. There are an amazing number of stand-out faculty and graduate students. A few of the faculty who were not on my committee but could well have been include Cecelia Bitz, Ed Waddington, Howard Conway, Dennis Hartmann, and Gerard Roe. I've benefited greatly from wading through statistical stuff with Justin Wettstein, and I would also like to thank Summer Rupper, Lora Koenig , and many other grad students for all of their help with work. Also, I'd have hardly any good ice core data without Joe Flaherty working in the isotope lab.

The glaciology group, the climate folks, and the Earth and Space scientists at the University of Washington have been very welcoming, as I walk the fuzzy line between these communities. No single group has been more consistently supportive and fun than my officemates, including Julia Jarvis, Summer Rupper, Kat Huybers, Shelley Kunasek, Noah Finnegan, Jeremy Smith, Ben Larson, Meg Smith, Shannon McDaniel, and Adam Haulter. In addition, other awesome grad students and friends not already mentioned include Jen Kay, Kim Comstock, Rob Elleman, and Yuko Ogata, to name a few.

I owe a lot to people outside this University, especially all of those involved in ITASE. Chris Shuman really got us going with the passive microwave data. Dan Dixon and Susan Kaspari have done remarkable work on the ice cores, and I must thank Paul Mayewski for leading the whole team. This work could not have been done without key contributions from other coauthors and collaborators Joey Comiso, Tas van Ommen, and Julie Jones. And there have been countless people involved in the logistics and funding of the field work. The National Science Foundation is a true lifeline funding a lot of good science, and I hope government support of NSF continues well into the future. I would also like to thank the international Scientific Committee on Antarctic Research, as they are supporting my next scientific adventure to Australia.

I would not be here without my family, which has given me unwavering love and support. Thanks, mom, dad, Marcus, and Gretchen.

INTRODUCTION

Antarctic climate – recent trends and variability

Signs of profound changes in Antarctic climate have emerged in recent years, including rapid warming on the Antarctic Peninsula (Vaughan et al., 2003), strengthening of the polar vortex (Thompson and Solomon, 2002), ice shelf collapse (Scambos et al., 2000), and ecological shifts (Doran et al., 2002). While these changes are striking, a complete characterization of Antarctic climate change has been difficult due to short and sparse meteorological observations. On the global scale, where confidence in the nature of observed changes is much higher, temperatures have risen markedly in the last hundred years, and early 21st century climate is likely to be outside the bounds of natural climate variability over the last millennium, consistent with anthropogenic influences on Earth's climate (e.g. Houghton et al., 2001; Karl and Trenberth, 2003).

There is a keen interest worldwide in studying Antarctica's role in global climate change as indicated by the direction of the research initiatives of the Scientific Committee on Antarctic Research, the international body that coordinates Antarctic scientific research, towards climate change issues (Summerhayes, 2005). Antarctica's complex interaction with the global climate system is a function of its physical characteristics. It is the coldest, windiest, highest, and driest continent on Earth. Nearly the whole continent is covered by a thick ice sheet, which contains 75 m sea level equivalent water (e.g. King and Turner, 1997). Due to the requirements of the surface energy balance over the ice sheet, which is characterized by high shortwave albedo and near black-body longwave emissivity, and to the presence of a surface-based temperature inversion, Antarctic surface climate is tightly coupled to the atmospheric circulation and to the climate of the mid-latitudes (e.g. van den Broeke et al., 2004; King and Turner, 1997). The ice sheet is a major heat sink in the Earth's atmosphere.

Warming of the oceans, sea-level rise, and warming of Antarctic climate in general have long been thought to increase the potential of the marine-grounded West Antarctic Ice Sheet (WAIS) to collapse (e.g. Bindschadler, 1998), which would lead to a major rise in global sea level. Recently, warmer oceans have been linked to accelerated thinning of the WAIS (Shepherd et al., 2004), and warmer surface temperatures over the Antarctic Peninsula region have been connected to rapid retreat of ice shelves (e.g. Scambos et al., 2000). Ice shelf retreat does not directly raise sea level, but it could accelerate the discharge of inland glaciers (e.g. Angelis and Skvarca, 2003).

Research focusing on the instrumental era of Antarctic observations (late 1950s to present) has led to a view that modern Antarctic climate is experiencing unusual regional trends compared to global trends due to large changes in the atmospheric circulation. While surface temperatures have risen elsewhere, a cooling trend over much of the Antarctic continent has been noted by a number of studies (Doran et al., 2002; Thompson and Solomon, 2002). Several studies have attributed this trend to a drift towards the positive phase of the Southern Annular Mode (SAM); (Thompson and Solomon, 2002; Kwok and Comiso, 2002; Shindell and Schmidt, 2004). The SAM is the leading pattern of variability in sea level pressure and tropospheric geopotential heights in the Southern Hemisphere (SH) extratropical latitudes, associated with anomalies in the westerlies and temperatures over the polar region (Thompson and Solomon, 2002; Kwok and Comiso, 2002). Studies have further linked the positive shift of the SAM (towards lower pressure over the polar region and stronger westerlies), which has been most pronounced in the summer and fall, to stratospheric ozone depletion and rising CO_2 concentrations (Thompson and Solomon, 2002; Shindell and Schmidt, 2004; Marshall, 2003; Marshall et al., 2004). This suggests that modern Antarctic climate trends are anomalous compared to natural variability and that anthropogenically-driven impacts are leading to interesting regional exceptions to the global trend towards warmer conditions. Other investigators (e.g. Bertler et al., 2004) have explored the interaction of the El Nino-Southern Oscillation (ENSO) with Antarctic climate, which is the most significant mode of interannual climate variability globally, involving anomalies in sea surface temperature, sea level pressure, winds, ocean circulation and near-surface temperature. However, the ENSO is still of uncertain significance to Antarctic climate (Turner, 2004).

Extending Antarctica's climate records

Available instrumental records are rather short to use in studies of the mechanisms behind Antarctic climate fluctuations. They are also limited when considering whether modern Antarctic climate trends are indeed unusual given historic variability. In principle, proxy climate information from ice cores in Antarctica provides a longer and more spatially detailed history of climate change than is available from direct observations. Deep ice core records from the Antarctic—from places such as Vostok and Byrd—are well known and have led to an appreciation of global climate change on the timescale of glacial-interglacial cycles over tens of thousands of years (e.g. Petit et al., 1999). In contrast, the upper (most recent few centuries)

portions of the cores have been largely overlooked and underappreciated. It is this portion of the records that would be most useful for establishing the reliability of ice core (technically the upper few tens of meters are *firn* cores) properties such as stable isotopes of water ($\delta^{18}O$ and δD, generally, δ) as proxies for temperature and other climate variables. Once reliable and physically plausible relationships are established, these records may be used to extend the instrumental record in a rigorous way that is consistent with the observed nature of Antarctic climate variability. What constitutes the key features of Antarctic climate variability presents an additional challenge, as there are only about a dozen continuous instrumental surface temperature observations from sites scattered across Antarctica since the late 1950s. Thus, we must also establish an understanding of the spatial structure of Antarctic climate variability in order to interpret the proxy record on the basis of the limited instrumental record.

Scope and goals of this dissertation

This work has grown out of, and supports the goals of, the United States International Trans-Antarctic Scientific Expedition (US-ITASE), a major ice coring and over-snow traversing effort in Antarctica. US-ITASE has as its chief objectives: (1) To determine the spatial variability of Antarctic climate (e.g. accumulation rate, air temperature, atmospheric circulation) over the last 200 years and, where data are available, the last 1000 years and longer and (2); To determine the environmental variability over the last 200 years and where data are available the last 1000 years and longer (Mayewski and Goodwin, 1996). US-ITASE is a multi-investigator project with researchers from several institutions (see Table 2.1). Without the framework and support of US-ITASE investigators, the scope of my work would have been much more limited. As the chapters will show, essential additional collaborations have been made with Josefino Comiso at NASA, Tas van Ommen in Australia and Julie Jones in Germany.

The major goals of my work include:

(1) Establishing an *a priori* expectation of major climate signals to be found in Antarctic ice cores by:

a. Developing the understanding of Antarctic climate signals, especially in space, through investigation of satellite-derived temperature and brightness temperature data;

b. Interpreting the major climate signals in a manner consistent with ground-based instrumental and atmospheric circulation data;

(2) Reconstructing Antarctic climate variability of the past two centuries from stable isotopes sampled in ice cores by:

a. Using the best available (high resolution, well-dated) ice core data;

b. Establishing the veracity of physical models of stable isotope signals;

c. Calibration of the isotopic signal in each core and among cores in terms of major climate signals ;

d. Validating the skill of the reconstruction and quantifying the uncertainty through statistical techniques commonly used in the paleoclimate community.

(3) Identifying future research needs in the areas of:

a. Selection of ice core drilling sites including criteria for climate variability;

b. Understanding the spatial variance of δ signals in relation to climate variables;

c. Using complementary means towards understanding of Antarctic climate, especially isotopic tracer models and non-Antarctic tree ring and instrumental data.

Chapter 1 is a study of the covariance between surface temperatures derived from infrared satellite observations and passive microwave brightness temperatures. The major modes of temperature variability are related to the primary atmospheric circulation patterns of the Southern Hemisphere. In Chapter 2, data from US-ITASE and other ice coring projects are introduced. Chapter 3 discusses the possibility of deriving stable-isotope-temperature calibrations from specific sites and from spatial aggregates of the data, on seasonal to interannual time scales. Chapter 4 builds upon ideas developed in the previous chapter, and presents the most significant results of this work, a 200-year Antarctic temperature reconstruction. In Chapter 5, available isotope data from 12 US-ITASE cores in West Antarctica are used in a compositing analysis to develop an empirical basis for linking isotope ratios to the atmospheric circulation. Finally, Chapter 6 provides concluding statements and a perspective on future research directions.

The major components of this dissertation, Chapters 1, 3, 4, and 5, have been written as stand-alone manuscripts. These sections have been or are intended to be published separately as scientific journal papers with myself as the first author. The following is a list of papers presented with a discussion about specific contributions from coauthors and from outside sources (reviewers, funders, etc.):

Chapter 1:

- Schneider, D.P., E.J. Steig, and J.C. Comiso. 2004. Recent climate variability in Antarctica from satellite-derived temperature data. *J. Climate*, **17**, 1569-1583.

The specific contributions of my coauthors were: Eric Steig guided my research and provided extensive editing and comments on the manuscript. Joey Comiso provided the AVHRR-derived satellite data and made suggestions on the manuscript. This work was supported by the U.S. National Science Foundation (grant numbers OPP-0196105, OPP-0126161) in association with the U.S. ITASE program. T_B data on CD-ROM from SMMR and SSM/I satellites (Gloersen et al. 1990; Maslanik and Stroeve 2001) were provided by the National Snow and Ice Data Center in Boulder, CO. NRA data were obtained from the online IRI/LDEO Climate Data Library at Columbia University (http://iridl.ldeo.columbia.edu). Gerard Roe provided code for autoregression modeling.

Chapter 3:

- Schneider, D.P., E.J. Steig, and T. van Ommen, High-resolution ice core stable isotopic records from Antarctica: towards interannual climate reconstruction, in press, *Annals of Glaciology,* v. **41**.

The specific contributions of my coauthors were: Eric Steig initiated many of the statistical analysis techniques, guided my research, oversaw the collection of ice core samples and the measurement of stable isotopes, and edited the manuscript. Tas van Ommen provided data from Law Dome and made suggestions on the manuscript. Ellen Mosely-Thompson kindly provided ice core data from Siple Station, while Talos Dome data were available online at the National Snow and Ice Data Center in Boulder, Colorado. Eric Steig and I were supported by the National Science Foundation, Office of Polar Programs, grant OPP-0196105. T. van Ommen was supported by the Australian government's Cooperative Research Centre's Program through the Antarctic Climate and Ecosystems CRC.

Chapter 4:

- Schneider, D.P., E.J. Steig, C. Bitz, D.A. Dixon, P.A. Mayewski, T. van Ommen, and J Jones, Ice core evidence for Antarctic climate change, in preparation.

This chapter is the product of collaboration between myself and several others. It is written for a broad audience. The ideas for the paper and its contents were mine. Eric Steig

provided input into planning the paper and made extensive comments and suggested revisions on several iterations of the manuscript. Because of this, a few sections are his writing. He has led the laboratory work. Cecilia Bitz obtained the model output from the CCSM3 that I discuss in the paper and she provided constructive comments. She also wrote the supporting description of the climate model. Daniel Dixon and Paul Mayewski are responsible most importantly for their leadership in the field and at the National Ice Core Laboratory, and also for the initial depth-age scales of the US-ITASE cores. They both provided numerous suggestions to improve the paper. Tas van Ommen contributed isotope data from the Law Dome ice cores and provided extensive constructive comments on various drafts of the paper. Julie Jones contributed several versions of her Southern Annular Mode reconstructions for use in the paper. She also made several helpful comments on a draft of the paper and wrote the supporting text about the method of her reconstructions. D.S., E.S., D.D., and P.M. have been supported by the National Science Foundation, Office of Polar Programs. C.M.B. was supported by NSF Atmospheric Sciences (ATM0304662); T.v.O. acknowledges support from the Australian Government's Cooperative Research Centres Programme through the Antarctic Climate and Ecosystems Cooperative Research Centre; and J.J. was funded by the German Federal Ministry for Education and Research (BMBF) under DEKLIM, and by the European Union under SOAP(Simulations, Observations, and Paleoclimate data (EVK2-CT-2002-00160).

CHAPTER 1

Recent climate variability in Antarctica from satellite-derived temperature data

1.1 Summary

Recent Antarctic climate variability on month-to-month to interannual time scales is assessed through joint analysis of surface temperatures from satellite thermal infrared observations (T_{IR}) and passive microwave brightness temperatures (T_B). Although T_{IR} data are limited to clear-sky conditions and T_B data are a product of the temperature and emissivity of the upper ~ 1m of snow, the two data sets share significant covariance. This covariance is largely explained by three empirical modes, which illustrate the spatial and temporal variability of Antarctic surface temperatures. T_B variations are damped compared to T_{IR} variations, as determined by the period of the temperature forcing and the microwave emission depth; however, microwave emissivity does not vary significantly in time. Comparison of the temperature modes with Southern Hemisphere (SH) 500-hPa geopotential height anomalies demonstrates that Antarctic temperature anomalies are predominantly controlled by the principal patterns of SH atmospheric circulation. The leading surface temperature mode strongly correlates with the Southern Annular Mode (SAM) in geopotential height. The second temperature mode reflects the combined influences of the zonal wavenumber-3 and Pacific South American (PSA) patterns in 500-hPa height on month-to-month timescales. ENSO variability projects onto this mode on interannual timescales, but is not by itself a good predictor of Antarctic temperature anomalies. The third temperature mode explains winter warming trends, which may be caused by blocking events, over a large region of the East Antarctic plateau. These results help to place recent climate changes in the context of Antarctica's background climate variability and will aid in the interpretation of ice core paleoclimate records.

1.2 Introduction

A number of studies have shown considerable interest in identifying and explaining Antarctic temperature trends over recent decades (Doran et al. 2002; Marshall 2002a; Thompson and Solomon 2002; Vaughan et al. 2001; van den Broeke 2000a). However, because the interannual variability of Antarctic climate is large, it is difficult to establish the significance of

surface temperature trends from sparsely distributed weather stations on the continent (King 1994). Furthermore, relatively little is known about the spatial structure of surface temperature variations across Antarctica. Such knowledge would, for example, improve the interpretation of ice core paleoclimate records, which are usually obtained from locations that are remote from weather stations.

Two important influences on Antarctica's climate variability, the Southern Annular Mode (SAM) and the El Niño-Southern Oscillation (ENSO), have been discussed by several studies, and increased tendency for these circulation patterns to stay in a particular phase may be driving surface temperature trends in the Antarctic (Gillett and Thompson 2003; Bromwich et al. 2003; Ribera and Mann 2003; Thompson and Solomon 2002; Kwok and Comiso 2002). We are therefore motivated to pay particular attention to the influence of these atmospheric patterns on Antarctic surface temperature anomalies, which, in this study, are derived from passive microwave brightness temperature (T_B) and thermal infrared satellite observations (T_{IR}).

In previous work with these data, Schneider and Steig (2002; hereafter SS02) presented a principal component analysis of T_B data and showed evidence for the SAM and ENSO-related signals in Antarctica. However, the T_B data, taken alone, can be complicated to interpret because of the effects of non-stationary microwave emissivity variations due to variations in snow characteristics, and occasional surface melt events. Kwok and Comiso (2002) examined newly available T_{IR} data, and also linked their variability to the SAM and ENSO. That study assumed, *a priori,* that indices of the SAM and ENSO would have skill in describing surface temperature anomalies, but it found mixed results. For example, the Southern Oscillation Index (SOI) does explain SST and sea-ice anomalies well over the Southern Ocean, but it does not have good skill at describing temperature anomalies on the Antarctic continent. Also, as Comiso (2000) and Shuman and Comiso (2002) discuss, the T_{IR} data set is biased by the absence of data for days with cloud cover. Shuman and Comiso (2002) was the first study to directly compare T_{IR} and T_B data, and generally found good agreement, but it only made comparisons at a few isolated locations with weather stations. Given the sparse distribution of Antarctic weather stations, it is desirable to further examine Antarctic climate with these satellite data. Other gridded products, such as the NCEP-NCAR Reanalysis data, are significantly less reliable for Antarctic climate studies, especially for surface conditions (Marshall 2002b; Hines et al. 2000).

In this paper, we analyze the T_{IR} and T_B data in order to reduce uncertainties in interpreting either satellite data set alone. First, we evaluate the T_{IR} data with methods that optimize the amount of variance that can be explained, in parallel to SS02. Secondly, we use the

two types of data to estimate the magnitude of microwave emissivity fluctuations. Next, the data are evaluated jointly using Maximum Covariance Analysis (von Storch and Zweirs 1999). The results of this analysis increase confidence in the interpretation of both data sets in terms of surface temperature variability. We examine the relationship between surface temperature variability and atmospheric circulation through comparison of the empirical modes of the satellite data sets with NCEP-NCAR geopotential height data. We conclude that, overall, the SAM explains the greatest variance in Antarctic temperatures. However, the second most important influence is not simply described by ENSO, but rather, reflects a combination of patterns previously referred to as the Pacific South American and wavenumber-3 patterns. We also suggest that blocking may be responsible for driving strong temperature trends in a little-studied region (0°-90°E) of East Antarctica.

1.3. Data

Surface temperature (T_{IR}) fields, at monthly resolution from January 1982 to December 1999, were derived for the Antarctic continent from thermal infrared channels of the Advanced Very High Resolution Radiometer (AVHRR) satellite instrument as originally discussed by Comiso (2000). Comparison with available ground-based observations shows that T_{IR} data provide good estimates of the near-surface air temperature (T_a), although they may be cooler than the actual T_a under strong surface inversion conditions (Comiso 2000). In addition, monthly means of T_{IR} data have a clear-sky bias because infrared surface temperature estimates cannot be made in cloudy conditions. Since the net effect of clouds on surface temperature in the Antarctic is warming (e.g. King and Turner 1997), monthly cloud-free averages from the infrared observations tend to be cooler than *in situ* station observations by ~0.5 K (Comiso 2000). Originally constructed on a 6.25 x 6.25 km polar stereographic grid, the T_{IR} data are averaged to a 25 x 25 km grid, so that they are co-registered with the passive microwave data. Anomalies are computed by subtracting the monthly climatology at each grid point.

Passive microwave brightness temperature (T_B) data used in this study are from the 37 GHz vertically polarized channel on the Scanning Multichannel Microwave Radiometer (SMMR) and Special Sensor Microwave Imager (SSM/I) satellite instruments from the same time period as the T_{IR} data. An important advantage of T_B data over T_{IR} data is that they can be obtained in all weather conditions. As discussed by SS02, T_B data cannot be interpreted as a pure surface temperature signal, because the variability in microwave emissivity is not known. Attenuation of

surface temperature changes through the penetration depth of the microwave emission—typically a few centimeters to a meter—means that amplitude is generally smaller for T_B variations than T_a variations. Surdyk (2002) emphasizes that changes in the snow temperature over the penetration depth have a much stronger influence on T_B variability than do emissivity changes. Surface melting, because of enhanced absorption of microwaves by liquid water during the melting event, and enhanced scattering after the snow re-freezes (Zwally and Fiegles 1994), accounts for the largest emissivity-forced component of T_B. This was evaluated by SS02, and found to be important primarily along the coast and on the ice shelves. A melt-masked, monthly anomaly dataset of T_B on the Antarctic continent is derived in the same manner as described by SS02 except where noted below.

Previous site-specific studies have found good agreement between T_{IR}, T_B, and T_a measurements made *in-situ* by Automatic Weather Stations (AWS). On monthly time scales, differences among the data have been found to be less than 1 K at most locations, if T_B data are corrected for emissivity (Shuman and Comiso 2002). However, these reported differences do not take into account the clear-sky bias, as AWS temperatures were compared to T_{IR} data only on days when both observations were available. Shuman and Comiso (2002) also found evidence for consistent offsets between T_a and T_{IR} data, notably at the South Pole, where it was observed that T_{IR} was ~4 K greater than T_a across the range of temperatures. This offset, which may be due to covering the South Pole at scan angles off of nadir, is not significant in our analysis because the mean T_{IR} values are subtracted from each grid point. Also, the T_B data are limited to areas north of 85°S, so the data sets are not directly compared in the South Pole region.

To examine the connections between the variability in Antarctic T_{IR} and T_B data and larger-scale SH atmospheric circulation variability, 1982-1999 500-hPa geopotential height anomalies (Z500) poleward of 20°S, on a 2.5° x 2.5° latitude-longitude grid, are used from the NCEP-NCAR Reanalysis (NRA) (Kalnay et al. 1996; Kistler et al. 2001). Various biases, most importantly spurious multi-annual trends, have been reported in these data (Hines et al. 2000; Marshall 2002b) but should be of little consequence to the purposes of this study. The 500-hPa level is the lowest standard pressure surface entirely above the surface of the ice sheet and the stable inversion layer, and NRA 500-hPa data compare more favorably to Antarctic station observations than do 850-hPa geopotential height or surface pressure fields (Marshall 2002b, Hines et al. 2000).

1.4. Methods

In Section 1.5, principal component analysis (PCA) of T_{IR} anomaly data is performed. Empirical orthogonal function (EOF, spatial) patterns and principal components (PC, temporal variations) are computed for data from all months of the year and broken down by season, December-January-February (DJF), March-April-May (MAM), June-July-August (JJA), and September-October-November (SON). In Section 1.6, the data sets are compared qualitatively, and in Section 1.7, spatially and temporally varying microwave emissivity (ε) is estimated using the Rayleigh-Jeans approximation. Comparison of the T_{IR} and T_B fields through Maximum Covariance Analysis (MCA) is used in Section 1.8 to diagnose the common spatial-temporal signals in the two data sets. Heterogeneous regression maps are shown to illustrate the spatial patterns of the MCA modes, while expansion coefficients show temporal variations of the modes. Next, the leading T_{IR} and T_B expansion coefficients are compared through spectral analysis. In Section 1.9, PCA is used to determine the leading patterns of variability in the atmospheric circulation at 500-hPa. Finally, regression analysis is performed among the various fields to show associated patterns.

1.5. T_{IR} data

1.5a. PCA of T_{IR} data

Applying PCA to the covariance matrix of monthly T_{IR} anomalies covering the Antarctic continent results in two modes with distinct eigenvalues that meet the separation criteria of North et al. (1982). The leading mode explains 52% of the variance in T_{IR}, while the second mode accounts for 9% of the variance. The first EOF, shown in Fig. 1.1a as a regression of T_{IR} anomaly data onto the first normalized principal component (T_{IR} -PC1, Fig. 1.1b) is associated most strongly with the high plateau of East Antarctica. Locally, high correlations in East Antarctica indicate that up to 80% of the variance in T_{IR} can be explained by this first mode, as determined by r^2 values. More moderate correlation of the same sign occurs over West Antarctica. Moderate correlation of opposite sign occurs on the northern reaches of the Antarctic Peninsula.

The second EOF (Fig. 1.1c) is centered on the Ross Ice Shelf and on the Marie Byrd Land region of the continent, where 40-60% of the T_{IR} variance is explained. Most of West

Antarctica is of the same sign, but the pattern changes sign over the Ronne-Filchner ice shelf (at 60°W) and most of East Antarctica. Some coastal areas near 120°E have the same sign as West Antarctica. Only a small fraction of the variance in East Antarctic temperatures can be explained by mode 2.

1.5b. Seasonality of T_{IR} modes

While the leading patterns of tropospheric circulation variability, including the SAM, exist year-round in the SH middle and high latitudes (Cai and Watterson 2002; Gong and Wang 1999; Thompson and Wallace, 2000a), the range of Antarctic temperature variability is much larger in winter months than summer months (King and Turner 1997; Shuman and Stearns 2001). In T_{IR}, the standard deviation of July monthly means is about twice that of January monthly means, averaged over the continent. In winter, longwave radiation terms dominate the surface energy budget and strong surface inversions develop during clear and calm weather. Therefore, the surface temperature in winter is very sensitive to factors that disturb the inversion, particularly changes in cloudiness and winds (van den Broeke 2000b; Warren 1996). Since PCA modes are designed to maximize variance explained, the leading T_{IR} modes may be more characteristic of winter than of summer temperature variability.

PCA is performed on seasonal subsets of the data: Summer (DJF), Autumn (MAM), Winter (JJA), and Spring (SON). The short time series diminish the statistical significance of the modes compared to the full data set; however, the following results can be supported. Mode 1 in every season dominates explained variance compared to the subsequent modes (Table 1.1), but explains slightly more variance in the transition seasons than the solstitial seasons. Compared to the full data set, the mode 1 EOF pattern is most similar in spring and summer, rather than the winter, as might be expected due to the larger variance in winter months. In spring and summer, a large part of the variance is explained over a broad region of East Antarctica, and most of the continent has the same sign. In autumn and winter, EOF 1 has considerably less coherent large-scale spatial structure. However, for all seasons, the correlation of the leading PC and the seasonal SAM index is about 0.5 – 0.6, as shown in Table 1.1, but is higher in the solstitial seasons. On the balance, these results suggest that the year-round leading modes in T_{IR} are not heavily biased towards a particular season.

In all except JJA, mode 2 explains the most variance in the 90°W to 180°W region of West Antarctica. The overall spatial patterns are less stable than in mode 1, and it is difficult to

relate them to the full-year pattern. However, the anomalies are generally consistent with a combination of the zonal wavenumber-3 and PSA patterns of atmospheric circulation variability, as discussed in Section 8. Since the atmospheric circulation patterns do exist throughout the year, and the traditional three month seasonal breakdown is not very representative of Antarctica's seasons, it is reasonable to base interpretations on the full-year data set. With a six-month seasonal breakdown, SSO2 found similar leading modes in T_B for winter half (April-September) and summer half (October-March) years.

1.6. Comparison of T_{IR} modes with leading modes in T_B

Qualitatively, the leading modes of T_{IR} and T_B (SS02) are similar. Mode 1 is characterized by covariance of the same sign throughout most of the continent, with the exception of some portions of the Antarctic Peninsula. Mode 2 has a center of action over the Ross Ice Shelf and adjacent inland areas in Marie Byrd Land. However, the differences in PCA modes of T_B and T_{IR} illustrate some contrasting features of the two datasets. Mode 1 explains 52% of the variance in T_{IR} but only 25% of the variance in T_B. Mode 2 explains 9% of the variance in T_{IR} and 18% of the variance in T_B. The degree of separation between the modes can be partially attributed to differences of spatial and temporal autocorrelation. While the monthly T_{IR} data have a typical (for an atmospheric variable) lag-1 autocorrelation coefficient of ~0.27, T_B data are temporally autocorrelated at ~0.60. Spatially, T_B data are quite variable, due to regional differences in snow physical properties, while the T_{IR} data vary on much larger length scales, reflecting more closely the surface temperature.

1.7. Emissivity variability at microwave wavelengths

The emissivity parameterization helps to quantify the effects of the physical properties of the snow layer from which the T_B signal emanates. T_B is the physical temperature of the snow times its emissivity (ε), integrated over the penetration depth (Zwally 1977; Surdyk 2002). This is the Rayleigh-Jeans approximation, allowing a calculation of 37 GHz ε through the relation $\varepsilon = T_B \times T_{IR}^{-1}$. On annual mean or longer timescales, using T_{IR} data in place of the physical temperature of the snow is valid, as mean T_B emissivity changes little and the mean annual surface temperature approximates the mean physical temperature of the snow (Zwally 1977, Surdyk 2002). Co-registration of T_{IR} and T_B data enables a map of ε to be calculated based on the

1982-1999 means (Fig. 1.2a). The pattern shows a spatial variation in ε of 0.25. This includes the melt areas, which have not been excluded from the T_B data in this section of our study. Although the average spatial variations in ε were removed from the analysis of SS02 by the use of anomalies and the masking of melt zones, the influences of spatially varying ε do affect the appearance of EOF-regression maps in some areas, especially near the margins of the ice sheet. Melting can temporarily make the magnitude of T_B anomalies greater than that of T_{IR} anomalies due to the high absorption of the liquid water.

Temporally, ε is negatively correlated with the annual cycles of T_{IR} and T_B when averaged over the continent, and the apparent magnitude of the seasonal change in ε is about 0.02 (Fig. 1.2b). However, this magnitude is partly artifact, as the T_B annual amplitude (19 K) is 30% less than the T_{IR} annual amplitude (27 K). This ~30% attenuation is indicative of an average penetration depth of less than 1 m (Surdyk 2002). Thus, the true seasonal variation in ε must be less than the apparent magnitude obtained when the attenuation is ignored (Surdyk 2002). An attenuation map can be produced by dividing the average magnitude of the T_B annual cycle by the magnitude of the T_{IR} annual cycle (not shown). By inference, the more damped the annual cycle, the deeper the penetration depth. The spatial pattern in attenuation is highly correlated with the emissivity map, showing that low emissivity corresponds to shallow penetration depth and vice versa, consistent with the theory that grain size is the dominant factor affecting both parameters (Surdyk 2002). Annual mean time series of T_{IR} and T_B are positively correlated, while the emissivity is anti-correlated with T_B and T_{IR} (Fig. 1.2c). The calculated interannual range in the value of ε is on the order of 0.01 with a standard deviation of 0.0034. This value of 0.01 is likely close to the real range in ε over the penetration depth because the annual mean surface temperature (from T_{IR}) approximates the annual mean temperature at depth. Thus, given the mean annual T_{IR} value of 239 K and the mean ε of 0.86, the interannual standard deviation in ε accounts for only ~0.8 K of (microwave brightness) temperature difference, well within the uncertainties of both data sets (Shuman and Comiso 2002) and well below the magnitude of temperature anomalies that are explained by our modes in Section 1.8.

1.8. Maximum Covariance Analysis of the data sets

Maximum Covariance Analysis (MCA) optimizes the covariance explained by pairs of structures in two data sets. Bretherton et al. (1992) and Wallace et al. (1992) provide a detailed discussion of the methodology, which is adhered to below. The name singular value

decomposition (SVD) is often applied to the entire method; here it is only used in reference to the algorithm used in extracting empirical structures via cross-covariance matrix decomposition. First, the cross-covariance matrix of T_{IR} and T_B anomaly fields is computed (with melting pixels masked as in SS02). The expansion coefficients of the T_{IR} and T_B fields are found by projecting the singular vectors from SVD onto the original gridpoint data of the respective field. These expansion coefficients are then normalized, and either field can be regressed upon them to display spatial structure. In the case that the T_{IR} (T_B) field is regressed upon a T_{IR} (T_B) expansion coefficient, the map is known as a homogeneous regression map, and in the case that the T_{IR} (T_B) field is regressed upon a T_B (T_{IR}) expansion coefficient, the map is referred to as a heterogeneous regression map.

No formal method has been developed for determining the significance of MCA modes, but some tests apply. The squared covariance fraction (SCF) of each mode is an indication of the fit between the two data sets. Another indication is the correlation coefficient between each mode's pair of expansion coefficients. Additionally, the cross-covariance matrix can be tested for relatedness (before applying MCA) with root mean squared covariance (RMSC, square root of the squared covariance (SC) after dividing by the product of the variance of the two data sets). The high T_{IR}-T_B RMSC of 0.22 implies strongly coupled fields that are suitable for MCA, as RMSC of 0.1 or greater is a typical guideline for strong correlation (Wallace et al. 1992).

MCA applied to T_{IR} and T_B fields yields three significant modes, with a SCF of 77%, 11%, and 5%, respectively. The modes' three pairs of expansion coefficients (T_{IR}x1 and T_Bx1; T_{IR}x2 and T_Bx2; T_{IR}x3 and T_Bx3) are correlated at 0.70, 0.61, and 0.78, respectively (Table 1.2). In both T_{IR} and T_B, the set of homogeneous regression maps for the leading two modes are almost identical to the leading spatial patterns from PCA of the data sets considered separately.

The set of heterogeneous regression maps, displayed in Fig. 1.3, are similar to cross-regressions and show the anomaly in the field on the map associated with one standard deviation of the opposite field's expansion coefficient. For mode 1, the T_{IR} field regressed onto T_Bx1 (Fig. 1.3a) is similar to the first EOF of T_{IR} anomalies, although less variance in T_{IR} is explained (23%). The T_B field regressed onto T_{IR}x1 (Fig. 1.3b) produces a pattern that is more smoothly varying than the first EOF of T_B (see SS02, Fig. 2a), and explains 11% of the variance. The amplitudes in Fig. 1.3b are smaller than those in Fig. 1.3a, implying attenuation of the surface temperature signal through the penetration depth. Also, where the covariance in Fig. 1.3b is the greatest in East Antarctica, notably between 75°S and 80°S, the emissivity is lowest, as shown in Fig. 1.2a, consistent with shallow microwave penetration depths and little attenuation. In Fig.

1.3c, the T_{IR} field is regressed onto T_Bx2, explaining 3% of the variance in T_{IR}, and the resulting pattern is similar to the second EOF of T_{IR}. Likewise, regression of the T_B field onto T_{IR}x2 (Fig. 1.3d), explains 4% of the variance, and produces a heterogeneous map similar to the second EOF of T_B. In this pair of maps, the amplitudes are comparable in magnitude, consistent with little attenuation, a shallow penetration depth, and low emissivity in the Ross Sea sector of Antarctica (Fig. 1.2a).

A third mode is diagnosed with MCA that was not prominent in the PCA results for the data sets when considered separately (although this third MCA mode correlates well with the fourth mode in T_{IR} data alone and the fifth mode in T_B data alone). It is retained for discussion because it projects onto the linear trends in the T_{IR} and T_B data sets and is reproducible, as discussed below. Because the T_{IR}x3 and T_Bx3 expansion coefficient time series have upward trends (see Fig. 1.4c, below), these time series and the T_{IR} and T_B gridpoint data are both detrended prior to the construction of the heterogeneous regression maps in order to avoid spurious correlations. If the trends are retained in the time series, the heterogeneous maps of mode 3 look very similar to annual mean trends in the T_{IR} and T_B data sets (see Kwok and Comiso 2002, Fig. 2, for trends in T_{IR}). Therefore, care must be taken not to include spurious correlations of unrelated trends in the maps. The map with T_{IR} data regressed onto T_Bx3 explains 4% of T_{IR} variance and shows positive anomalies in T_{IR} throughout much of East Antarctica (Fig. 1.3e). The anomalies of greatest magnitude occur from 0° to 60°E. Similarly, the map of T_B data regressed onto T_{IR}x3, explains 4% of T_B variance and shows positive T_B anomalies, but of weaker magnitude, in the same area of East Antarctica.

The results outlined above strongly imply that there is meaningful covariance between T_{IR} and T_B data sets. However, it must be established with confidence that the correlations have not arisen by chance. As a first test of reproducibility, T_{IR} and T_B anomaly data are detrended prior to MCA. In this case, the same three modes are produced, but without the trend in the third mode. Second, as a test of the statistical robustness of the MCA results, the T_{IR} and T_B data sets are divided into subsets. Data for odd months only are used, and then, data for even months only. Odd and even month RMSC, SC, SCF, and correlation coefficients between expansion coefficient pairs are comparable in magnitude to the statistics for the full data sets for each of the first three modes (Table 1.3), indicating that the first three modes meet reproducibility criteria.

Another test of statistical robustness, based on the following Monte Carlo procedure, further demonstrates the strong relationships between T_{IR} and T_B anomaly data. Following the method of Wallace et al. (1992), the temporal order of the T_{IR} field is scrambled randomly while

the order of the T_B field remains unchanged. RMSC, SC, SCF and correlation coefficients are computed for each of 1000 random runs (Table 1.3). The significance of the observed runs and the subsets clearly stands out above the random runs. The observed squared covariance is an order of magnitude larger than the mean SC of the scrambled runs, the SCF of the observed first mode is about two standard deviations above the mean of the scrambled runs, and the correlation coefficients among expansion coefficient pairs for the first three modes are well above the mean of the scrambled runs. Finally, the RMSC values of the random data sets are smaller than the value of 0.1 that would indicate strong correlation. This leaves little doubt as to the significance, above the 99% confidence level, of the leading MCA modes and the strong relationship between the T_{IR} and T_B fields.

The three pairs of normalized expansion coefficients show the time variability of the three surface temperature modes from MCA (Fig. 1.4). The expansion coefficients of the first two modes are well correlated with the original PCs from each data set considered separately, as can be seen in Table 2. For instance, T_{IR}-PC2 correlates with T_{IR}x2 at r = 0.96 and similarly high correlations exist for the other matches. Therefore, the time series that explain the most covariance between the T_{IR} and T_B data sets also explain the most variance in the individual data sets.

The power spectra of each expansion coefficient time series are estimated with a Hanning window providing 13 degrees of freedom (Fig. 1.5). Also shown in Fig. 1.5 is the theoretical spectrum, with 95% confidence limits, for the first order red noise autoregressive process (AR(1)) that provides the best fit to each time series (von Storch and Zweirs 1999). There are no significant spectral peaks at the 99% confidence level. Each time series is consistent with red noise, but with different degrees of "redness," which can be quantified by comparing the AR(1) coefficients from the best-fit theoretical spectrum.

If it is assumed *a priori* that T_{IR} spectra provide a direct measure of the variability in the surface temperature, then T_B spectra should reflect the attenuation of that variability at depth (see Fig. 10 of Surdyk 2002). Because both the penetration depth (as discussed in Section 1.7) and the surface forcing (as indicated by the T_{IR} and Z500 modes) are spatially variable, the degree of attenuation and "memory" in the TB time series will also be spatially variable, and this is reflected in differences among the pairs of AR(1) coefficients. The MCA procedure is therefore unable to completely remove the effect of spatially varying snow structure, but it does show that the T_B and T_{IR} have a common forcing—the surface temperature. The strong covariance between the data sets suggests that effects of the clear sky bias in T_{IR} data and snow emissivity influences

on T_B data do not mask the underlying large-scale modes of surface temperature variability on monthly timescales or longer.

1.9. Influence of atmospheric circulation on Antarctic temperatures

1.9a. Principal Component Analysis of 500-hPa geopotential height anomalies

To define the leading patterns of SH atmospheric circulation during the time period of this study in a consistent manner with the analysis of temperatures in Section 1.5, PCA is applied to monthly Z500 anomaly data poleward of 20°S. For equal-area weighting, the data are weighted by the square root of the cosine of their latitude prior to analysis. The original unweighted Z500 data are regressed against each normalized PC, showing anomalies corresponding to one standard deviation of the corresponding PC. Three patterns of interest are resolved, explaining 24%, 12%, and 10% of the (weighted) variance respectively. The latter two patterns are not well separated under the criteria of North et al. (1982). However, they have been reported by a number of studies and found in many different data sets (Carleton 2003; Cai and Watterson 2002; Mo and White 1985). Our results are consistent with the definition of the first Z500 pattern as the SAM (Fig. 1.6a), the second Z500 pattern as the Pacific South American (PSA) pattern (Fig.1.6b), and the third pattern as the zonal wavenumber-3 pattern (Fig. 1.6c) as named by other studies (Cai and Watterson 2002; Mo 2000). The third pattern is sometimes called the PSA-2 pattern (Mo 2000). The signs are displayed for consistency with the modes in T_{IR} and T_B and the regression patterns discussed below.

1.9b. Correlations and regression patterns

Associations between Antarctic temperatures and patterns of atmospheric circulation can be illustrated with a variety of methods. The temporal correlations among the PCs of Z500, the expansion coefficient pairs from MCA, and the SOI are summarized in Table 1.4. The first PC of Z500 forms a representative SAM index (Thompson and Solomon 2002), and it has strong correlation with the first MCA mode ($r(T_{IR}x1, SAM) = 0.58$ and $r(T_Bx1, SAM) = 0.61$) and weak correlation with the other modes. Z500 PC2 correlates well with the SOI ($r = 0.43$), and has moderate correlation with both modes 1 and 2 in T_{IR} and T_B. Z500 PC3 has a weak correlation with the SOI and the best correlation with mode 2 in T_{IR} and T_B ($r(T_{IR}x2$, Z500 PC2) = 0.39 and

r(T_Bx2, Z500 PC2) = 0.32). Mode 3 from MCA has only weak correlation with the Z500 patterns.

Regression patterns reinforce the connections implied by the various correlation coefficients. Since T_{IR} and T_B data are highly correlated, regressions involving Z500 data discussed here are made only with T_{IR} data for illustration. Regressions of T_{IR} data onto the normalized PCs of the three leading Z500 patterns are shown in Fig. 1.7. The SAM explains 17% of the variance in T_{IR} anomalies (Fig. 1.7a), the PSA pattern explains 6% of the variance (Fig. 1.7b), and the zonal wavenumber-3 pattern explains 3% of the variance (Fig. 1.7c). The first regression pattern is quite similar to the first T_{IR} EOF (Fig. 1.1a). During the positive phase of the SAM, relatively strong westerlies encircle Antarctica near 60°S, which tends to enhance warm air advection over the northern Peninsula, while the cool anomalies on the rest of the continent are indicative of adiabatic cooling (Thompson and Wallace 2000a).

As seen in Fig. 1.7b, in East Antarctica, the PSA pattern explains much less variance in surface temperature than does the SAM, but the spatial structures of temperature anomalies are generally similar. In the Peninsula and most of West Antarctica, the PSA pattern explains variability of the same sign as in East Antarctica. However, the PSA pattern is associated with temperature anomalies of opposite sign near 150°W, 75°S, consistent with the anticyclonic 500-hPa height anomaly centered near 60°S, 125°W (Fig. 1.6b).

The PSA regression pattern resembles the regression of T_{IR} data upon the SOI that was shown in Fig. 3b of Kwok and Comiso (2002). For comparison to the PSA pattern in geopotential height, we show the pattern in Z500 associated with the Southern Oscillation, formed by regressing Z500 data onto the negative SOI to illustrate anomalies typical of El Niño years (Fig. 1.8). The zonally elongated north-south dipole structure over the far southern Pacific closely resembles the ENSO warm minus cold year mean 500-hPa height difference of Renwick and Revell (1999 Fig. 5) and the ENSO-associated patterns of other studies (e.g. Mo and Higgins 1998, Kidson 1999; Bromwich et al. 2003). In contrast to the 6% of T_{IR} variance explained by the PSA pattern, our calculations indicate that only 0.5% of the variance in T_{IR} anomalies on the Antarctic continent is explained by the regression of T_{IR} data upon the monthly SOI. However, circulation indices such as the SOI may not adequately capture the variability that is truly associated with ENSO (Carleton 2003; Kidson and Renwick 2002). ENSO-related forcing in the tropics is thought to project primarily onto the PSA pattern of variability on interannual to interdecadal timescales in middle to high latitude SH geopotential height field (Cai and Watterson

2002, Garreaud and Battisti 1999). The amount of T_{IR} variance explained by the SOI does improve somewhat, to 3%, if the data are first filtered with a 12-month running mean.

It is interesting that the pattern in Antarctic T_{IR} explained by the PSA pattern also resembles the correlation (although of opposite sign) of winter temperatures at Faraday station with the T_{IR} gridpoint data (King and Comiso 2003, Fig. 1). Although King and Comiso (2003) suggested that the climate variability of the Antarctic Peninsula is unrelated to the rest of Antarctica, our results show a connection through the PSA pattern. As illustrated in Fig. 1.6b, the strong anticyclonic anomaly in the far southeastern Pacific is accompanied by low geopotential height over most of Antarctica. Thus there is a connection between the anomalous meridional advection along the western Peninsula implied by the southeastern Pacific center of action and contemporaneous decreases in geopotential height over most of the continent.

As shown in Fig. 1.7c., the wavenumber-3 pattern explains positive temperature anomalies over the same area of West Antarctica associated with the second surface temperature mode, consistent with the strong positive and negative height anomalies centered along 60°S near 90°W and 155°W, respectively. The wavenumber-3 pattern also explains weak temperature anomalies of the same sign in East Antarctica, unlike the second temperature mode, in which West and East Antarctica are out of phase. This is likely due to the additional influence of the PSA pattern on the second surface temperature mode. While the PSA pattern in Z500 is associated with geopotential height fluctuations over East Antarctica, the wavenumber-3 pattern has very little correlation with heights over this region.

As a consistency check, Z500 data are now regressed upon T_{IR} expansion coefficients from the leading MCA modes. As above, the time series of mode 3 are detrended prior to regression. Although T_{IR} expansion coefficients are used here for illustration, regressions involving T_B expansion coefficients are very similar. The first Z500 regression pattern (Fig. 1.9a) closely resembles the SAM pattern in Z500 (Fig. 1.6a), especially in the Eastern Hemisphere. In the west, the PSA (Fig. 1.6b) pattern appears to have an influence on both the first and second regression patterns (Fig. 1.9a and 1.9b). However, the second regression pattern (Fig. 1.9b) most strongly correlates with the Z500 wavenumber-3 pattern (Fig. 1.6c). The third regression pattern (Fig. 1.9c) resembles the SAM, but has anomalies of much weaker magnitude. The positive anomalies in East Antarctica near 45°E are suggestive of a ridge in the mid-troposphere extending inland through East Antarctica. This resembles the wintertime blocking episodes discussed by Hirasawa et al. (2000) and Enomoto et al. (1998), who documented warm, moist air being pumped from the north all the way to the polar plateau. The positive temperature

anomalies associated with the third mode (Fig. 1.3e) correspond to the "strip" of annual mean warming on the East Antarctic ridge observed by Kwok and Comiso (2002). Inspection of monthly trends shows that in winter months, warming trends in T_{IR} occur over a much broader area than this strip, and Comiso (2000) described several anomalously warm July episodes in East Antarctica. Since the winter months account for most of the trend in the mode 3 expansion coefficients, it is likely that the events explained by mode 3 and these warm episodes are part of the same phenomenon.

1.10. Discussion and Conclusions

Previous studies have shown that Antarctic 37 GHz T_B data and T_{IR} data are both well correlated with surface air temperatures (Shuman and Comiso 2002; Surdyk 2002; Shuman and Stearns 2001; Comiso 2000), but this is the first to fully examine the consistency of these relationships across the continent. The PCA and MCA results demonstrate that the most important empirical modes in the T_{IR} and T_B data sets are well correlated with each other. The strength of the connection between T_{IR} and T_B increases confidence in the quality of both data sets. A general difference between the data sets is that the T_B data are les spatially autocorrelated and more temporally autocorrelated than the T_{IR} data because of the dependence of T_B on both emissivity and temperature integrated over a layer of snow and firn. The degree of dampening of T_B signals depends on the period of the surface forcing and the penetration depth of the microwave emission. Lower emissivity regions indicate a shallow penetration depth and relatively high-amplitude T_B fluctuations, which results in the highest T_{IR} and T_B covariance. The spatial pattern in emissivity apparently changes very little in time, and most likely represents spatially differing snow and firn structures.

Spatial and temporal patterns of T_{IR} and T_B variability, and more generally, surface temperature variability, in Antarctica are consistent with well-documented patterns of variability in extratropical SH atmospheric circulation. It is clear that the most important influence on Antarctic temperature anomalies from month-to-month to interannual timescales is the SAM. This first mode is well separated from other modes in both Z500 data and the satellite data sets. Looking at data from all months, strong temperature trends associated with this mode are not seen. However, inspection of trends by month over the length of the record shows that T_{IR} observations are consistent with a late spring and summer cooling trend, possibly driven by an

increasing tendency of the SAM to stay in its positive phase during these seasons (Thompson and Solomon 2002).

The PSA pattern has an influence on the first two surface temperature modes. The wavenumber-3 pattern of variability, however, has a relatively stronger influence on the second surface temperature mode, shown by its association with large temperature anomalies in the West Antarctic sector inland of the Ross and Amundsen seas. Anomalies of opposite sign in East Antarctica suggest that the PSA pattern exerts a stronger influence there. Since ENSO-related variability projects primarily onto the PSA and the wavenumber-3 patterns, Antarctic climate records often show ENSO-like spectra (SS02; Ichiyanagi et al. 2002; Bromwich and Rogers 2001; White et al. 1999).

Some persistent trends in the available satellite record are associated with the third mode, which cannot, within the scope of this study, be clearly linked to the principal patterns of atmospheric circulation variability. However, blocking events over inland East Antarctica have been documented with station data (Hirasawa et al. 2000; Enomoto et al. 1998) and provide a plausible explanation for the trends in temperature and the pattern seen in Z500 on our regression map (Fig. 1.9c). During these episodes, rises of ~40 K can occur in two days or less at remote interior stations such as Dome Fuji and Plateau, and T_a can take more than a month to return to its value before the rise (Enomoto et al. 1998; Kuhn et al. 1973). The upward trend in the T_{IR} and T_B expansion coefficients comes primarily from the winter months, when the blocking episodes most often occur and the surface temperature is extremely sensitive to circulation changes. In addition, changes in cloud cover and winds associated with blocking will destroy the surface inversion, adding to the magnitude of the surface temperature anomalies (Hirasawa et al. 2000). At present, however, the satellite record is too short to establish the long-term significance of the trends, and the monthly temporal resolution of this study limits our ability to further characterize the causes of variability in the third temperature mode.

The results of this study show that the surface temperature variability of Antarctica is well represented by both the T_{IR} and T_B data sets. Nonetheless, it is important to note that biases in the T_{IR} data associated with cloud cover, and in the T_B data associated with attenuation and possible emissivity changes, have not been completely removed. Ongoing improvements to the data include a technique for filling in cloud gaps in infrared observations with emissivity-corrected T_B observations (Shuman, personal communication 2002) and a method suggested by Winebrenner et al. (2005) that models T_B data on the basis of T_a variations and which could lead

to an improved parameterization of snow properties and their influence on T_B. Analyses of updated data sets may result in minor changes to the empirical modes we have calculated.

Currently, a gap exists between our understanding of Antarctica's short instrumental and satellite records, and deep ice cores from Antarctica (e.g. Petit et al., 1999; Morgan et al. 2002). Future work will include evaluating the stability of the temperature and circulation modes discussed here on longer timescales. Some prior work hints that these modes operated in the past. For instance, long ice core paleoclimate records from locations spread thousands of kilometers apart in East Antarctica are well correlated with each other, consistent with our first mode, while records from West Antarctica and some East Antarctic cores appear to reflect local climate, consistent with our second mode (Watanabe et al. 2003; Steig et al. 2000). East Antarctic isotopic records from the ice cores may be tied to the SAM over a large area (Noone and Simmonds 2002b), while West Antarctic ice core records would be expected to be strongly linked to circulation variability in the Southern Pacific, which in turn is teleconnected to the tropical Pacific during strong El Niño and La Niña events (Bromwich et al. 2003). Century-scale reconstructions of the major modes of SH atmospheric circulation from tree rings (Jones and Widmann 2003) and a network of intermediate-depth Antarctic ice cores (Mayewski 2003) will help to fill in the gap between our understanding of modern climate variability and our theories of past climate variations.

Table 1.1 Variance explained by first two PCA modes of T_{IR} and correlation with the SAM index by season.

Season	**Mode 1**	**Mode 2**	**r(SAM index*, T_{IR}-PC1)**
DJF	49%	14%	0.63
MAM	50%	9%	0.49
JJA	49%	13%	0.68
SON	57%	7%	0.50
Full Year	52%	9%	0.57

* The SAM index is the first principal component of 500-hPa geopotential height as discussed in the text.

Table 1.2. Correlation coefficients among PCs of T_B and T_{IR} considered separately and expansion coefficients from MCA. Sign is ignored.

	T_B-PC1	**T_{IR}-PC1**	**T_B-PC2**	**T_{IR}-PC2**	**T_B-X1**	**T_{IR}-X1**	**T_B-X2**	**T_{IR}-X2**	**T_B-X3**	**T_{IR}-X3**
T_B-PC1	1.00	0.46	0.00	0.11	0.81	0.47	0.21	0.05	0.01	0.04
T_{IR}-PC1		1.00	0.05	0.00	0.68	0.99	0.01	0.11	0.00	0.02
T_B-PC2			1.00	0.48	0.03	0.04	0.96	0.56	0.14	0.02
T_{IR}-PC2				1.00	0.09	0.02	0.54	0.96	0.13	0.36
T_B-X1					1.00	0.70	0.07	0.00	0.07	0.00
T_{IR}-X1						1.00	0.00	0.09	0.00	0.00
T_B-X2							1.00	0.61	0.11	0.00
T_{IR}-X2								1.00	0.00	0.15
T_B-X3									1.00	0.78
T_{IR}-X3										1.00

Table 1.3. Summary of MCA reproducibility tests and Monte Carlo results.

Run	SC	RMSC	SCF(%) modes(1,2,3)	$r(T_Bx,T_{IR}x)$ modes(1,2,3)
1000 Scrambled Runs				
Highest	$6.3x10^4$	.098	(82,31,18)	(.34,.39,.38)
Lowest	$1.6x10^4$	.050	(29,04,03)	(.14,.16,.16)
Mean	$3.1x10^4$	.068	(55,14,09)	(.23,.28,.28)
Std. Dev.	$7.2x10^3$	.008	(10,04,02)	(.03,.04,.04)
Observations				
All months	$3.28x10^5$	.223	(77,11,05)	(.70,.61,.78)
Odd months	$3.27x10^5$	.241	(77,11,05)	(.74,.54,.80)
Even months	$3.32x10^5$	.222	(70,16,06)	(.69,.67,.75)

Table 1.4. Summary of correlation coefficients among modes in Z500, SOI, and MCA expansion coefficients. Sign is ignored.

	SOI	**T_Bx1**	**T_{IR}x1**	**T_Bx2**	**T_{IR}x2**	**T_Bx3**	**T_{IR}x3**
Z500-PC1	0.16	0.61	0.58	0.06	0.05	0.06	0.15
Z500-PC2	0.43	0.25	0.31	0.24	0.17	0.06	0.06
Z500-PC3	0.18	0.09	0.16	0.32	0.39	0.02	0.00
SOI		0.02	0.04	0.19	0.14	0.06	0.11

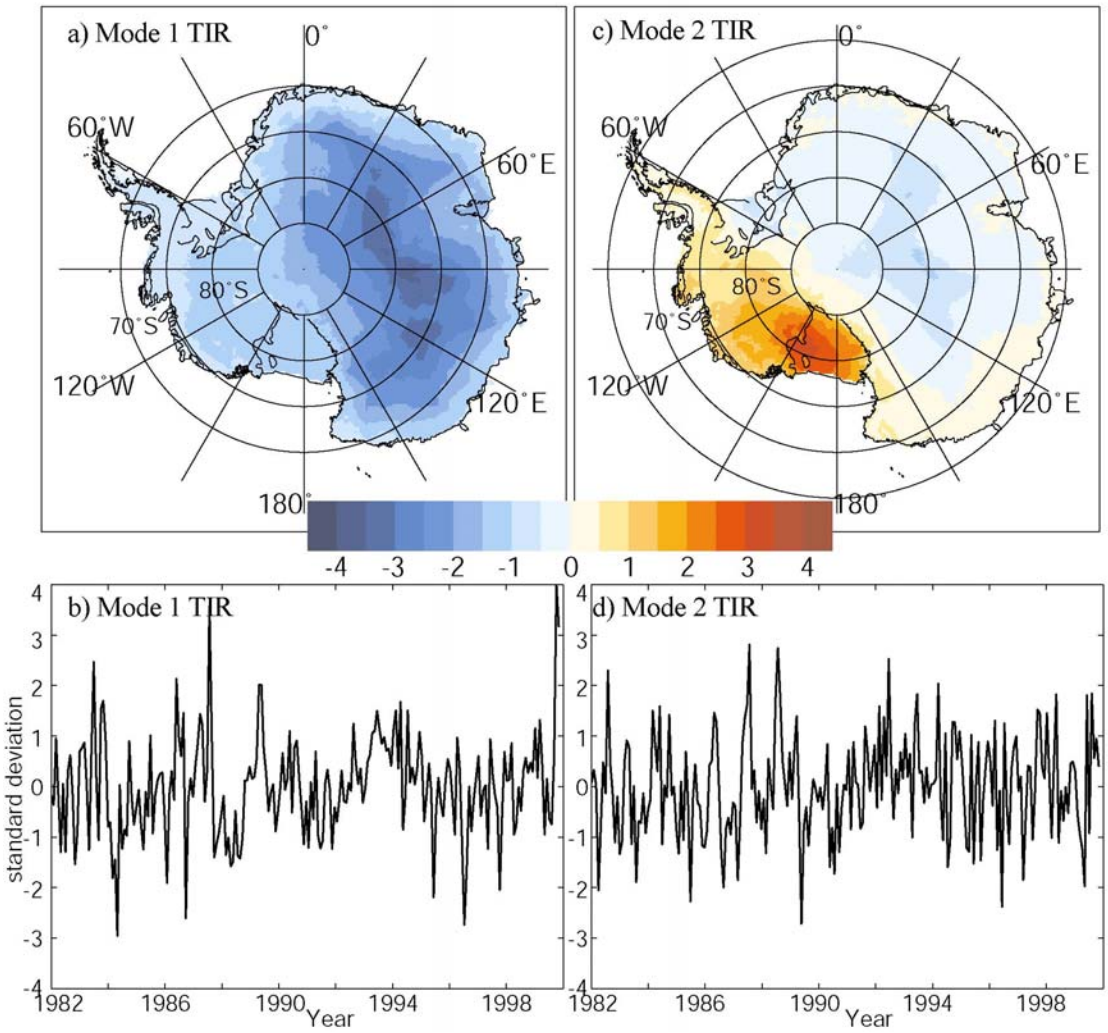

Figure 1.1. Results from PCA of monthly 1982-1999 T_{IR} anomaly data. (a) EOF-1 shown as a regression coefficient between each grid point and the first normalized PC. (b) The first normalized PC corresponding to the EOF pattern above. (c) As in a but for the second EOF. (d) As in b but for the second PC. Color scale is in K, corresponding to a typical anomaly associated with each mode, that is, the value of one positive standard deviation of the respective PC.

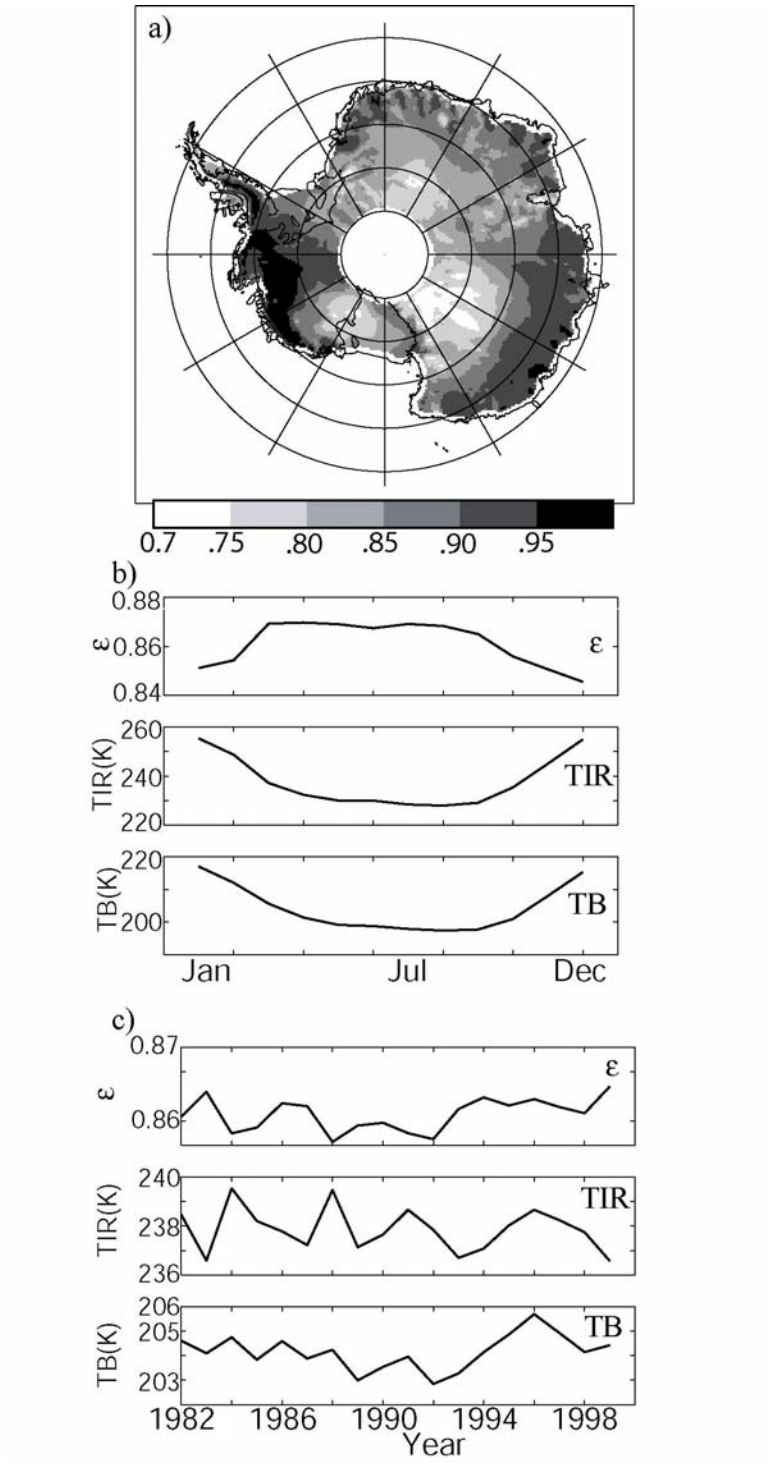

Figure 1.2. (a) Mean microwave emissivity at 37 GHz vertical polarization of the Antarctic ice sheet based on 1982-1999 mean values of T_{IR} and T_B. (b) Continent-averaged annual cycles of emissivity, T_B, and T_{IR} based on 18-yr means of each month. (c) Continent-averaged interannual variations of emissivity, T_B, and T_{IR}.

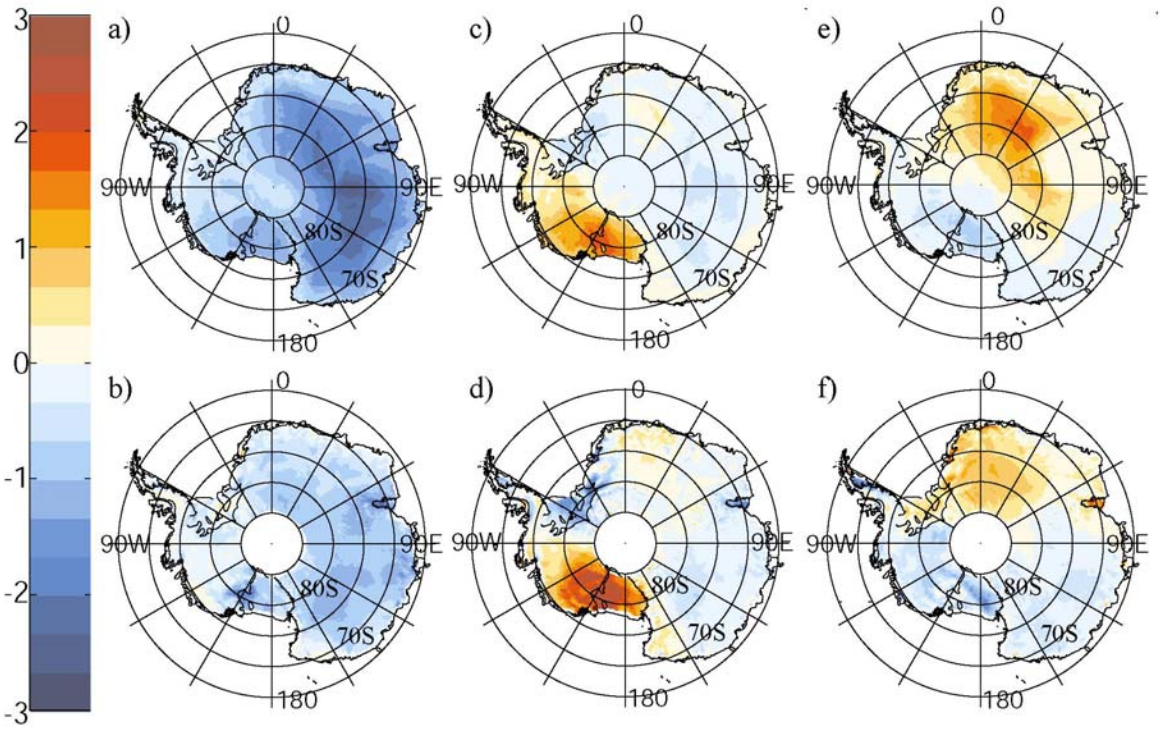

Figure 1.3. Heterogeneous regression maps from MCA of T_{IR} and T_B fields. The top panels (a,c,e) are covariances from the T_{IR} field regressed upon the first, second, and third normalized T_B expansion coefficients, respectively. The bottom panels (b,d,f) are covariances from the T_B field regressed upon the first, second, and third normalized T_{IR} expansion coefficients, respectively. Color is in units of K, corresponding to one standard deviation of the respective expansion coefficient.

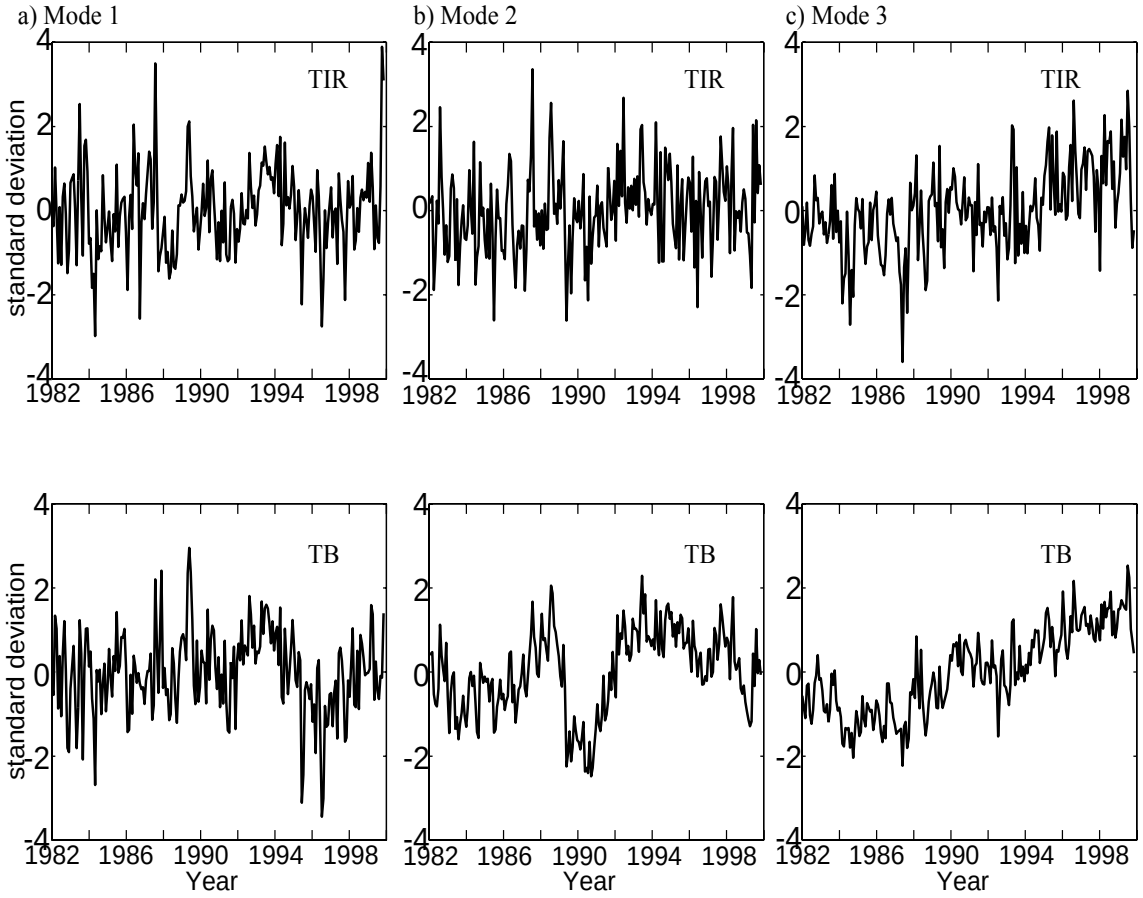

Figure 1.4. Expansion coefficients of the first three MCA modes (a-c, respectively) corresponding to the heterogeneous maps in Fig. 1.3.

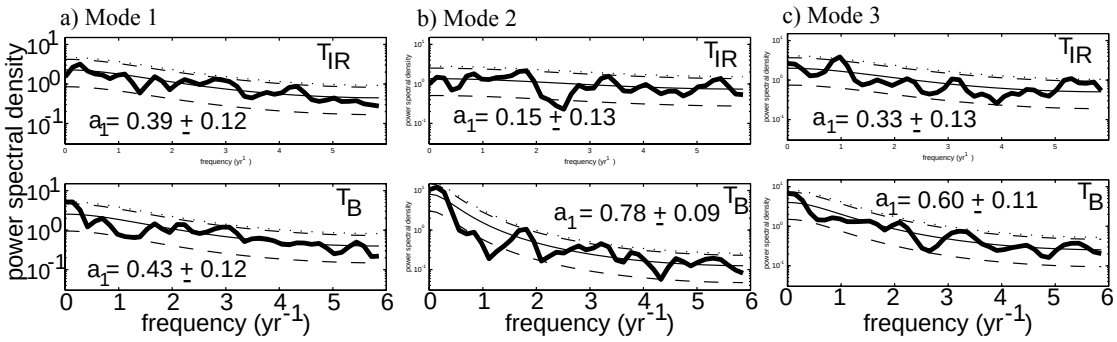

Figure 1.5. Power spectra (heavy solid lines) of the MCA expansion coefficients shown in Fig. 1.4. for (a) first, (b) second, and (c) third modes. Also shown (thin solid lines) are the theoretical spectra of the AR(1) (red noise) process that best fits the original time series. 5% and 95% confidence levels are indicated by dashed lines; 99% confidence level by dotted lines. The coefficients a_1 of the best-fit spectra are also indicated inside the plots.

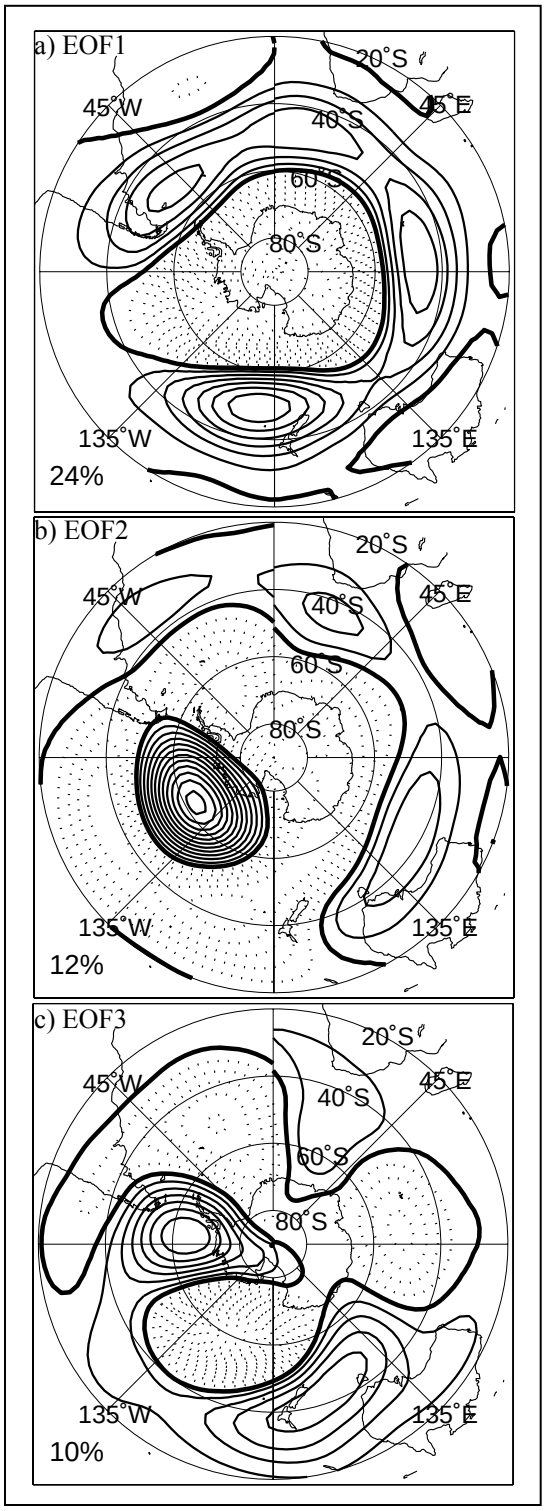

Figure 1.6. The leading modes in monthly 500-hPa geopotential height, 1982-1999. The (a) first, (b) second, and (c) third EOFs, shown as the Z500 data regressed upon the leading normalized PCs. Percentage of variance explained indicated at lower left. Contour interval 5m, zero contour heavy solid line, negative contours dotted, positive contours solid.

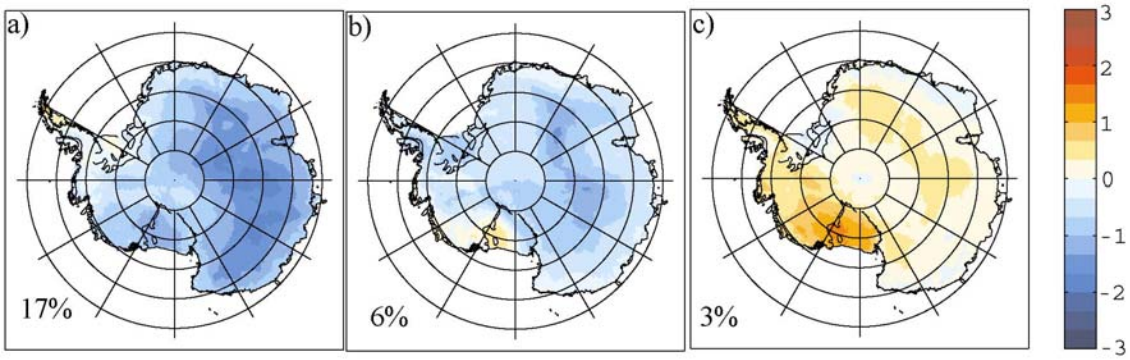

Figure 1.7. Regressions of T_{IR} gridpoint data upon the first three Z500 normalized PCs (a-c, respectively). Percentage of variance explained indicated in lower left. Color scale is in K, corresponding to one standard deviation of the respective PC time series.

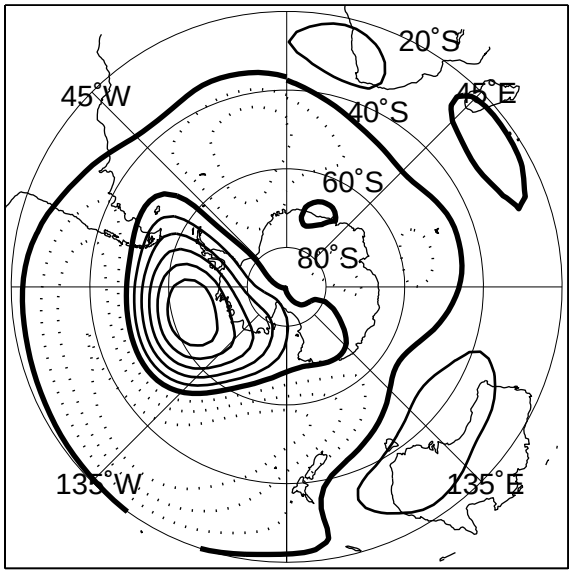

Figure 1.8. Regression of 1982-1999 monthly Z500 data upon the SOI with sign reversed to show anomalies typical of the ENSO warm phase. Units, contours as in Fig. 1.6.

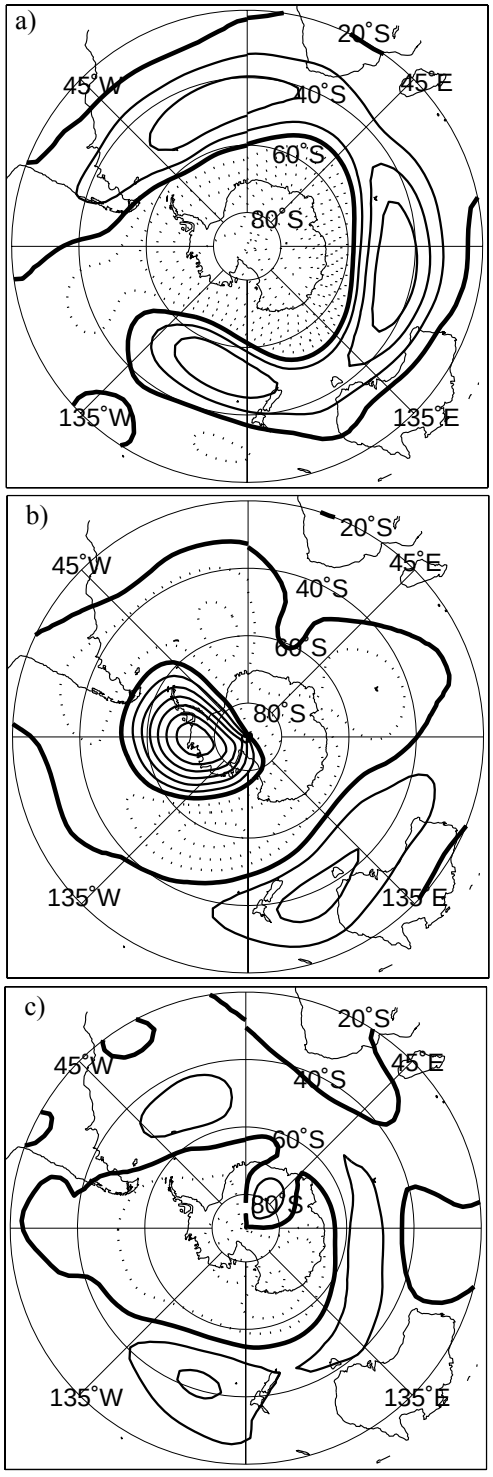

Figure 1.9. Regression of Z500 data upon the (a) first, (b) second, and (c) third normalized T_{IR} expansion coefficients shown in Fig. 4. Units, contours as in Fig. 1.6.

CHAPTER 2

New high-resolution ice cores from Antarctica: Sites, climatology, and stable isotope measurements

2.1 Selection of Ice Coring Sites

While the major features of Antarctic climate variability were highlighted in Chapter 1, climatological considerations, rather than the desire to obtain a record from a "center of action" of one of the modes of variability, often dictates the selection of ice coring sites. Climatologically, the best case scenario is generally a site with high snow accumulation and low annual mean temperature. Accumulation plays a role in how precisely an ice core can be dated, and in how deep a core must be drilled to reach a desired age horizon. To suit ice core studies with the goal of developing high-resolution (interannual) reconstructions of the major modes of variability, mean accumulation rates should be sufficiently high at the coring site so as to allow the clear identification of annual layers in properties such as stratigraphy, stable isotope ratios, and major ion chemistry. Counting of these layers through the core is the principal method of developing a depth-age scale. Another key in the accurate dating of high-resolution ice cores is the identification of volcanic eruption markers, as peaks in non-sea-salt sulfate (nss-SO_4^{2-}) concentration. Mean annual air temperature plays a role in determining the accumulation rate; however, its more direct importance in ice core site selection is that it indicates how well species are likely to be preserved after deposition. At warm sites, surface melting can lead to diffusive changes of chemical species and stable isotopes down through the firn column (e.g. Cuffey and Steig, 1998). Warm conditions also lead to the more rapid diffusion of stable isotopes, potentially compromising any high-resolution signals that may have been gained by choosing a site with a high accumulation rate. Firn permeability and porosity, tied to accumulation and temperature, can also be of importance in post-depositional alterations of chemical compounds (e.g. Neumann, 2003; Rick and Albert, 2005).

2.2 Estimated temperature and accumulation rate climatology

There is an expectation of correlation between temperature and accumulation rate through the Clausius-Clapeyron relation. The spatial patterns of mean annual temperature (Figure 2.1) and accumulation rate (Figure 2.2) across Antarctica, however, have notable regional differences. The close association of temperature with elevation is quite visually stunning

(Figures 2.1a and 2.1b); but there is not such a persistent relationship between temperature and accumulation rate. In West Antarctica, for example, the Ross Ice Shelf and its drainage area on the continent are relatively warm, but the accumulation rate is low. Around Byrd station, the accumulation rate pattern has been well mapped (Morse et al., 2001). Accumulation in this region decreases from the high elevation (~1800 m) and cold (~-30°C) divide towards the lower elevation and warmer ice streams and ice shelf area. Near the Amundsen Sea Coast, east of the divide, accumulation rates are among the highest in Antarctica. This pattern of accumulation in West Antarctica appears to arise at least in part from the quasi-permanent Amundsen Sea Low, which is centered near the coast at 135°W (e.g Bromwich et al., 2004; Morse et al., 2001). On its north-eastern flank, warm, moist air can be advected into West Antarctica from the Amundsen Sea. If the accumulation pattern is a function of distance from the predominant moisture source and is modified by orography, the Siple Coast region and the Ross Ice Shelf lie on the dry side of the divide. Figure 1.6a suggests that the strength of the ASL is strongly modulated by the SAM.

2.3. Ice coring Projects

The International Trans-Antarctic Scientific Expedition (ITASE) has as its chief goal the documentation and understanding of environmental change in Antarctica over the last 200 years, a time period which spans the largely pre-industrial and the industrial era. The central contribution of the project has been the collection and analysis of a spatial array of ice cores all across the continent. The United States' effort (US-ITASE) has largely focused on West Antarctica. US-ITASE is a collaboration of many institutions and principal investigators, with distinct but complementary topics of study (Table 2.1). Most of the investigators or their graduate students and postdocs participated in field work in the Antarctic over four field seasons from 1999-2002. I participated in years two and three (2000 and 2001), and Eric Steig participated in year four (2002). Over the course of the four field seasons, nineteen moderately deep (60 – 120 m) cores were collected (Figure 2.3). Ice-penetrating radar profiles and global positioning system (GPS) surveys of surface elevation have been made between the sites along the lines shown in Figure 2.3. High-frequency radar (400 MhZ) was used to quickly asses whether the stratigraphy at a potential site was well-behaved, and GPS helped to identify and avoid locations with potential peculiarities in the local accumulation pattern due to the interaction of prevailing winds with terrain.

In addition to the climatological considerations outlined above, US-ITASE had additional practical concerns in the selection of sites. Chief among these was the avoidance of heavily crevassed terrain, which was identified in advance through studies of satellite data and guarded against in the field through continuous real-time monitoring of high-frequency ice penetrating radar reflections.

The University of Washington contribution to US-ITASE has been primarily through the analysis of samples for stable isotope ratios (δ^{18}Oand δD). Field work included the sampling of snowpits and shallow cores for stable isotopes, density, and stratigraphy, to supplement the main ice core data at each site. Core processing was done at the National Ice Core Laboratory in Denver, Colorado in the summers following the field seasons (2000-2003), and Steig and I participated in each of these processing sessions. At the University of Washington, measurements of δ^{18}O have been made using CO_2 equilibration (Epstein and Mayeda, 1953) coupled to a Micromass Isoprime mass spectrometer with an estimated precision of 0.07‰, and δD has been analyzed using Cr reduction (Schoeller et al., 2000) coupled to a ThermoFinnegan DeltaPlus mass spectrometer with a precision of 1‰. Sampling intervals have been on the order of 2-5 cm.

2.4. Summary of US-ITASE sites and isotope measurements

Table 2.2 presents general site characteristics of all of the US-ITASE cores and the two complementary cores from Siple Station and Law Dome, along with measurements of accumulation rate and stable isotopes from the ice cores. Latitude, longitude, and elevation were determined with GPS. The T_{IR} data, discussed in Chapter 1, are used to indicate the mean annual temperature. Accumulation rate data are derived from the chemistry-based depth-age scales of University of Maine researchers in conjunction with the core density measurements (ice core mass and geometry was measured in the field). The ages of the deepest part of the cores are estimated from the chemistry based chronologies. Stable isotope measurements are from the University of Washington stable isotope laboratory.

As of this writing, seven of the US-ITASE cores have complete measurements of either δ^{18}O and/or δD through the entire core, and an additional five cores have measurements complete in their upper ~20 m. University of Maine researchers (primarily Dixon) have dated several of the US-ITASE cores based on annual signals in major ion chemistry, especially in nss-SO_4^{2-}. Major volcanic eruptions (e.g. Pinatubo (1991), El Chichon (1982); Agung (1961); Krakatoa

(1883); Tambora (1815)) had nss-SO_4^{2-} peaks associated with them in nearly all of the cores, assuring accurate cross-dating of the records (Dixon et al., 2005; Steig et al., in press).

Four of the cores which have both chemistry based chronologies and complete stable isotope measurements are at least the targeted 200-years long. I have corroborated the dating of three of these cores (2000-1, 2000-5, and 2001-5) through the counting of annual cycles in δD or $\delta^{18}O$. Because of the difference (~1 month) in the seasonal timing of summer stable isotope peaks and nss-SO_4^{2-} peaks, I made slight adjustments to the chemistry based chronologies before applying them to the isotope data. The chemistry based depth-age scales assign nss-SO_4^{2-} peaks to January 1st of each year. Sulfate tends to lag the isotope peak, which occurs earlier in the summer, closer to January 1st. Thus, to achieve accurate calendar-year annual averages of stable isotopes, the adjustment procedure centered stable isotope peaks on January 1st. Figure 2.4 illustrates the difference in chemistry based and adjusted age scales for core 2001-5. In Chapters 3 and 4, I use the three age-adjusted cores in my analyses of variance and in calibrations with meteorological data. Core 1999-1 is excluded because the warm temperature, low accumulation rate, and high firn permeability (Rick and Albert, in press) of the site appears to have led to strong isotopic diffusion, and there may be additional complicating affects associated with local elevation change (Kaspari et al., 2005). In Chapter 5, I use all of the US-ITASE records for which isotope measurements are currently available spanning the last ~40 years, developing depth-age scales directly from stable isotopes in cases where chemistry based chronologies have not yet been derived.

The mean behavior of stable isotopes versus site characteristics such as temperature and elevation can be derived from the data in Table 2.2. Isotope ratios are first plotted versus elevation as the independent variable (Figure 2.5a), because elevation is more accurately known than mean temperature. The number of measurements is small, but a fairly linear relationship is shown between isotopes and elevation. The point from Law Dome, which is rather warm for its elevation, is an outlier compared with the other data points. Figure 2.5b displays $\delta^{18}O$ versus mean annual temperature. A least-squares linear fit can be made through these points with a slope of 0.78‰ / °C, and the r^2 value of 0.78 is quite good. However, this should be cautiously interpreted, and not taken as a calibration curve for stable isotope ratios. One can see that removing just one of the points, notably the Law Dome point, would change the δ-T slope calculated from the data (to 0.42 ‰ / °C). More reasons for such caution are discussed in Chapter 3. These include the fact that the temperature data used are from the T_{IR} data set, which represent surface temperature rather than the condensation temperature, which in theory is more

physically linked to stable isotope fractionation (e.g. Jouzel et al., 1997). The T_{IR} data are also representative of clear-sky conditions, though obviously the data are quite good for general climatological studies, as for example in Chapter 1 and as suggested by the expected good relationship of T_{IR} and elevation. Such a relationship, however, cannot necessarily be well-defined from the few sparse data points at the locations of the ice cores. In Figure 2.6, T_{IR} is plotted versus elevation for the 24 sites listed in Table 2.2. One can derive a good linear fit with a slope of -10.9 °C / km and an r^2 of 0.87; however, it is apparent from the figure that a uniform lapse rate does not apply everywhere across Antarctica. Such variation could be attributed to, for example, the differing strength of the surface inversion. This example further illustrates how using a "one size fits all" spatial δ-T slope defined from just a few data points could be problematic for calibrations. In Chapters 3 and 4, I discuss alternative methods of calibrating the stable isotope measurements in terms of temperature anomalies.

Time series of the seven records with at least chemistry based depth-age scales are displayed in Figure 2.7. Common characteristics include a stable long-term mean, and high interannual to decadal scale variability. Visually, some covariance among the records can be seen, and more quantitative analyses are discussed in the following chapters.

2.5 Summary

The US-ITASE project has collected a rather large array of ice (or firn) cores with the goal of achieving widely spatially distributed records spanning the last 200 years. The total depth of core collected (~1400 m) is comparable in scale to the deep core from Law Dome (~ 1200 m) and is about half that of the well-known ~2800 m, 110,000 year long Greenland Ice Sheet Project Two deep core (e.g. Meese et al., 1997). Core sites were selected on the basis of climatological, glaciological, and practical factors. Fortunately, most of the sites meet the desirable criteria of relatively high accumulation rates (>12 cm H_20 yr^{-1}) and low mean annual temperature (~-30°C). Furthermore, most of the cores can be dated with a high degree of precision and accuracy on the basis of major ion chemistry, and for a few cores thus far, the high-resolution of the measurements allows the timescales to be fine-tuned so that summer stable isotope peaks are defined as January 1st. The vast amount of data available is too great to discuss in detail in this thesis, though some preliminary analysis has been done, and important scientific questions can be addressed, as discussed in the following chapters. Above, the spatial covariance of mean isotope ratios with factors such as mean annual temperature and elevation has been illustrated. Linear

relationships are found, in agreement with first-order expectations (for instance, more depleted isotope ratios with colder temperatures), however, caution is advised in the application of such relationships to temporal δ-T calibrations.

Table 2.1. Summary of US-ITASE Project, 1999-2002 traverses

Topic	Principal Investigators	Grad students/ postdocs	Institution
Lead ITASE coordination	Paul Mayewski		University of Maine
Stable isotopes	Eric Steig, Christopher Shuman (NASA), Jim White (Colorado)	David Schneider	University of Washington
Glaciochemistry, accumulation from ice cores	Paul Mayewski	Dan Dixon, Susan Kaspari	University of Maine
Deep radar	Bob Jacobel	Brian Welch	St. Olaf
Shallow radar	Steve Arcone	Blue Spikes, Jim Laatsch	CRREL, University of Maine
Mass balance, accumulation from radar	Gordon Hamilton	Blue Spikes	University of Maine
Satellite image analysis	Gordon Hamilton	Leigh Stearns	University of Maine
Snow and firn microstructure	Mary Albert	Ursula Leeman	CRREL
Hydrogen peroxide, formaldehyde	Roger Bales	Markus Frey	Desert Research Institute (Nevada)
Trifluoroacetate	Joe McConnell	Markus Frey	University of California Merced
Meteorology	David Bromwich	Andy Monaghan	Byrd Polar (Ohio State)

Table 2.2. Site characteristics of US-ITASE and other core sites.

Core Name	Year Drilled	Latitude	Longitude	Elevation (m)	Mean accumulation (cm H_20 yr^{-1})	Mean annual temp. (°C)	Mean $\delta^{18}O$ (‰)	Mean δD (‰)	Depth of main core (m)	Bottom age (year)
South Pole		-90.00	0.00	2900	7.8	-46.73	n/m	n/m		n/m
US-ITASE 02-5	2002	-88.00	-107.98	2747	n/m	-43.21	n/m	n/m	78	n/m
US-ITASE 02-4	2002	-86.50	-107.99	2586	16.0	-40.12	n/m	-345	72	1753
US-ITASE 02-3	2002	-85.00	-105.00	2396	n/m	-35.55	n/m	n/m	75	n/m
US-ITASE 02-2	2002	-83.50	-104.99	1957	n/m	-32.66	n/m	n/m	119	n/m
US-ITASE 02-1	2002	-82.00	-110.01	1746	n/m	-29.48	n/m	n/m	118	n/m
US-ITASE 01-6	2001	-76.10	-89.02	1228	40.0	-25.93	n/m	n/m	18	1977
US-ITASE 01-5	2001	-77.06	-89.14	1239	34.0	-27.00	-31.5	n/m	115	1780
US-ITASE 01-4	2001	-77.61	-92.25	1483	n/m	-30.15	n/m	n/m	68	n/m
US-ITASE 01-3	2001	-78.12	-95.65	1620	35.0	-30.40	n/m	-253	70	1853
US-ITASE 01-2	2001	-77.84	-102.91	1336	46.0	-27.83	-30	n/m	71	1889
US-ITASE 01-1	2001	-79.16	-104.97	1842	n/m	-31.61	-32.0	n/m	73	n/m
US-ITASE 99-2	1999	-81.20	-126.17	1040	n/m	-25.75	n/m	n/m		n/m
US-ITASE 99-1	1999	-80.62	-122.63	1350	15.0	-26.75	-32.6	-253	58	1724
US-ITASE 00-7	2000	-79.13	-122.27	1495	n/m	-30.36	n/m	n/m	63	n/m
US-ITASE 00-6	2000	-78.33	-124.48	1639	n/m	-30.99	-33.2	n/m	60	n/m
US-ITASE 00-5	2000	-77.68	-124.00	1828	13.0	-31.90	n/m	-264	60	1715
US-ITASE 00-4	2000	-78.08	-120.08	1697	19.0	-31.03	n/m	-262	58	1798
US-ITASE 00-3	2000	-78.43	-115.92	1742	n/m	-30.72	n/m	-250	60	n/m
US-ITASE 00-2	2000	-78.73	-111.50	1675	n/m	-30.55	-31.0	n/m	61	n/m
US-ITASE 00-1	2000	-79.38	-111.24	1791	23.0	-31.10	-33.0	-258	105	1652
Byrd Station		-80.01	-119.56	1503	16.0	-28.86	n/m	n/m		
Law Dome 2000	varies	-66.78	112.82	1370	67.0	-19.40	-22.3	n/m	1260	~80,000 yrs BP
Siple Station	1983	-75.92	-84.15	1054	56.0	-25.00	-29.7	n/m	302	1420
n/m = not measured										

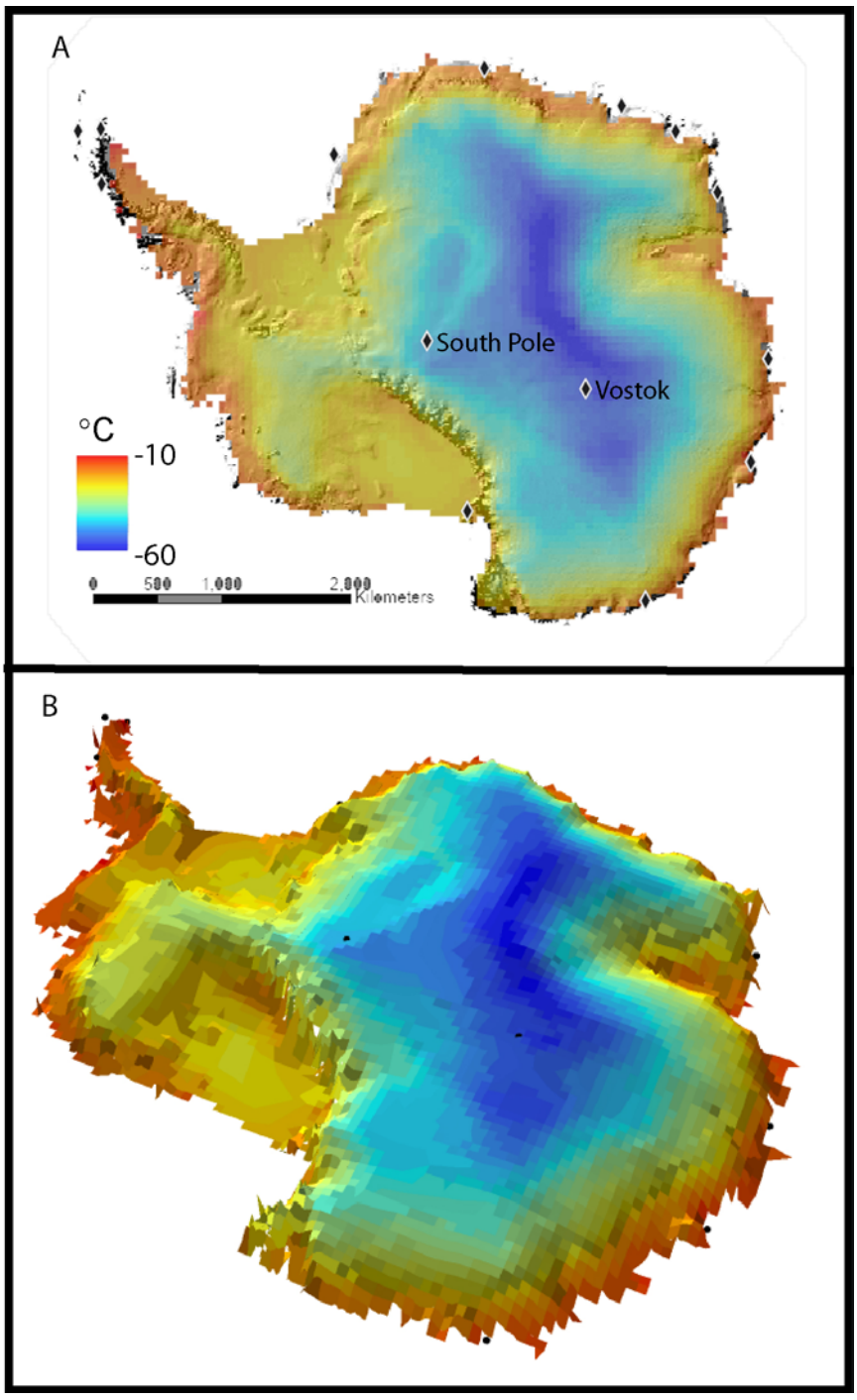

Figure 2.1. Maps of mean annual temperature. (a) Mean annual temperature (1982-1999 average) from the T_{IR} data set draped over surface elevation from the Liu et al. (1999) digital elevation model. (b) Same as in (a), except projected in a three-dimensional perspective.

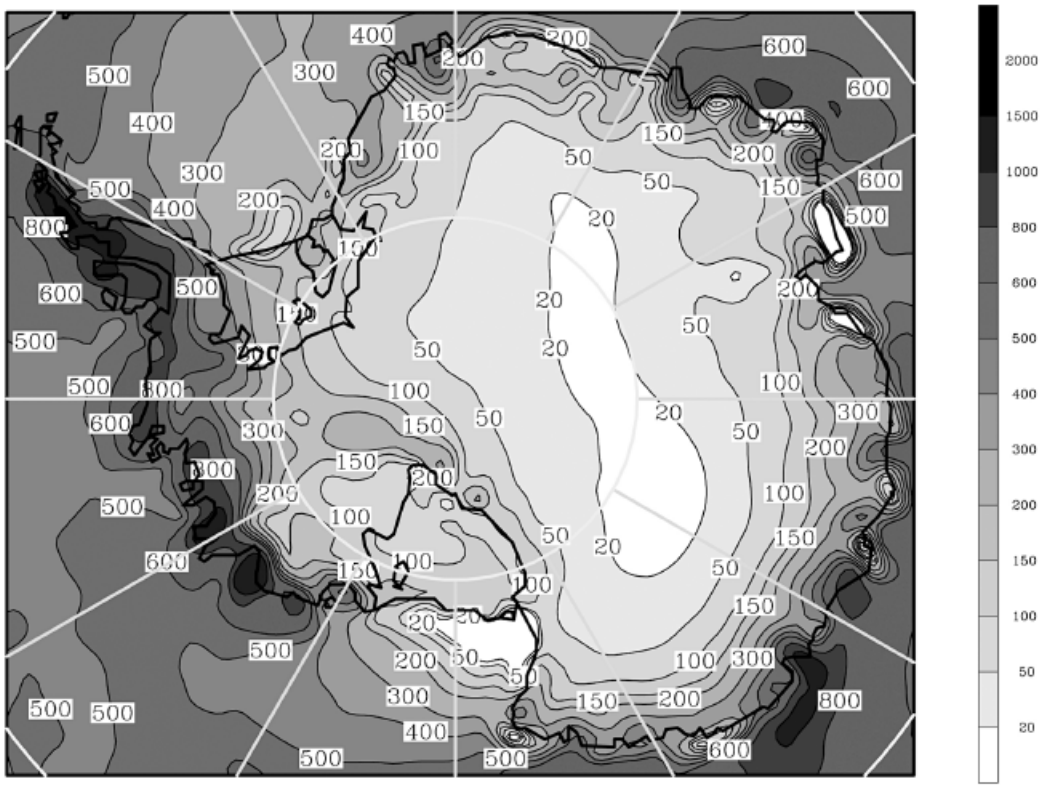

FIG. 3. Annual precipitation minus sublimation for Jul 1996–Jun 1999 simulated by Polar MM5 (mm yr^{-1} water equivalent).

Figure 2.2. Map of mean annual accumulation rate (mm yr^{-1} H_2O). From Bromwich et al (2004) simulation by the Polar mesoscale climate model 5 (MM5). The simulated accumulation values and spatial pattern compares favorably to the compilation of accumulation data (derived from stakes, snow pits, ice cores, radar traverses, and passive microwave brightness temperatures) of Vaughan et al. (1999).

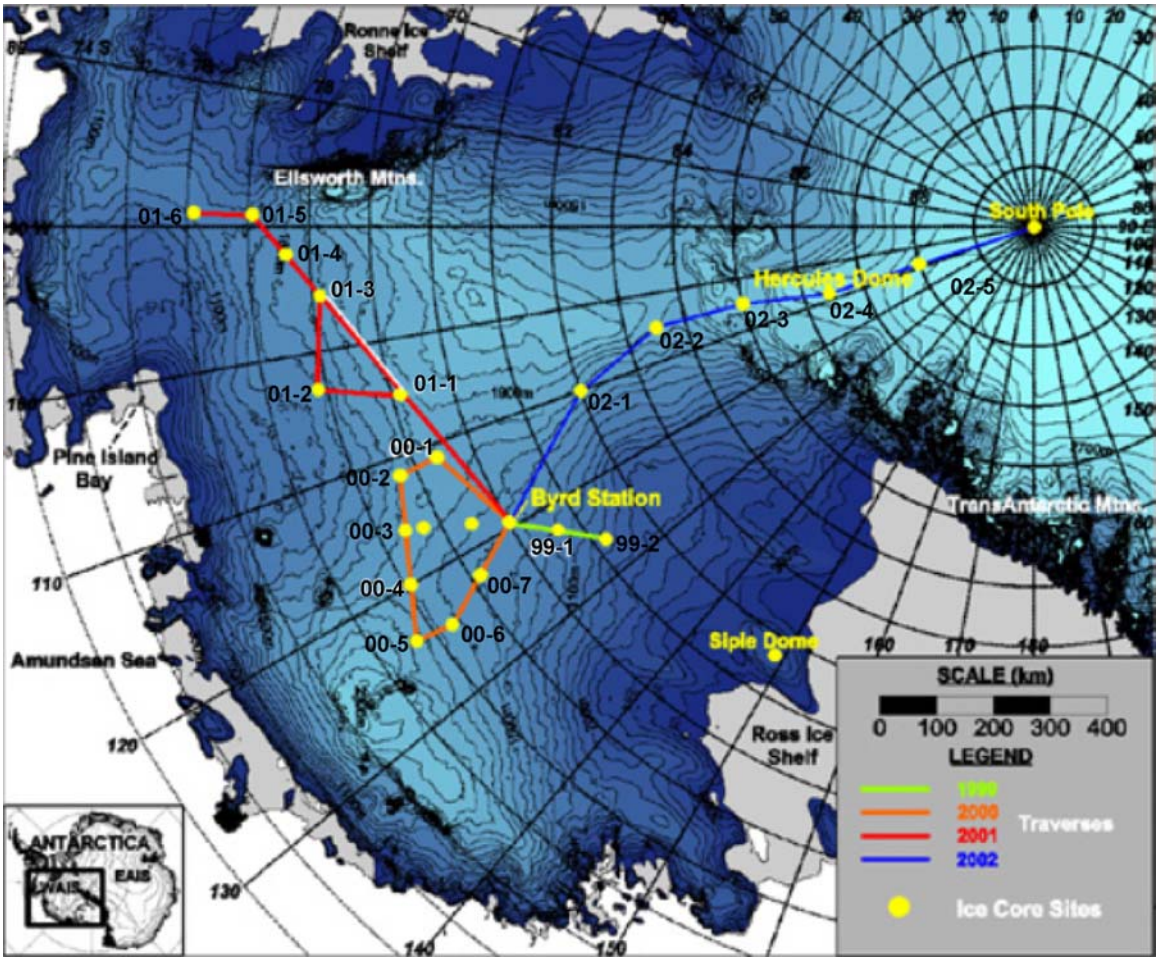

Figure 2.3. Map of US-ITASE (1999-2003) traverse routes. The ice core sites are indicated by yellow dots, with colored lines representing the routes of the over-snow traverses, and black contour lines indicating the surface elevation (m). After Mayewski et al. (2003).

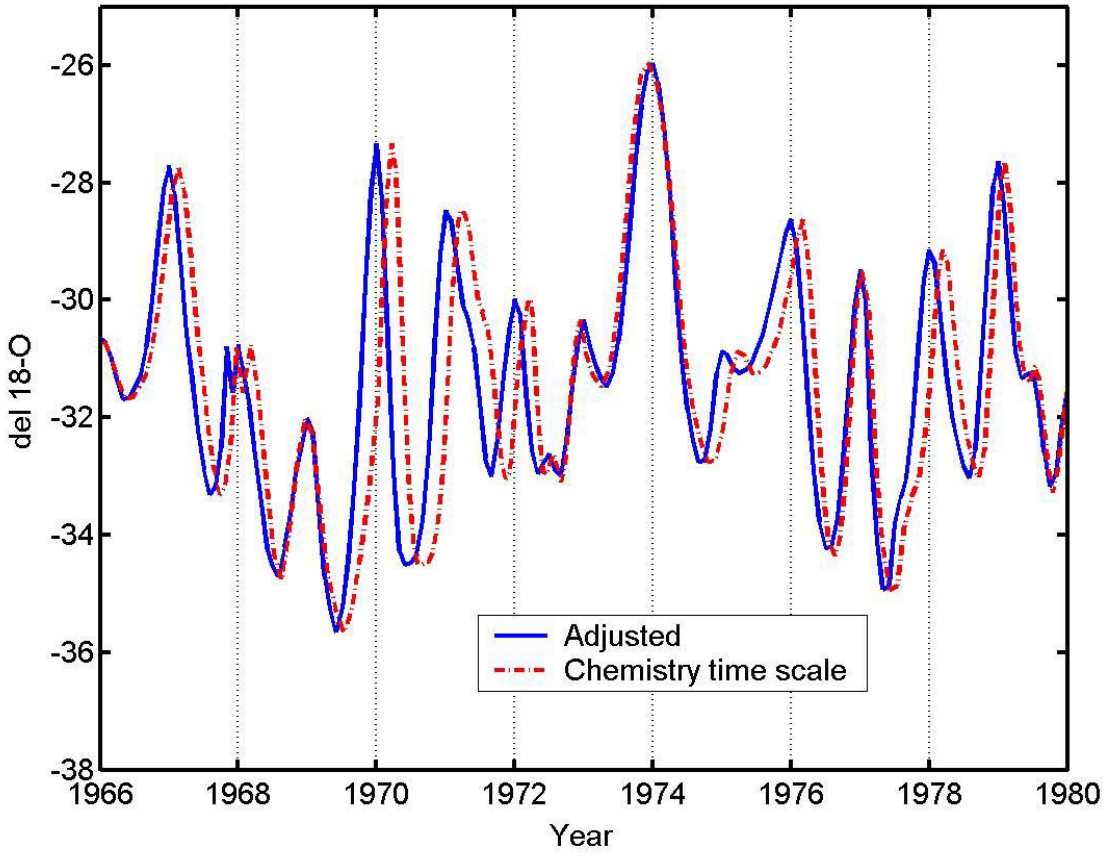

Figure 2.4. Section of $\delta^{18}O$ data from core 2001-5. Shown are the $\delta^{18}O$ series versus the timescale based on the counting of annual peaks in nss-SO_4^{2-} and other chemical ions and the $\delta^{18}O$ series versus the timescale based on adjustment of the chemistry-based timescale so that maximum values of $\delta^{18}O$ are attributed to January 1st of each year. The yearly tick markers indicate January 1st.

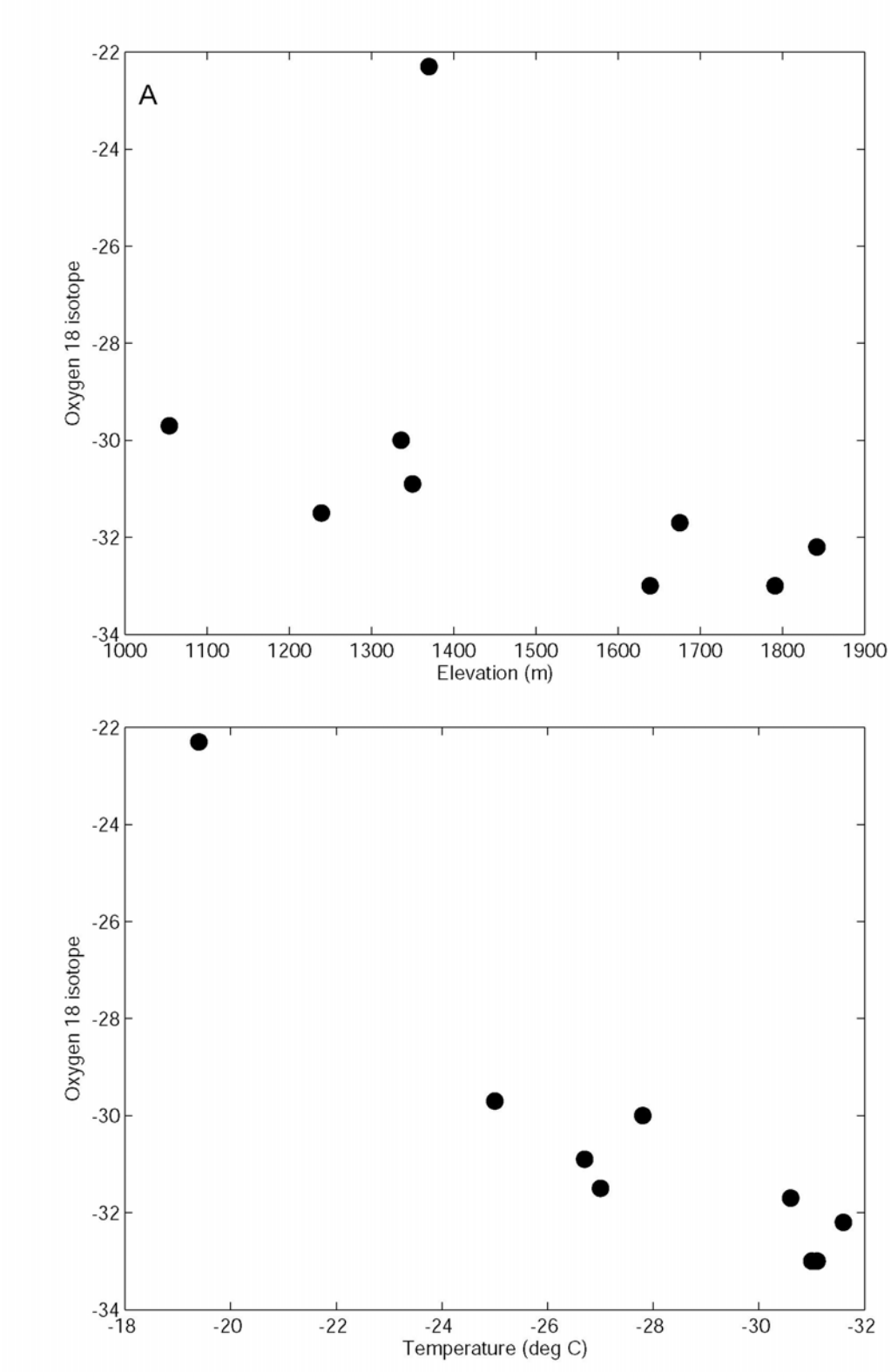

Figure 2.5 Mean values of $\delta^{18}O$ versus elevation (a) and temperature (b) from the data in Table 2.2.

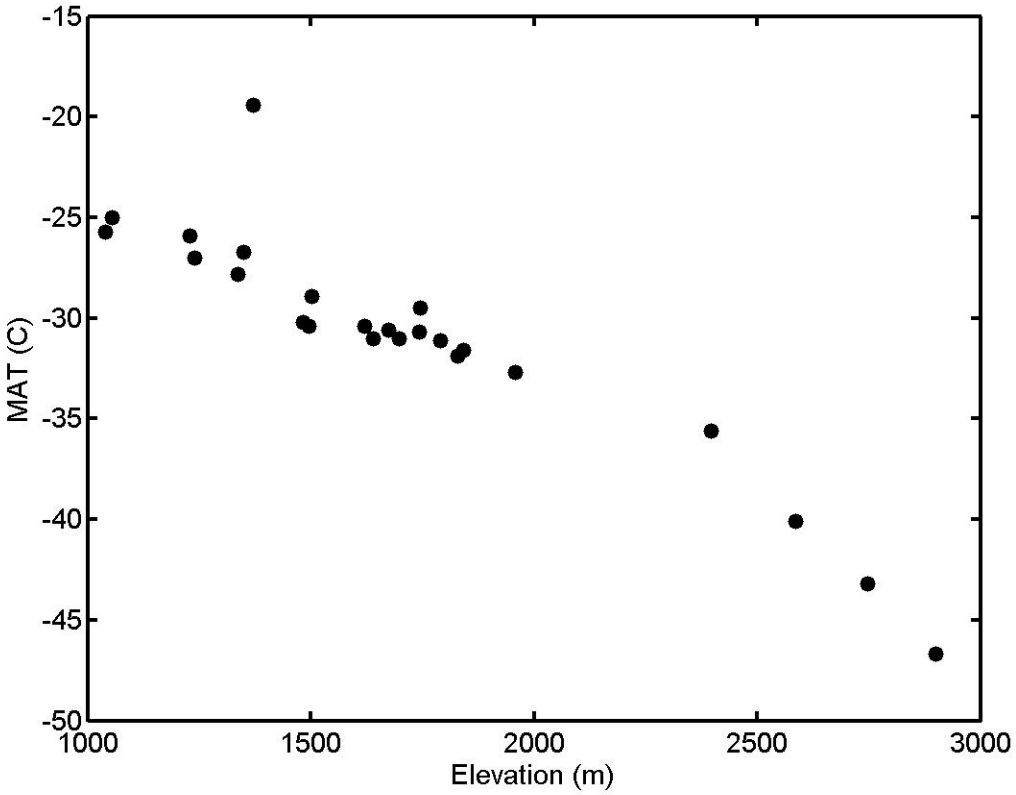

Figure 2.6. Mean annual temperature versus elevation at selected ice core sites.

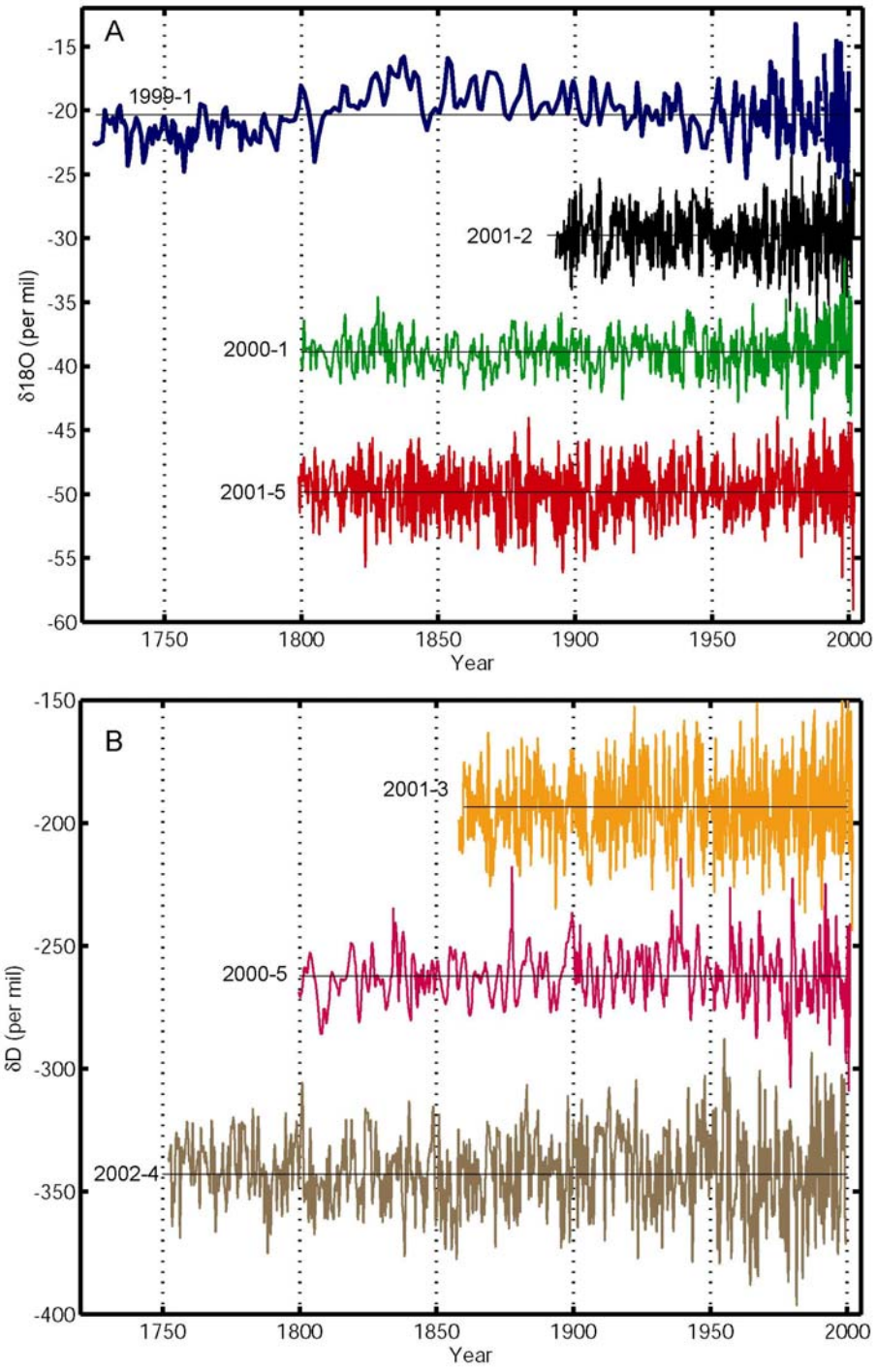

Figure 2.7. Time series of $\delta^{18}O$ and δD from seven US-ITASE cores. Mean values are adjusted for clarity of presentation.

CHAPTER 3

High resolution ice core stable isotopic records from Antarctica: Towards interannual climate reconstruction

3.1. Summary

Ice core records are a key resource for reconstructing Antarctic climate. However, a number of physical processes preclude the simple interpretation of ice core properties such as oxygen isotopic ratios in terms of climate variables like temperature or sea level pressure. We show that well-dated, sub-annually resolved stable isotopic records from the US-ITASE traverses and other sources have a high correlation with local seasonal temperature variation. However, this temporal relationship cannot be simply extended to quantitative interannual resolution reconstructions of site temperature. We suggest that a consistent and important target for ice core calibrations is a composite of annual mean temperature records from Antarctic weather stations, which covaries strongly with the dominant mode (from principal component analysis) of temperature variability in the Antarctic. Significant correlations with this temperature index are found with individual ice core records, with a composite of the ice cores, and through a multiple linear regression model with the ice cores as predictors. These results imply that isotopic signals, like the instrumental temperature mode itself, have a strong response to large-scale atmospheric circulation variability, which in the Antarctic region is dominated by the Southern Annular Mode.

3.2 Introduction

Globally averaged temperatures have risen markedly in the last hundred years, and early 21st century climate is likely to be outside the bounds of natural climate variability over the last millennium (e.g. Houghton and others, 2001; Karl and Trenberth, 2003). Relatively little can be said with any certainty, in this context, about recent climate change in Antarctica, because the instrumental record is too short and geographically sparse. Proxy climate information from ice cores in Antarctica provides a longer and more spatially detailed history of climate change than is available from direct observations.

Isotopic ratios of oxygen and hydrogen in polar ice cores have been used extensively as temperature proxies and, when calibrated with instrumental data, are often viewed as a paleothermometer. However, many physical factors in addition to temperature determine the

isotopic content of accumulated snow and ice, making extraction of proxy climate information from ice cores a difficult task in practice. Classically, a Rayleigh distillation model, with control parameters of the initial isotopic mass of the water vapor in an air parcel and the fraction of vapor mass that remains when precipitation forms at the deposition site, is used to explain highly correlated spatial and seasonal isotope-temperature relationships (e.g. Dansgaard, 1964). More sophisticated general circulation models suggest several other controlling factors, which include the seasonal timing of precipitation, the source region conditions, and the mixing of air parcels (e.g Cole and others, 1999; Noone and Simmonds 2002a; 2002b; Werner and Heimann, 2002).

Recent studies focused on Antarctica have found a disparity among different ice core sites of both the spatial and temporal isotope-temperature slopes, and potentially large imprints of source region conditions on the isotopic signal (Vaughan and others, 2003; Masson-Delmotte and others, 2003; van Ommen and Morgan, 1997; van Lipzig and others, 2002). To date, few interannual calibrations of ice cores have been attempted (Masson-Delmotte and others, 2003), although interpretations of stable isotopes as proxies of site temperature are frequently offered (e.g Thompson and others, 1990; Stenni and others, 2002; Vaughan and others, 2003; Mayewski and others, 2005), usually on lower-resolution (decades to centuries) time scales.

Large-scale features of the atmospheric circulation can strongly affect the isotopic ratios of precipitation through modulation of the condensation history of air masses reaching Antarctica, the location of the moisture source region and the isotopic signature of the source water. The effect that circulation anomalies have on local temperature may only explain a small part of the local isotopic response (Noone and Simmonds, 2002a, 2002b; Masson-Delmotte and others, 2003). Thus, a single isotopic record may not be well related to local temperature changes, but may more strongly reflect large-scale circulation features. Additionally, each location will be subject to local noise, caused by variations in precipitation timing, accumulation rate, post-depositional alteration and local circulation regimes.

Here, we consider both the sensitivity of stable isotopes to seasonal and interannual variations in local temperature, and, in keeping with the modeling studies discussed above, also use multiple records to reconstruct a spatially averaged interannual temperature history representative of the Antarctic region as a whole. While seasonal correlations are very strong, a single temporal isotope-temperature relationship that is common to all sites cannot be well defined. Focusing on reconstructing the regional temperature record, as inferred from Antarctic weather stations, we find that standard linear techniques (multiple linear regression and compositing) applied to multiple ice core time series yield consistent and promising results. The

signal common to the instrumental and ice core records reflects the dominance of the Southern Annular Mode on both isotopic and temperature variations over the continent (Noone and Simmonds, 2002b; Schneider and others, 2004).

3.3 Data

We use three ice cores from the United States International Trans-Antarctic Scientific Expedition (US-ITASE) (cores 2000-1, 2000-5, and 2001-5) for which high resolution (sub-annual) isotopic measurements and precise dating have been completed (Dixon and others, 2005; Steig and others, in press). More analyses on the US-ITASE data, which will include more than two dozen ice core profiles, are ongoing. We also use isotopic records that are at least annually-resolved from three previous drilling projects: Siple Station (Thompson and others, 1990), Talos Dome (Stenni and others, 2002), and Law Dome. The Law Dome record consists of Law Dome DSS97, a single core available at quasi-monthly resolution to 1996, and Law Dome 2000, a stack of 1 to 3 cores from the same site, including DSS97, available at annual resolution to 1999. The dating of the Law Dome cores is discussed by Palmer and others (2001) and van Ommen and others (2005). A map depicting the locations of these cores is displayed in Figure 1, and site characteristics are listed in Table 1.

Timescales for the US-ITASE cores are based on well-resolved seasonal cycles in ice core chemistry, with validation from volcanic horizons of known age (Dixon and others, 2005). On the basis of several validation tests, Steig and others (in press) estimate an accuracy of $<\pm 1$ year and a precision of ±2 months for these cores. We make minor adjustments to the time scales described by Dixon and others (2005), since a "core chemistry year," defined primarily by annual non-sea-salt sulfate peaks, will not always line up precisely in depth with an "isotopic year," defined as the interval between summer isotopic peaks. The isotopic peaks are assigned to January 1st. This avoids aliasing that may arise from the difference in timing (± 1 month, Steig and others, in press) of the isotopic and sulfate peaks, biasing the isotope record towards a particular season. Adjustment of the timescale is practical only in the highest-resolution portions of the isotope records where annual cycles are clearly defined. This is the case for the portions of the ice core records discussed here. It should be noted that the number of years in the two slightly different time scales is not different; only sub-annual adjustments are made. Isotopic peaks have also been assigned to January 1st in the Law Dome records.

To facilitate calibration against meteorological data, the ice core timescales are linearly interpolated to monthly resolution between summer markers for the US-ITASE and Law Dome cores. This assumes a constant accumulation rate throughout the year. While this assumption is not strictly valid, these sites have relatively high annual accumulation rates (Table 3.1) and as shown below, the isotopic cycles are clearly defined and have high (r^2 ~0.96), significant correlations with seasonal variations in temperature. Specific significance levels (when above 90%) cited henceforth are based on a two-tailed *t*-test while reducing the number of degrees of freedom to account for autocorrelation in the data (see Bretherton and others, 1999, Section 5).

Throughout this paper, we use the shorthand "δ" to refer interchangeably to oxygen and deuterium isotope ratios, unless distinction is necessary. $\delta^{18}O$ and δD in units of per mil (‰) are reported as = $(R/R_{VSMOW} - 1)$ where R is the ratio of $^{18}O/^{16}O$ or D/H and VSMOW is Vienna Standard Mean Ocean Water (VSMOW). All data are normalized to the VSMOW/SLAP (Standard Light Antarctic Precipitation) standards from the International Atomic Energy Agency.

Instrumental climate observations are needed to facilitate the interpretation of proxy ice core data, but long continuous meteorological records at ice core sites in Antarctica are rare. Satellite-derived surface temperatures are now available (Comiso, 2000), providing an important data source for this purpose. Although satellite-derived temperatures are an imperfect estimate of the true surface temperature because of a clear-sky bias that is stronger in the winter, the correlation with ground-based observation on monthly to interannual timescales is very high (e.g. Shuman and Comiso, 2002; King and Comiso, 2003). For each location discussed below, we select the 18-year (1982-1999) temperature time series (T), at monthly resolution, from the approximately 50 km * 50 km grid point in which the ice core site lies. The spatial resolution was reduced from the original satellite data by averaging adjacent pixel values. These data are limited in their temporal length, which poses problems for their use in interannual calibrations, but they are well suited for climatological δ-T correlations and the inference of spatial patterns of temperature variability (Kwok and Comiso, 2002; Schneider and others, 2004).

3.4 Results

3.4.1 Local correlations with temperature

Various methods have been used to calibrate ice core δ in terms of temperature variations. For example, van Ommen and Morgan (1997) proposed that the seasonal variation in

local temperature and isotope ratios could be applied to longer-term ice core records that extend back into the last glacial period. Many other studies have instead applied modern spatial δ-T scaling to ice core δ profiles (e.g. Petit and others, 1999). The seasonal temporal slope may be an improvement over the spatial slope. The latter has been shown to underestimate changes in temperature and to vary regionally (Jouzel and others, 1997), and there is no clear physical reason to link the spatial and temporal slopes (Bradley, 1999; van Lipzig and others, 2002). Below, we adapt both methods for use with the satellite data before proceeding to and comparing the results with interannual δ-T correlations.

Records in Table 3.1 are listed in order of decreasing mean annual temperature. As shown here, the mean $\delta^{18}0$ values are increasingly depleted following this trend. On the basis of these data, a spatial slope of 0.8 ‰/°C for $\delta^{18}O$ can be derived, consistent with δ-T slopes reported previously for Antarctica (e.g. Zwally and others, 1998). Shown in Figure 3.2 are the seasonal variations in $\delta^{18}O$ and T at four locations where sub-annual measurements are available. Each monthly value is an average of about 18 years of data for that month. For comparison with the other cores, δD values from core 2000-5 have been scaled by a factor of 1/8, to approximate $\delta^{18}O$ variability. Table 3.2 summarizes the correlations between T and δ and the equation of the linear best-fit line at each of these sites.

While all of the correlation coefficients are highly significant, the slopes vary and are all lower than the overall spatial slope. From Figure 3.2, it is apparent that the scaling of the y-axes, 0.50‰/C, approximates the actual relationship at Law Dome, while the other three sites have smaller slopes, which are given in Table 3.2. The temperature cycles are not sinusoidal but rather exhibit a broad winter minimum and short summer maximum, a well-known feature of Antarctic climatology (King and Turner, 1997). The isotopic cycles closely follow the shape of the temperature cycles, supporting a consistent δ-T relationship through the course of the year, but one that is specific to each site.

The difference in slopes among sites can at least in part be attributed to diffusion, which reduces the amplitude of the δ cycle at warmer and lower accumulation rates sites. We estimate the degree of diffusive loss, using an effective diffusion length calculated for local temperature and accumulation rate at each site, with the methods described in Cuffey and Steig (2002). The average amplitude loss can be estimated using the following equation from Johnsen and others (2000):

$$l = 100\left(1 - e^{-2(\pi L/\lambda)^2}\right) \tag{3.1}$$

where *l* is the relative (%) amplitude of the seasonal cycle compared with the original amplitude, L is the diffusion length, and λ is the annual layer thickness. In Table 2, *l* has been estimated, and the corresponding δ-T slope has been compensated for this effect. As expected, the seasonal δ -T slopes are increased by a larger factor for the lower accumulation rate sites. Perhaps due to additional loss of the seasonal cycle amplitude by sublimation and redeposition of water vapor in the upper few cm of the firn (e.g. Neumann, 2003), which is not taken into account in this diffusion model, the corrected slope values still vary significantly among the ice cores.

To investigate interannual variability in δ and its relationship with T, annual mean values of δ based on the calendar year are calculated for each of the cores discussed above; annual data for Siple Station and Talos Dome were obtained from other investigators. Accumulation rates are high enough in the US-ITASE, Siple Station and Law Dome cores that seasonal variations are obvious and the apparently limited diffusion should mean that accurate annual averages can be calculated, as the length over which diffusion acts is less than the thickness of an annual layer. At 2000-5, a relatively low accumulation core, clear annual isotopic cycles are sometimes absent, though the calculated diffusion length is still less than the average annual accumulation rate. At Talos Dome, on the other hand, there are obvious δD cycles only in the upper 7-8 m of the firn, and the age control is less reliable (Stenni and others, 2002) than that of the other cores discussed here. Thus, this core may be less reliable than the others as an annually resolved record.

Interannual variations in δ have a much poorer fit with T than do seasonal variations, and the δ-T correlation coefficients are quite low and not statistically significant (Table 3.3) perhaps due in part to the short length and high variance of the records. The δ-T slopes derived are not stable, as removing just a few outlying data points substantially alters the slope. For instance, in 2000-1, if just two data points are removed from the timeseries, than the slope changes from 0.42‰/°C to 0.90‰/ °C. For the Law Dome cores, the calibration is somewhat more stable, but there is still a discrepancy (although smaller than that of the other cores) between the seasonal and interannual slopes. One reason may be that physical processes governing the seasonal variation of temperature (e.g insolation) and the interannual variation of temperature (e.g. advection) are quite different. Thus, some researchers have suggested that isotopic fractionation should not be expected to respond in the same way to these processes (e.g. Cole and others, 1999).

3.4.2. Correlations with large-scale and longer-term temperature indices

Possibly, a stronger δ-T relationship could be found with accumulation-weighted annual values of δ and inversion-top temperatures (e.g. van Lipzig and others, 2002), but that is beyond the limits of available data. However, noise in individual records can be reduced through calculating averages or composites of ice cores and of the instrumental records with which they are compared.

An appropriate composite of instrumental data against which to evaluate all of the ice cores simultaneously should be one that is broadly representative of the study region. Although there are significant patterns of spatial variability in Antarctic climate, to first order temperature anomalies are remarkably coherent across the continent. A principal component analysis of satellite-derived temperatures covering the entire continent reveals that it is dominated by one mode, which has the same sign of anomaly nearly everywhere except for the northern Peninsula and explains 52% of the monthly variance and 62% of the variance in annually-averaged data (Schneider and others, 2004). This mode would seem an ideal target against which to calibrate spatially dispersed ice cores. Unfortunately, the satellite data cover too short of a period to provide a reliable interannual calibration; additionally, not all of our ice core records overlap temporally with these data. Therefore, we use meteorological observations from staffed Antarctic research stations to derive a longer climate index that adequately describes the time variability of the leading spatial temperature pattern, while leaving higher-order and more complex spatial patterns for future studies.

The Reference Antarctic Data for Environmental Research (READER) project provides the most recent update of Antarctic station data (Turner and others, 2004), with data available online (www.antarctica.ac.uk/met/READER/). In this data set, there are 14 stations with at least 30 years of monthly surface air temperature data from the late 1950s to present. Eight of these stations, which are indicated in Figure 3.1, have complete monthly records from 1961 to 1999, except for Scott Base, in which two months are missing in 1994 that we fill in with climatology. Principal component analysis applied to these stations results in a leading mode which explains 35% of the variance and has positive weights at each of the stations. The principal component associated with this mode is correlated with the simple mean of the constituent stations at $r = 0.98$. The mean was formed by subtracting the 1961-1990 monthly climatology from each station record before averaging all of the station anomalies. This composite index, denoted as A8, correlates with the mean and first principal component of the satellite data for 1982-1999 at $r = 0.72$ (significant at 95%), so it can be considered representative of the Antarctic as a whole.

Further support for this idea is shown by the correlation of annual values of A8 with the gridded satellite data (Figure 3.1). Nearly all areas have a positive correlation, except for the northern part of the Peninsula. Over the whole continent, A8 explains 28% of the full spatial-temporal interannual variance in satellite-derived Antarctic temperatures. A8 is thus a useful benchmark for ice core calibrations; it explains far more variance than other indices which are commonly invoked. For instance, the Southern Oscillation Index explains only 0.5% of the variance in Antarctic temperatures (Schneider and others, 2004).

Table 3.4 lists the correlations of δ and T at each site with A8. Correlations for the short satellite period are compared with the full length of A8. For the period 1982-1999, only Talos Dome δ has a significantly different correlation with local T than with A8. Also, correlations of A8 and δ are consistent with the correlations of A8 and T at the majority of the sites. For the longer period, most of the correlations of A8 and δ reach significance at the 90% level or above, but the magnitudes are not consistently greater than for the shorter period. Correlations among the four longest cores are mostly not significant (Table 3.5) despite the consistent and significant correlations with A8.

A composite index of annual ice core time series is constructed by the averaging of all of the ice cores available during the overlap period with A8. The five cores included are those listed in Table 3.4, excluding Talos Dome because of its negative correlations. Because each δ series has a different mean and variance, the time series are normalized before computing the composite. The mean δ value over the 1961-1990 overlapping reference period (1961-1983 for Siple Station) is subtracted from the time series and the result is divided by the standard deviation of the record during the same reference period. Over the period 1961-1983, when all five cores are included, A8 and the composite are highly correlated ($r = 0.67$, significant at 95%). For the full record, the correlation is $r = 0.62$, significant at the 99% level. Also, the slight warming trend in A8 (+0.0024 °/yr) from 1961-1999 is closely tracked by an upward trend in the composite. In detail, this period is composed of a warming to 1981, with a cooling tendency thereafter that is seen in both A8 and the ice core composite (Figure 3.3). These correlations are remarkable given the obvious disparity in the spatial sampling of the stations comprising A8 and the ice cores comprising the composite, and given the intrinsic uncertainties of the δ time series.

3.4.3. Scaling relationships with Antarctic-wide temperature anomalies

A straightforward way to express the ice core composite in terms of the temperature variations measured in A8 is through a single regression. This may not result in an optimal or reliable estimate of temperature variability, because as we have shown, there are differences in the sensitivity of the isotopic time series to temperature variations among the ice cores and across different time scales. Thus, multiple regression is also considered, since it can be objectively used to select which combination of ice cores best predicts the target time series, A8.

If the ice core composite is simply scaled against A8, the regression coefficient in the equation, A8 = 0.52*composite - 0.08, has a 95% uncertainty range of +/- 0.30. A verification test, giving an indication of the stability of the regression, shows that regression coefficients for an early time period, 1961-1980, and a late time period, 1981-1999, are well within this 95% uncertainty band. The scaled composite time series does not change the correlation with A8 from the unscaled composite. The trend (+0.0061 ° C/yr) and the variance (0.10 ° C) of the scaled composite are over-and under- estimated, respectively, compared to the target A8 time series.

Correlations of individual cores with A8 (see Table 3.4) show that some δ records are better than others in tracking the climate index. Stepwise multiple linear regression, where at each step a δ record is added to the predictors in the order of decreasing correlation with the predictand (Table 3.6), ultimately leads to similar results as the simple composite. With the four long ice core records and a 1961-1999 calibration period, the coefficients used to predict A8 are those in the last row of Table 3.6. The predicted time series (A8proxy) is highly correlated with A8 (r = 0.59, significant at 99%, Figure 3.3). The 1961-1999 trend in A8proxy (+0.0037° /yr) is very close to the trend in A8 itself. The variance in the reconstruction (0.09° C) is underestimated compared to the variance in the station time series (0.27 ° C).

A simple but strict cross-validation exercise is performed to test the ability of the predictors to predict time periods independent of the multiple regression. The data are split into an early and a late period, 1961-1980, and 1981-1999. Coefficients from the early period fitting are used to predict the late period and vice versa. Values of r^2 for the cross-validation are presented in Table 3.6. The somewhat low values are indicative of the problem of a limited data set and of extreme year-to-year variability in the target index, A8. Given the short time periods involved, single years can significantly change the cross-validation r^2 value. Since we do not have the luxury of a long cross-validation data set, we also use a less strict test that is often applied to short data sets (e.g. Wilks, 1995). This involves removing one year at a time, predicting the missing year, and compositing the single-year predictions into a verification time series, as was recently applied to tree rings by Jones and Widmann (2003). With this verification

scheme, A8 and the verification time series are correlated at r = 0.45, significant at 95%, indicative of the overall stability of the reconstruction, but again a reflection of the fact that not all individual years are correctly predicted, as can clearly be seen in Figure 3.3.

Reconstructions using the multiple linear regression and composite methods are correlated with each other at r = 0.95 (significant at 99%) and have a similar magnitude of correlation with A8. Thus, although the seasonal site-specific δ-T slopes vary, the similarity of the multiple linear regression results and composite results suggests that it is appropriate, in this case, to weight the normalized isotopic records equally.

3.5. Discussion

Results presented above show a strong relationship between monthly estimates of δ and T over the course of the seasonal cycle. However, on an interannual timescale, to the extent that they can be consistently defined, linear transfer functions are of little value when the correlation coefficient of δ with T is low. This finding of low interannual δ-T correlation is consistent with that of isotopic modelling studies (Cole and others, 1999; Noone and Simmonds, 2002a; Werner and Heimann 2002).

Compared with local T, a large-scale climate index, A8, does not substantially improve the amount of variance that can be explained in a single record of δ over the same time period. Over the 39-year time period, the magnitude of variance explained in δ by A8 is not systematically increased, but the statistical significance of the correlation is improved (Table 3.4). While the ice cores have only a modest correlation with site T and with A8 during 1961-1999, they are not all correlated with each other (Table 3.5), but they are consistently correlated with A8 (except for Talos Dome), so they are not redundant predictors. This attests to the large-scale representativeness of A8 and the physical processes it reflects. It implies not only temperature changes over a broad area of the ice sheet (see Figure 3.1), but also circulation changes (Schneider and others 2004), which in turn alter precipitation timing, winds, moisture origin and transport pathways, and condensation histories. These are the same factors which a number of studies have shown influence interannual variations in δ (Noone and Simmonds 2002a, 2002b; Werner and Heimann, 2002; Cole and others, 1999; van Lipzig and others, 2002), and which are, as Noone and Simmonds (2002b) discuss, systematically altered by the Southern Annular Mode (SAM). A composite of five normalized δ profiles explains a substantial amount of variance (roughly 45%) in A8. Through multivariate techniques or by simply scaling the composite, the

ice core reconstruction can be expressed in terms of temperature variations, with the two methods yielding very similar results. White and others (1997) used a similar method of computing an ice core composite for central Greenland and explained a comparable amount of variance through a multiple linear regression. However, that regression relied upon a number of climate indices which were not all independent of each other, whereas we have only used one primary index, A8. When using just one climate index, Greenland temperatures, White and others (1997) found a lower correlation than we have—r = 0.47 with their ice core composite.

The SAM is the prominent feature in mid to high latitude tropospheric atmospheric circulation (Thompson and Wallace, 2000a). Because the SAM is a roughly zonally symmetric oscillation, it affects temperature anomalies at Antarctic stations and in the continental interior apart from the Peninsula region in the same sense (Thompson and Wallace 2000a; Schneider and others, 2004). Regression of its index against satellite-derived surface temperatures explains about 18% of the variance on both monthly and interannual timescales (Schneider and others, 2004). Similarly, A8 is significantly correlated (at 99%) with the 1969-1998 SAM index of Thompson and Solomon (2002), which is based on radiosonde measurements of 500-hPA geopotential heights, at r = -0.78. As noted above, Noone and Simmonds (2002b) show that Antarctic isotope variability is also strongly controlled by the SAM. However, due to the high covariance between A8 and the SAM index, it is somewhat arbitrary whether variability in the ice core composite is attributed to the SAM, to temperature, or to a combination of the two. On the other hand, it is notable that, without any fitting, the ice core composite more closely tracks the variations and trends in A8 than in the SAM (r(composite, SAM index 1969-1998) = -0.33). Thus, the ice core composite cannot be simply viewed as a surrogate for the SAM index, though if viewed as a temperature index, it clearly has a relationship with the SAM consistent with that from modern instrumental observations.

3.6. Conclusions

In the ice core records we have examined, site-specific δ-T correlations are strong on a seasonal basis, and reinforce use of stable isotopes as temperature proxies. On the other hand, differences among seasonal slopes cannot be fully explained in terms of simple diffusion models, though more complete models may provide an improved assessment of the slope differences. Furthermore, differences between seasonal slopes and interannual slopes probably arise from different physical processes acting on both the variation of site temperature and the history of air

masses en route to the deposition site. At the interannual scale, a regional temperature index (A8) explains as much or more variance in local δ records as the site T, and embodies many of the relevant physical processes, as shown by its covariance with temperatures across the continent and with the SAM.

We suggest that the statistical reconstruction methods described here, with a focus on larger-scale processes as opposed to site-specific phenomena, are a viable approach towards reconstruction of interannual climate variability from ice cores. Our results demonstrate that meaningful estimates of the interannual variability and trends in 40 years of Antarctic temperature anomalies can be made with either a multiple linear regression model or a scaled composite on the basis of several well-dated, high resolution ice core records. Each additional record, with the exception of Talos Dome, improves the variance explained in temperature; thus we anticipate that additional high-resolution, well-dated ice core records will further improve the statistical skill of the calibration. As more data are added, however, records which clearly do not hold a significant physical relationship with the target index (e.g. Talos Dome) should be avoided. Verification exercises can be used to determine the reliability of such models. These calibration results are important because they suggest that the primary signal of temperature variability in the Antarctic may be reconstructed from δ records. Moreover, they are not simply fortuitous as physical models independently show the strong linkages among δ records, temperatures, and the SAM (Noone and Simmonds, 2002b). These results suggest promise for meeting one of the major goals of ITASE: quantitatively reconstructing the last ~200 years of climate variability in the Antarctic.

Table 3.1. Ice core records investigated in this study.

Core name	Lat.	Lon.	Elevation (m)	Mean annual temperature from satellite	Period of record (this study)	Isotope analyzed	Mean δ 1961-1990	Accumulation rate 1982-1999, water equivalent (m/yr)
Law Dome	66.78 S	112.82 E	1370	-19.4°C	1961-1999	$\delta^{18}O$	-22.3‰	0.67
Siple Station	75.92 S	84.15 W	1054	-25.0°C	1961-1983	$\delta^{18}O$	-29.7‰	0.56
US ITASE 2001-5	77.06 S	89.14 W	1246	-27.0°C	1961-2000	$\delta^{18}O$	-31.5‰	0.38
US ITASE 2000-1	79.38 S	111.23 W	1791	-31.1°C	1961-2000	$\delta^{18}O$	-33.0‰	0.26
US ITASE 2000-5	77.68 S	123.99 W	1828	-31.9°C	1961-2000	δ D	-264‰	0.12
Talos Dome	72.37 S	158.75 E	2316	-37.8°C	1961-1996	δ D	-292‰	0.09

Table 3.2. Mean monthly seasonal calibrations of δ with local T. If the correlation is significant, it is indicated in parentheses.

Core Name	**Equation of regression line**	**r^2**	**Amplitude loss due to assumed diffusion**	**Slope corrected for amplitude loss (‰/°C)**
Law Dome DSS97	$\delta^{18}O = 0.38T - 14.9$‰	0.96 (99%)	1%	0.38
2001-5	$\delta^{18}O = 0.21T - 26$‰	0.97 (99%)	2%	0.21
2000-1	$\delta^{18}O = 0.11T - 29$‰	0.94 (99%)	13%	0.13
2000-5	$\delta D = 0.55T - 246$‰	0.94 (99%)	20%	0.69

Table 3.3. Interannual calibrations of δ with local T.

Core Name	Equation of regression line	r
Law Dome 2000	$\delta^{18}O = 0.44T - 14$‰	0.39
Law Dome DSS97	$\delta^{18}O = 0.49T - 13$‰	0.51
2001-5	$\delta^{18}O = 0.09T - 29$‰	0.06
2000-1	$\delta^{18}O = 0.42T - 19$‰	0.29
2000-5	$\delta D = 2.9T - 1.7$‰	0.36
Talos Dome	$\delta D = 3.43T - 159$‰	0.25

Table 3.4. Correlations of local variables (δ and T) with a large-scale temperature index (A8). If the correlation is significant, it is indicated in parenthesis.

Site Name	**r, 1961-1999A8 and δ**	**r, 1982-1999 A8 and δ**	**r, 1982-1999 A8 and T**
Siple Station	0.68 (95%)		0.00
Law Dome 2000	0.42 (95%)	0.66 (90%)	0.47
2001-5	0.19	-0.13	0.26
2000-1	0.33 (90%)	0.28	0.39
2000-5	0.38 (95%)	0.44	0.21
Talos Dome	-0.11	-0.24	0.60

Table 3.5. Ice core records correlation matrix 1961-1999. If the correlation is significant, it is indicated in parenthesis.

Core Name	Law Dome 2000	2001-5	2000-1	2000-5
Law Dome 2000		-0.09	0.18	0.26
2001-5	-0.09		-0.01	-0.10
2000-1	0.18	-0.01		0.35(90%)
2000-5	0.26	-0.10	0.35(90%)	

Table 3.6. Stepwise multiple linear regression models. Coefficients, read across in each row, are those applied to the respective ice core time series to predict A8. R^2 values indicate how much variance is explained in A8 by the prediction at each step, with the significance level shown in parenthesis. At right, in italics: cross-verification exercise in which the prediction is verified in a time period independent of the calibration.

	Law Dome 2000 coefficients	**2000-5 coefficients**	**2000-1 coefficients**	**2001-5 coefficients**	**1961-1999 calibration, no verification (r^2)**	***1961-80 calibration; 1981-99 verification (r^2)***	***1981-99 calibration; 1961-80 verification (r^2)***
Step 1	0.22				0.18 (95%)	*0.44*	*0.02*
Step 2	0.15	0.18			0.26 (95%)	*0.24*	*0.05*
Step 3	0.09	0.11	0.17		0.29 (99%)	*0.22*	*0.05*
Final model	0.18	0.13	0.08	0.13	0.35 (99%)	*0.07*	*0.11*

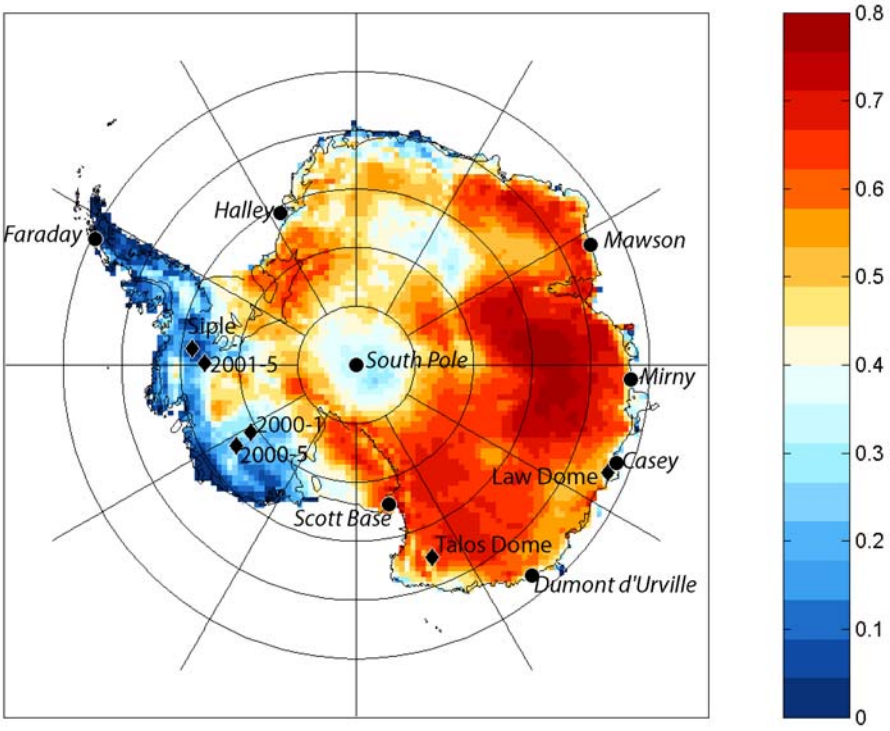

Figure 3.1. Map of Antarctica, with ice core sites indicated by a diamond, and stations with surface air temperature observations, which are used to construct A8, indicated by a large dot. Background color is the correlation coefficient of A8 with annual mean satellite-derived surface temperature anomalies at each grid box from 1982-1999.

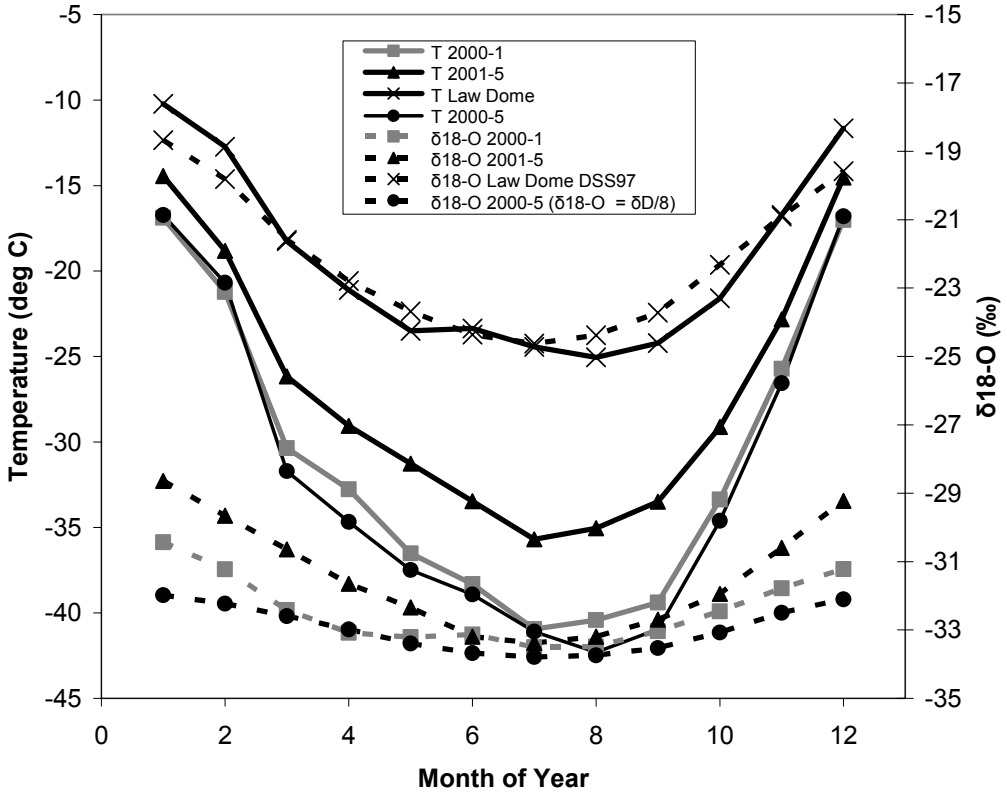

Figure 3.2. Plot of 18-yr monthly mean satellite-derived temperatures and corresponding isotopic values at various sites.

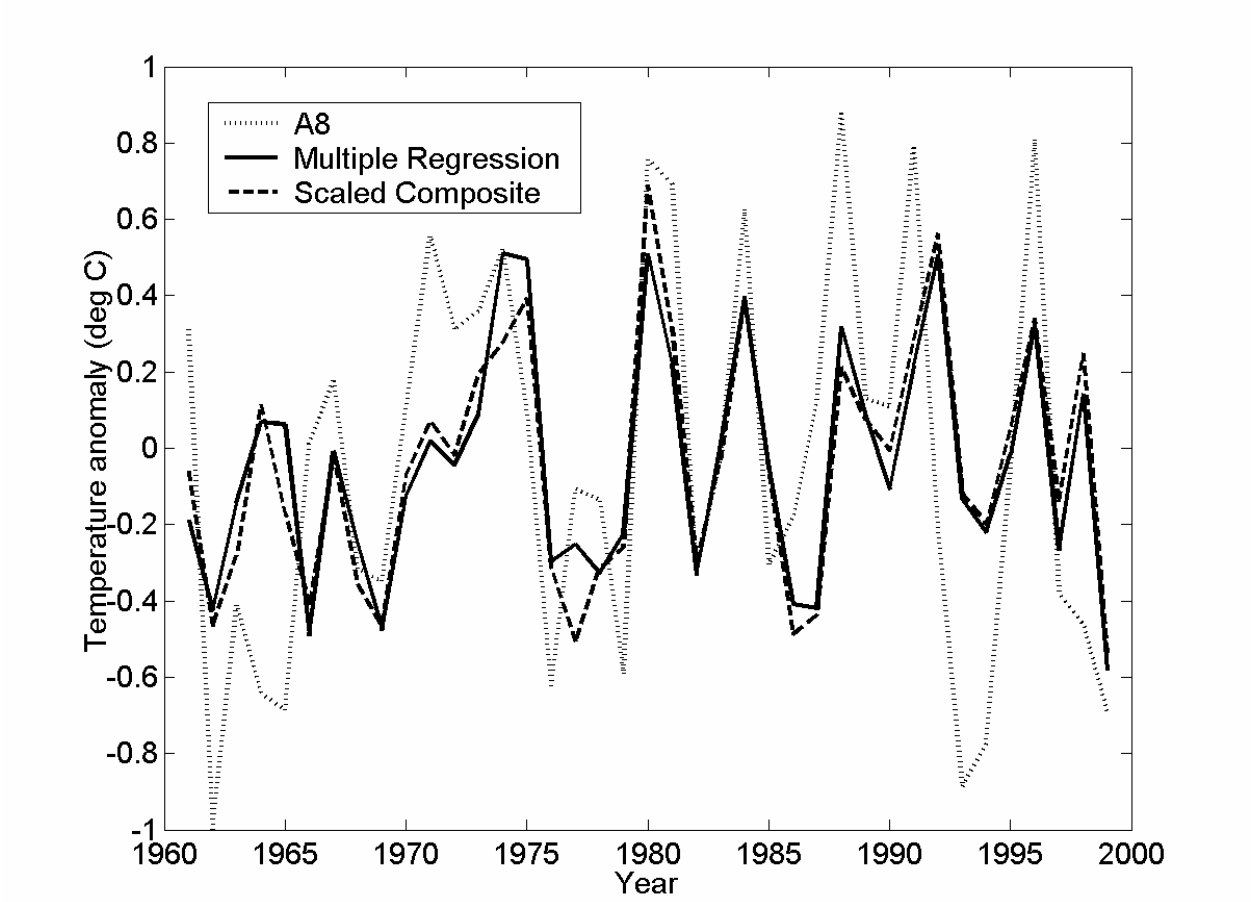

Figure 3.3. Estimates of annually averaged Antarctic temperature anomalies from A8, a multiple linear regression model with ice cores as predictors, and a scaled ice core composite.

CHAPTER 4

Ice core evidence for Antarctic climate change

4.1 Summary

Little is known about the variability in Antarctic surface temperatures prior to the late 1950s. We present an annual resolution 200-year reconstruction of Antarctic temperature anomalies based on a calibration of ice core stable isotope profiles. We demonstrate that both observed and reconstructed Antarctic temperatures exhibit high variability that is dominated by the Southern Annular Mode (SAM), the primary feature of atmospheric circulation in the high-latitude Southern Hemisphere (SH). Antarctic temperatures show periods of increase in common with the observed SH mean temperature record (1856-1999), but show a smaller, less significant long-term increase. The difference in trends is due in part to the positive trend of the SAM since the 1970s. These results differ from climate models, which depict significant long-term Antarctic warming.

4.2 Text

Although there has been a dramatic surface warming on the Antarctic Peninsula since the 1950s *(1,2)*, indications of climate change are much less clear over the rest of the Antarctic continent. Recent work has shown that any indications of long-term change in Antarctic temperatures (possibly as a reflection global warming) are likely to be mixed with the expression of a major circulation feature, the Southern Annular Mode (SAM); *(3 - 5)*. The SAM leads to large monthly to interannual temperature variability, and affects the Peninsula and the main Antarctic continent in different ways *(3 - 5)*. It is a roughly zonally symmetric see-saw in atmospheric mass between the Antarctic and the mid-latitudes, characterized by anomalies in the westerlies and the strength of the polar vortex *(3 - 6)*. A trend towards the positive phase of the SAM, implying a greater pressure difference between the polar region and the mid-latitudes, has occurred since the 1970s *(3, 6)*. The shift towards a stronger vortex is especially pronounced in the summer and fall months, a phenomenon that has been attributed to stratospheric ozone depletion in combination with the increasing concentration of atmospheric CO_2 *(3, 7, 8)*. The trend in the SAM can explain a fraction (up to 50%) of the increase in summer surface

temperature on the Peninsula, and a larger fraction of the summer and fall cooling that has been observed over the continent in the last ~20 years *(3, 4)*.

In situ meteorological observations from the Antarctic are short in length (30-50 years) and sparse in spatial coverage (Fig. 4.1). Most authors examining near-surface temperature records that extend back to the International Geophysical Year of 1957-58 have noted warming at most of the meteorological stations *(1, 2, 9)*. In contrast, a spatial extrapolation of station trends showed a net cooling of the continent between 1966 and 2000 *(10)*. Satellite-derived temperature data, which begin only in the 1980s, also indicate cooling over much of the continent *(4, 9)*. Here, we present a target time series from the instrumental record for calibration and an ice-core based temperature reconstruction to place these trends in the context of the past 200 years.

It has been suggested that the disparate trends reported by various studies are a consequence of spatial analysis techniques and/or of different data types *(2, 11)*. A more fundamental problem for interpretation of Antarctic climate change is the length of the records. From updated instrumental records, we average the temperature records at eight non-Peninsula stations to form a composite index that is in agreement with the temperature trends highlighted above. This index of Antarctic temperature anomalies, which we define as A8, exhibits an increasing trend since 1958, but also captures the decline in temperature since 1966 and the sharper decreasing trend since the beginning of the satellite era (Fig. 4.2). None of these trends are statistically significant *(12)*. The sharp trend in the most recent decades arises primarily from several cold years in the 1990s. Separation of A8 into its seasonal components shows that the cold annual mean conditions in the 1990s are due to anomalously low summer and fall temperatures (Fig. 4.5.S2), consistent with the seasonal timing of the positive SAM trend *(3, 6)*. The interannual variations of the A8 index are also anti-correlated with the SAM index (Table 4.1). These results are consistent with the first-order pattern of Antarctic temperature variability, which, as defined from satellite data, is characterized by spatial homogeneity in the sign of anomalies across the main part of the continent *(5)*. Thus, A8 captures the large-scale, SAM-dominated variability that is shared by the station records and also reflected in the satellite data (Figs.4.1 and 4.2; see also supporting text). The El Nino-Southern Oscillation may also influence Antarctic temperatures, however, its effects appear to be limited to the Ross Sea *(13)* and Antarctic Peninsula regions *(2)*. We focus on the first-order pattern of Antarctic temperature variability, extending the A8 index back to 1800.

The ice core proxy data we use are time series of stable isotope ratios (of oxygen and deuterium, i.e. $\delta^{18}O$ and δD; hereafter δ), which are commonly interpreted in terms of local

temperature, justified on the basis of Rayleigh-fractionation models and positive spatial and temporal correlations with air and surface temperature *(14 - 16)*. Atmospheric general circulation models with isotopic tracers show that on the continent, positive covariance between temperature and isotope variability is also expected because both are strongly controlled by, and are negatively correlated with, variability in the SAM *(14)*. The influence of the SAM thus leads to an expectation of spatial homogeneity in the anomalies of both temperature *(4, 5)* and stable isotopes *(14)* across the continent.

The δ records used in our reconstruction of A8 each have significant correlations with the seasonal cycle of local site temperature and with interannual variations in A8 and similar indices in the overlapping instrumental period *(16, 17; supporting text*). These records include previously published records from Law Dome *(18)* and Siple Station *(19)*, and three new ice core records obtained by the International Trans-Antarctic Scientific Expedition (ITASE); *(16, 17)*. Core sampling has been completed at sub-annual resolution, enabling precise and accurate dating *(17)*. Independent depth-age scales of the ITASE cores were obtained from the counting of annual peaks in non-sea salt sulfate, other ions, and δ in each record. Absolute ages were identified by volcanic eruption peaks in sulfate. Isochronal layers have been traced between some of the cores using reflections from high-frequency ice-penetrating radar, confirming dating consistency. Ice core records excluded from our reconstruction (Fig. 4.1) are either not accurately resolved at annual resolution, not correlated with A8 or local indices of temperature, or not yet completely sampled at high resolution *(supporting text)*.

A single δ record integrates a number of climate processes *(15)*, and typically contains additional noise that is not directly related to the large scale climate signal. To reduce noise and to estimate the large scale signal, we normalize the δ time series and combine them into a single composite at annual resolution. The composite has a significant correlation with A8 (1961-1999, $r = 0.58$, $p < 0.01$) that does not vary significantly over different time periods of the calibration interval. The amount of δ variance attributable to temperature, 34%, is in agreement with results from atmospheric general circulation model studies of near-coastal Antarctic sites *(15)*. The composite does not show a strong seasonal bias: correlations with seasonal A8 indices confirm that the annual correlation is the greatest *(supporting text)*.

To calibrate the reconstruction, the ice core composite is standardized to have the standard deviation and mean of the target A8 index over the 1961-1999 overlap interval when the station data are most complete (Fig. 4.3a). 95% confidence intervals are estimated as twice the standard deviation of the residuals added to the estimated uncertainty associated with the scaling

factor *(12)*. This "composite plus scale" method *(20)* is relatively robust to the problem of underestimated variance, which can be especially pronounced at decadal scale and lower frequencies in linear regression-based reconstructions *(21)*. We test for linearity in the calibration at lower frequencies using 5-year average data, and also consider secular change in the temperature and/or location of the oceanic moisture source of Antarctic precipitation, which can affect the sensitivity of δ records to temperature change on the continent *(e.g. 22; supporting text)*. Although supporting data are limited, nearly identical results are found with the 5-year average calibration, and no evidence of any significant trend in source conditions that would compromise the low-frequency reliability of our reconstruction is found. Low-frequency temperature variations could be also damped by the occurrence of a long term trend in the seasonality of accumulation rate; that is, if warmer temperatures have overall contributed to greater accumulation through the Clausius-Clapeyron relation, this would tend to increase the winter/summer accumulation ratio, and bias the isotope record towards more depleted winter values. This possibility cannot be entirely ruled out, but there is no evidence of any long term increase in accumulation in the cores we use *(23)*.

Our reconstruction (Fig. 4.3a) is in good agreement with the instrumental observations from the continent. In the calibration interval, the reconstruction reflects the increase in A8 to ~1990 and the decrease in temperature thereafter, and shows significant correlation with interannual variations. There is not a significant 200-year linear trend in the reconstruction. The cores used in the reconstruction have slight positive 200-year trends (Fig. 4.6.S3), though the trends are sensitive to starting and ending years. While we have used only five ice cores to derive our reconstruction, we are aware of no other ice core δ records from the continent that suggest significant warming within the past two centuries, so our results can be interpreted as generally representative of the Antarctic continent. The greatest local warming has been inferred from the isotope record at Siple Dome *(24)*, though our analysis indicates that the 1800-1995 trend is not statistically significant.

Our reconstruction shows large interannual to decadal scale variability, and it is important to understand the origin of this variability, and to determine whether signals of climate change are obscured by the high variance. The expression of the SAM in Antarctic temperatures (and in δ) on the interannual scale is known from observations and models—an anti-correlation of anomalies between the Peninsula region and the continent *(3 – 5, 14)*. The station of Orcadas is situated near the Peninsula (Fig. 4.1). The surface temperature record from this site, which is the longest record near Antarctica, extending back to 1904, exhibits a good correspondence with

Peninsula records since 1958 *(1)*. Correlation statistics (Table 4.1) show that the temperature record from Orcadas is negatively correlated with A8. Also, Orcadas temperature and mean sea-level pressure (MSLP) records are positively and negatively correlated with the instrumental SAM index, respectively.

The Orcadas records provide key instrumental bases for inferring the behavior of the SAM over the last century *(2)*. Over this period, our reconstruction of A8 is negatively correlated with Orcadas temperature, and positively correlated with Orcadas MSLP (Table 4.2). This demonstrates that the expression of the SAM in Antarctic temperatures persists on longer timescales than those observed, and gives confidence in the interannual reliability of our reconstruction.

A recent, independent reconstruction of the annual mean SAM index *(25; supporting text)* is another basis for characterizing the SAM signal in our reconstruction. Correlations of the SAM reconstruction with our reconstruction and with the Orcadas data (Table 4.2) are low at annual resolution, but the signs are consistent with observed modern relationships. The low correlation may be related to the fact that the SAM reconstruction is derived mainly from sea level pressure data at mid-latitude stations, which are generally not highly correlated with Antarctic temperature. At decadal time scales, the statistical significance of the correlations improves, and the signs remain consistent with instrumental observations (Table 4.2). There is thus a clear signature of the SAM in our Antarctic temperature reconstruction, on interannual and decadal timescales.

Over the Antarctic instrumental era, hemispheric and global mean temperatures have increased and temperatures over most of the Antarctic continent have changed little *(26)*. The annual mean temperatures observed in Antarctica in the 1990s are some of the lowest indicated by observations, and our reconstruction shows that they are some of the lowest since the beginning of the 20th century. In contrast, in the 1990s, temperatures averaged over the globe reached record highs *(26)*. Nevertheless, the SH mean temperature record *(12)* and the Antarctic temperature show common periods of increase from ~1910 to ~1945, and from the 1960s to ~1990 (Fig. 4.3a and Fig. 4.3b). The intervening period (~1945 to ~1965) is suggestive, as are the 1990s, of the combined effects of background climate change and the SAM. In this period, our reconstruction indicates a pronounced cooling. SAM reconstructions and early observations indicate persistently positive SAM values in the latter part of this period *(6, 25, 27)*, which may explain the Antarctic cooling. The SAM's cooling effect would have been on top of the cooling

effect of large-scale climate forcings, including industrial aerosols, that is reflected in the level trend of the SH mean in this interval *(26)*.

Over long time periods, the little change exhibited by our temperature reconstruction seems enigmatic compared to other climate trends. Close to Antarctica, Orcadas has experienced a warming of 2.0 ± 0.82°C per 100 yr ($p < 0.01$) from 1904-2002. The SH mean increased at a rate of 0.44 ± 0.09 °C per 100 yr ($p < 0.01$) between 1856 and 1999. Our reconstruction shows a trend of only 0.21 ± 0.26 °C per 100 yr over the same interval (Table 3). The large 95% confidence interval overlaps with that of the SH mean, but the trend of the reconstruction is only significant at the $p < 0.15$ level. Therefore, we cannot isolate a long-term change in the temperature of the Antarctic continent that is significant above the variability.

Has the observed positive trend in the SAM affected Antarctic temperatures sufficiently as to reduce the magnitude of long-term change on the Antarctic continent? Reconstructions of the SAM index show little evidence that the circulation pattern has undergone a long-term, century-scale change *(25, 27)*. The Orcadas MSLP record shows no trend over its length, a further indication of no major long-term changes in the SAM. Although the summer SAM index peaked in the 1960s *(27)*, the peak of the annual mean index at this time was much less pronounced *(25)*. The most substantial positive trend in the annual mean SAM index has occurred since the mid-1970s *(3, 6, 25)*. In the period ending in 1975, the trend of our temperature reconstruction is not appreciably different from that of the SH mean (Table 3). In the period since 1976, the Antarctic trend towards cooling contrasts sharply with that of the SH mean. The fraction of the temperature trend that is linearly congruent with the SAM trend can be found by regressing A8 onto the annual mean values of the SAM index and multiplying the coefficient by the trend in the SAM index. The result suggests a rate of decrease of -3.0°C per 100 years, which accounts for most (83%) of the difference in the rates of change between the continent and the SH mean for 1976-1999. Thus, we suggest that the recent change in the SAM may largely explain the differences between the trends of Antarctic temperatures and that of the SH mean temperature over the last century.

To accurately estimate future Antarctic climate change, it is essential to know if climate models can correctly depict past Antarctic climate change. To illustrate one climate model's depiction of climate change over the continent, we use the mean of eight ensemble members of 20th-century integrations of the Community Climate System Model 3 (CCSM3); *(supporting text)*. The trend in the 2-m temperature over the Antarctic continent, excluding Peninsula locations north of 75° S, is significantly positive from 1880-1999 (Table 4.3), in contrast to the results of

our reconstruction. In addition, the CCSM3 Antarctic temperature trends are about 20% greater than the model's SH mean temperature trend. In the CCSM3, and in comparable models, zonally-averaged 20th century warming is at a minimum at ~60°S due to local ocean heat uptake *(28)*. South of this belt, however, over the continent, the warming trend increases with latitude (not shown). The CCSM3 does not suggest nearly as strong of a polar amplification of warming in the Antarctic as in the Arctic, where the sea-ice albedo feedback dominates *(29)*, but nonetheless our reconstruction suggests that the model still overestimates Antarctic warming.

Considering confidence intervals, model trends in the periods before and after 1975 (Table 4.3) are more consistent with observations, and the 2-m temperature reaches a plateau in the 1990s (Fig. 4.3b). However, over the length of the model data, the model's SAM correlations with 2-m temperature on the continent are rather weak, -0.20 ($p < 0.05$) and 0.14 (not sig.), for annual resolution and 10-yr smoothed data, respectively. The magnitudes are smaller than observations and even smaller than those of the reconstructions. Unlike implied by the reconstructions, the correlation becomes positive at the decadal time scale, suggesting a decoupling of model temperatures from the SAM. Notably, the SAM trend in the CCSM3 ensemble mean is large (1958-2000, 4.7 ± 1.9 normalized SAM units ($p < 0.01$)), greater than that observed *(6)*, but there appears to be a limited model 2-m temperature response. Most models agree in the strengthening of the SAM *(30)*, but even those with well-resolved stratospheric dynamics (perhaps a requirement for representing Antarctic climate processes *(3, 7, 8)*), like the Goddard Institute for Space Studies model, tend to show enhanced surface warming over Antarctica relative to the hemispheric mean *(31)*.

Our ice core based reconstruction indicates that Antarctic temperatures over the past 100 to 200 years have been strongly influenced by circulation features, especially the SAM. The Antarctic temperature history resembles that of the SH as a whole, showing common periods of warming. The central estimate of the linear positive trend of the reconstruction less than that of the SH mean over the ~150 year overlap period, though it is only since the mid-1970s when the rates of change substantially diverge. Antarctic climate change is thus strongly coupled to circulation changes. Climate models generally overestimate warming on the continent, and it will be a challenge to bring models into closer agreement with the ice core record.

4.3 Supporting text of Chapter 4 (Data and Methods)

I. DATA

A. Meteorological station data

Surface temperature data from Antarctic stations shown in Fig. 4.1, and the MSLP data from Orcadas, were obtained from http://www.antarctica.ac.uk/met/READER/ and are discussed in *(S1)*. We chose records that are negatively correlated with the SAM (by convention of the definition of the SAM, see section D below), eliminating stations from the Antarctic Peninsula. We also chose records with the most complete and continuous monthly observations (comprising 100% of daily observations in most cases, except notably after 2000, see the data source for metadata and missing data reports) so that a homogeneous calibration time series could be derived. Missing data, absent from our temperature index, are: 1958-1959, Casey and Novolazarevskaya; 1960, Novolazarevskaya; 2002, Novolazarevskaya; 2003, Novolazarevskaya and Scott Base. Scott Base also has two missing values in 1994 that are filled in with climatological values, but this station still is used in the 1994 annual mean. A separate monthly climatology (1961-1990) was computed for each station and removed to form monthly anomaly time series. The anomaly time series were then averaged to form a composite Antarctic anomaly time series that we name A8. Annual values are finally computed by averaging over the calendar months of the monthly A8 index.

EOF analysis *(e.g. S2)* was performed on the monthly data from 1961-2001 to confirm that the stations selected have meaningful covariance. The first EOF explains 39% of the total monthly spatial-temporal variance. All stations have positive weights in the first EOF, and the first PC is correlated at better than $r = 0.99$ with the A8 index. Variance explained in each station record by A8 and the first PC is indicated in Fig. 4.4.S1. Also shown in the figure is the spatial correlation across the continent of A8 with the satellite-derived temperature data field *(S3, S4)*. The signs of the correlation coefficients are positive nearly everywhere over the continent, explaining ~26% of the total variance of the satellite-derived temperatures. Furthermore, the spatial pattern of the A8 regression upon satellite data is very similar to the first EOF of the satellite data, also shown in Fig. 4.4.S1.

Seasonal A8 indices showing unusually cold summer-fall conditions in the 1990s are shown in Fig. 4.5.S2, showing that the annual index indeed captures large-scale variability associated with the SAM.

B. Ice core data in reconstruction

For use in the reconstruction, we chose well-dated, well-sampled ice core time series that can be treated in an analogous way to the station data (i.e. removing climatological means and

compositing). Each core has $\delta^{18}O$ or δ D in units of per mil (‰), reported as $\delta = (R/R_{VSMOW} - 1)$ where R is the ratio of $^{18}O/^{16}O$ or D/H and VSMOW is Vienna Standard Mean Ocean Water (VSMOW). All data are normalized to the VSMOW/SLAP (Standard Light Antarctic Precipitation) standards from the International Atomic Energy Agency. The five isotopic ice core records used in the reconstruction are displayed in Fig. 4.6.S3.

The strategy for dating, averaging, and compositing the δ records over the 1961-1999 overlap interval with the instrumental record is discussed elsewhere *(S5, S6)*. Briefly, each core has at least annual mean resolution (although sampling resolution in most cases is higher). The 1961-1990 mean δ value is subtracted from the entire 200-year record and each record is further divided by its standard deviation of the 1961-1990 baseline period. The five time series are finally stacked into an "ice core composite" referred to as *ice* below, which is used in our reconstruction of A8, as discussed in the text and below.

C. Ice cores not used in reconstruction

We considered other Antarctic ice core δ time series reported as annually-resolved for our reconstruction. Qualitatively, these records agree with our finding of an insignificant 200-year change in δ. However, these records are not used in our reconstruction for one or more of the following reasons: (a), The data are not available to us; (b) The time series are stated as annual, but due to low snow accumulation rates at the site, dating accuracy and precision are not sufficiently high for interpretation of δ as interannual temperature variations. Diffusion of δ in these low accumulation records dampens interannual variations; (c) The time series does not correlate well with seasonal and/or interannual variations in site temperature and/or with A8; (d) Sampling and analysis is not yet complete.

These cores (locations shown in Fig. 4.1.) with references and reasons (a-d) for rejection indicated in parentheses are:

Hercules Dome (S7, d)
Talos Dome (S8, b, c)
Dronning Maud Land stack (S9, b, c)
Plateau Remote (S10, a, likely b and c as well)
Berkner Island (S11, b, c)
Dyer Plateau (S12, a, also location on Peninsula outside our main area of focus)
Siple Dome (S13, c).

D. The instrumental SAM index

We gratefully acknowledge G. Marshall for providing data for the SAM index for 1958-2000. As discussed in *(S14)*, he computes two monthly resolution zonal mean sea level pressure indices from six stations at roughly 40° S and six stations at roughly 65° S. From these zonal mean indices, we subtract the 1961-1990 mean. Then the indices are divided by their 1961-1990 standard deviations. To obtain the SAM index, the normalized zonal mean at 65° S is subtracted from the normalized zonal mean at 40° S, i.e. SAM = $P^*_{40°S} - P^*_{65°S}$ where P* indicates the normalized pressure indices. As needed, an annual SAM index is used by averaging the monthly values over the calendar months.

E. Climate Model (CCSM3) Antarctic Data

The CCSM3 is a global coupled atmosphere, ocean, sea ice, and land model. The ensemble of runs used in this paper has an atmosphere component with spectral triangular truncation at wavenumber 85 (T85), which is equivalent to 1.4° in the horizontal (for land as well). The atmosphere has 26 vertical levels. The ocean and sea ice have zonal resolution of 1.125 deg and the meridional resolution of 0.54°, except in the subtropics and tropics where the resolution is finer. The model is well documented and may be downloaded freely from http://www.ccsm.ucar.edu .

The eight ensemble members were initialized at different times from a 500-yr long, pre-industrial control run. The 20th century forcing included time-varying greenhouse gases (CO_2, CH_4, N_2, Halocarbons), the direct effect of sulfate emissions, solar and volcanic variability, and aerosols. Temporally and spatially varying tropospheric ozone was prescribed as computed from an off-line atmospheric chemistry model up to the model tropopause, as defined by temperature gradient. Time varying, zonal-mean stratospheric ozone was prescribed from a NOAA dataset *(S15)* in the top two model levels. Ozone was interpolated between these two limits in the third level from the top to the model tropopause. Model runs in years 2000-2005 were forced with the SRES A1B scenario. The forcing and model results are described in more detail *(S16)*.

F. Southern Hemisphere mean temperature

Southern Hemisphere mean annual temperature anomalies (base period 1961-1990) from land and ocean instrumental records (shown in Fig. 4.3 and used in calculations in Table 4.3) were obtained from http://www.cru.uea.ac.uk/cru/data/temperature/. The time series is updated

by P.D. Jones and colleagues at the Climatic Research Unit, University of East Anglia, United Kingdom and discussed in *(S17)* as well as by the IPCC reports *(S18)*.

G. The reconstructed SAM index

In this paper, we use an 1866-2001 annual mean SAM reconstruction in comparison with our Antarctic temperature reconstruction and a 1905-2001 SAM reconstruction in comparison with the Orcadas data (Table 4.2). The SAM reconstructions were carried out using multiple linear regression to estimate the annual SAM index from the leading principal components (PCs) of normalized station SLP (so-called principal component regression (PCR)). The station data were kindly provided by Phil Jones *(S19)*, and Rob Allan and Tara Ansell.

For model fitting we define the SAM index as the first PC of detrended ERA40 annual mean SLP for the domain 20^{o}S-75^{o}S, and the SAM as the first empirical orthogonal function (EOF) of these data. The predictor PCs for model fitting are derived from detrended annual means of the station SLP records. To select those stations containing a SAM signal, we correlated the detrended station SLP with the detrended SAM index for the period 1958-2000 (the period of overlap between the ERA40 and station data), and retained those that were significantly correlated at the 5% level. The stations selected are shown in Table 4.4.S1 below. To obtain the reconstruction, the undetrended station records were normalized by dividing by the standard deviation from the fitting period, and the PCs were calculated by projecting the normalized values on the EOFs defined in the fitting period. Multiplication of these PCs with the PCR weights derived from the fitting data yields the reconstruction. Further information on the reconstruction method can be found in the supplementary online material of *(27)*.

Three reconstructions were undertaken: back to 1866 (10 stations), back to 1905 (16 stations), and back to 1951 (27 stations). For the 1855/1905/1951 reconstructions, the cross-validation gives a correlation of 0.72/0.85/0.81 respectively between the reconstructed AAOI and the detrended ERA40 AAOI, and a reduction of error of 0.48/0.62/0.68 respectively. The 1951 reconstruction includes stations from the Antarctic and Southern Indian Ocean centres of action, and was undertaken to test how well the 1905 and 1866 reconstructions using fewer stations perform. The 1905 reconstruction performs well, as it is highly correlated with 1951 reconstruction, with 0.92 for interannual values and 0.96 for 9-year running means of the data. The lower correlations between the 1866 and 1951 reconstructions (0.84 interannual, 0.60 9-year running mean), indicate that less confidence can be had in the 1866 reconstruction.

II. METHODS

A. Antarctic temperature reconstruction scaling, estimates of uncertainty, and low-frequency reliability

Our reconstruction is best considered an estimate of the annual mean temperature. While some δ records may have a seasonal bias, precipitation in West Antarctica tends to be seasonally quite uniform *(S6)*, while very high resolution Law Dome core has been demonstrated to have little bias *(S20)*. Additionally, the correlation of the ice core composite (*ice*) with station temperatures is greatest with the annual mean as shown in Table 4.5.S2.

The reconstruction of annual mean values of A8 presented, $\mathbf{R_1}$, is obtained as

$$R_1(t) = \left((\sigma_{A8}/\sigma_{ice}) * ice(t)\right) + \left(\overline{A8} - \overline{ice} * (\sigma_{A8}/\sigma_{ice})\right) \qquad \textbf{(4.1)}$$

where *ice* is the ice core composite, and σ is the standard deviation, for *ice* and A8, from 1961-1999. The first term on the right scales the standard deviation and the second term scales the mean. Although a least-squares regression could alternatively be used in reconstruction, we find that this method substantially underestimates the variance of Antarctic temperatures (on all timescales). Among Antarctic stations comprising A8, the variance of the annual mean temperature ranges from 0.35 to 1.2°C *(S21)*, while the variance of the A8 index is 0.28°C for 1961-1999. Gridded satellite data have a higher variance of 0.78°C averaged over the continent. For the full (1800-1999) reconstruction, $\mathbf{R_1}$ has a variance of 0.23°C. Importantly, as noted in the text, *ice* has a significant correlation with A8 of $r = 0.58$. The correlation results do not change substantially for different calibration intervals (i.e. if the length of the calibration data are cut in half; Table 4.6.S3). The scaling of the reconstruction does not impact *r*, so are we not "explaining" any more or less variance in A8 by using the scaling instead of a regression method, and as such a different scaling would not impact the other correlations that we report (i.e. Table 4.1). The 2σ (i.e. 95%) confidence intervals of $\mathbf{R_1}$ are defined as twice the root-mean-square error of the regression (A8 vs. *ice*) times the standard deviation of the predictand (i.e. A8), or equivalently, twice the standard deviation of the residuals, A8 – $\mathbf{R_1}$ *(e.g. S22)*, which yields $2\sigma_{R1} = \pm 0.94$ °C. In addition to this uncertainty, we also take into account the uncertainty of the standard deviation ratio, σ_{A8}/σ_{ice}, that we used to scale the reconstruction to A8, although there are

few data available to estimate this. We split our data roughly in half and find the range of ratios shown in Table 4.6.S3.

The range in $\boldsymbol{\sigma_{A8}/\sigma_{ice}}$ is 0.79 to 0.95. The standard deviation of the difference of a reconstruction using 0.79 and one using 0.95 is 0.09°C, which we add to the $2\sigma_{R1} = \pm 0.94$°C, for a total estimated uncertainty of ± 1.03°C.

An unavoidable question in all paleoclimate studies is whether proxies have a time-scale dependent sensitivity to the climate data of interest. For instance, if isotope ratios were less sensitive to temperature at decadal scale than at interannual timescales, this would tend to bias the record towards lower decadal variability. We have a very short target time series for addressing this problem; however we can partly address this by using 5-year averages of A8 and *ice* over the 1960-1999 period and replacing these values in the reconstruction equation 4.1 above. The resulting reconstruction is compared to 5-year average values of the annual mean reconstruction and results are found to be nearly identical (Fig. 4.7.S4). Thus, at least over these time scales, the scaling factor is linear.

We can address concerns about possible low frequency bias indirectly by considering likely causes of such bias: changes in the seasonality of precipitation and changing moisture source conditions. We noted in the main text that there is no evidence of accumulation change that would be expected if there are significant changes in accumulation seasonality. If changes in moisture source have occurred, these will be reflected in deuterium excess ($d = \delta D - 8*\delta^{18}O$), which is sensitive to evaporation temperature *(S23)*. While d measurements are available for only one of the cores used in the reconstruction, US-ITASE 2000-1, in this core there is small but statistically insignificant significant trend (0.45 ‰ per 100 years). Using the methods of Kavenaugh and Cuffey (S23) to correct the δD values for d, we find that the magnitude of the slight trend in δD in this core is actually *reduced*. This further supports one of the chief conclusions of our paper, that century scale trends in Antarctic temperatures have been small over the last two centuries.

C. Trend estimation

Throughout the text, we report all trends (slope of least squares linear regression of time series versus time) with their 95% confidence intervals and an estimate of the significance level (e.g. 90% (or $p < 0.1$), 95% (or $p < 0.05$), or 99% (or $p < 0.01$)) at which the trend is different from zero, stating it is insignificant if $p > 0.1$. The method we use for assessing the significance level is the "adjusted standard error + adjusted degrees of freedom (see *(S24)*, equations 1-6)."

The effective number of samples is estimated from the lag-1 autocorrelation of the regression residuals. It is used to both find the critical *t*-value for the stipulated confidence interval and in determining the standard error of the trend. The 95% confidence interval is estimated as the critical *t*-value times the standard error (see (S2), equation 8.3.7).

D. Correlation coefficients

Throughout the text, we also give correlation coefficients ("r") and the level at which they are different from zero as determined by a two-tailed *Student's t* test (e.g. (S2), equation 8.7). As in the estimate of the significance level of the trend, we also adjust the number of independent samples to account for autocorrelation. However, we do not adjust the critical *t* value.

Table 4.1. Correlation statistics (14) of annual resolution, instrumentally-derived definitions of Antarctic temperature anomalies (A8) and the SAM index for 1958-2000. Also included are surface temperature (T) and mean sea level pressure (MSLP) data from the Orcadas station. The Orcadas MSLP data are available only to 1991. ***Bold italics***, $p < 0.01$; **Bold**, $p < 0.05$; *Italics*, $p < 0.10$. Linear trends have been removed from the time series.

	A8	**SAM**
A8		***-0.51***
SAM	***-0.51***	
Orcadas T	***-0.43***	***0.33***
Orcadas MSLP	0.04	**-0.38**

Table 4.2. Correlation statistics (14) of annual and 10-year smoothed, reconstructed estimates of Antarctic temperature anomalies from ice cores and the reconstructed SAM index from mid-latitude stations for 1866-1999. Also included are temperature (T) and mean sea level pressure (MSLP) data from the Orcadas station. The Orcadas MSLP data span 1905-1991 and the temperature data span 1905-1999. For 10-year correlations, the beginning and ending five years of the time series are not included to avoid end effects of the filter. ***Bold italics***, $p < 0.01$; **Bold**, $p < 0.05$; *Italics*, $p < 0.10$. Linear trends have been removed from the time series.

	Antarctic recon.		**SAM recon.**	
	1-yr.	10-yr.	1-yr.	10-yr.
Antarctic recon.			-0.15	***-0.28***
SAM recon.	*-0.15*	***-0.28***		
Orcadas T	***-0.39***	**-0.25**	0.16	**0.25**
Orcadas MSLP	**0.27**	**0.30**	0.03	***-0.42***

Table 4.3. Trends (°C per 100 years; (14)) in SH mean instrumental record, Antarctic reconstruction, ensemble mean CCSM3 2-m Antarctic temperature and ensemble mean CCSM3 SH mean. Annual resolution data are used in all cases. ***Bold italics***, $p < 0.01$; **Bold**, $p < 0.05$; *Italics*, $p < 0.10$. The 95% confidence interval (±) of the CCSM3 trends are given as twice the standard deviation of the trends of the individual ensemble members, rather than the convention used for the other time series (14).

Time period	SH mean	Antarctic recon.	CCSM3 Antarctic	CCSM3 SH mean
1856-1999	***0.44 ± .09***	0.21 ± .26	****0.75 ± .14***	****0.56 ± .07***
1856-1975	***0.32 ± .10***	0.21 ± .35	****0.60 ± .25***	****0.47 ± .12***
1976-1999	***1.40 ± .59***	**-2.2 ± 3.8	1.70 ± 3.5	1.20 ± .86

*Data begin in 1880; **A8 instrumental record used

Table 4.4.S1. The stations used to produce the SAM reconstructions, and their latitudes and longitudes.

Stations used in the 1866 reconstruction	**Latitude (°S) and longitude (°E)**
Ascuncion (Paraguay)	25.27, 57.63
Auckland (New Zealand)	36.90, 174.80
Buenos Aires (Argentina)	34.58, -58.48
Christchurch (New Zealand)	43.50, 172.60
Cordoba (Argentina)	31.40, -64.19
Dunedin (New Zealand)	45.90, 170.50
Goya (Argentina)	29.10, -59.30
Hokitika (New Zealand)	42.70, 171.00
Tahiti (Soc. Islands)	17.54, 149.62
Wellington (New Zealand)	41.30, 174.80
Additional stations for the 1905 Reconstruction	
Apia (Samoa)	13.80, -171.80
Catamarca (Argentina)	28.60, -64.45
Chatham (New Zealand)	44.00, -176.60
Rarotonga (Cook)	21.12, -159.82
Salta (Argentina)	24.90, -65.50
Sarmiento (Argentina)	45.60, -69.10
Additional Stations for the 1951 Reconstruction	
Aitutaki (Cook)	18.80, -159.80
Alofi (Niue)	19.10, -169.90
Bellingshausen (Antarctica)	62.20, -58.90
Cambell Island (-)	52.60, 169.20
Esperenza/Hope Bay (Antarctica)	63.40, -57.00
Faraday (Antarctica)	65.30, -64.30
Ile Nouvelle Amsterdam (-)	37.80, 77.50
Macquarie (Australia)	54.50, 159.00
Nandi (Fiji)	17.80, 177.50
Penhryn (Cook)	9.00, -158.10
Trelew (Argentina)	43.20, 65.30

Table 4.5.S2. Seasonal correlations of the ice core composite with A8.

Season	***r* (A8, *ice*)**
SON	0.35
MAM	0.28
JJA	0.44
DJF	0.23
Annual	0.58

Table 4.6.S3. Variation of calibration factors over different time periods.

Period	σ_{A8}/σ_{ice}	***r* (A8, *ice*)**
1961-1999	0.85	0.58
1961-1980	0.79	0.69
1981-1999	0.95	0.52

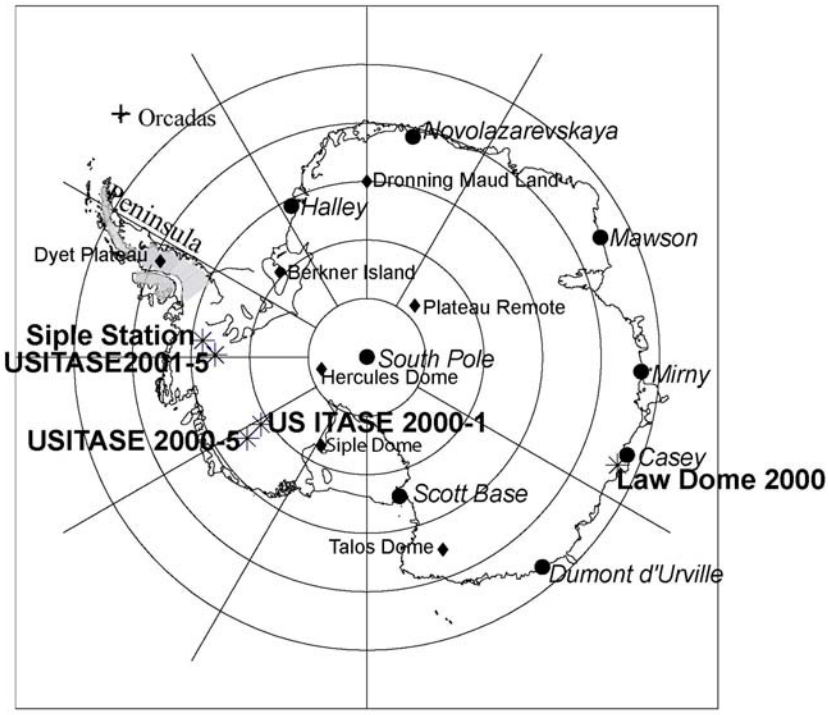

Figure 4.1. Map of Antarctica, indicating selected stations and ice core sites. Filled circles and italic font, stations with monthly temperature data spanning 1958-2003 used to form the A8 index in Fig. 4.2; Asterisks and bold font, ice core sites with δ records used in the reconstruction; Diamonds and small font, other ice core sites with consistent long-term histories (except for the Peninsula location noted in the text) not directly used in the reconstruction; Plus symbol, Orcadas station. (data sources in supporting text).

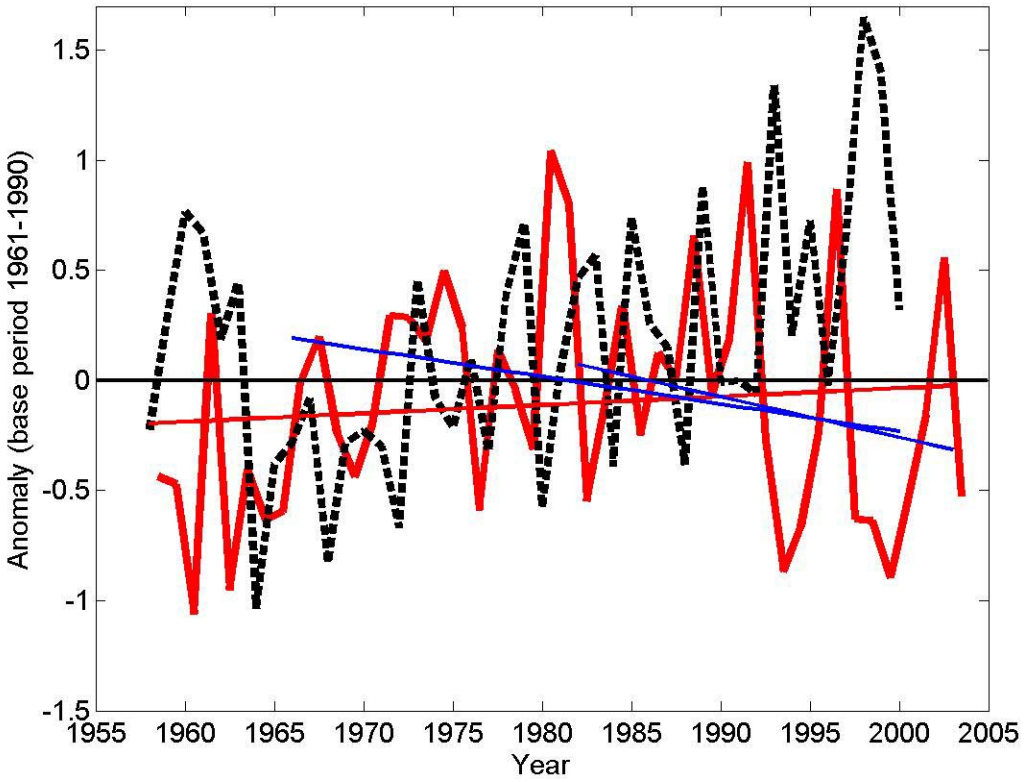

Figure 4.2. Annual values of composite Antarctic surface temperature anomalies (A8, 1958-2003) and the SAM index, 1958-2000 (14). Thick red line and filled red circles, A8 (°C); Thin red line, linear trend of A8 1958-2003; Long and short blue lines, 1966-2000 (see (8)) and 1982-2003 (the era of satellite observations) linear trends of A8, respectively; Black dashed line, SAM index (normalized pressure data).

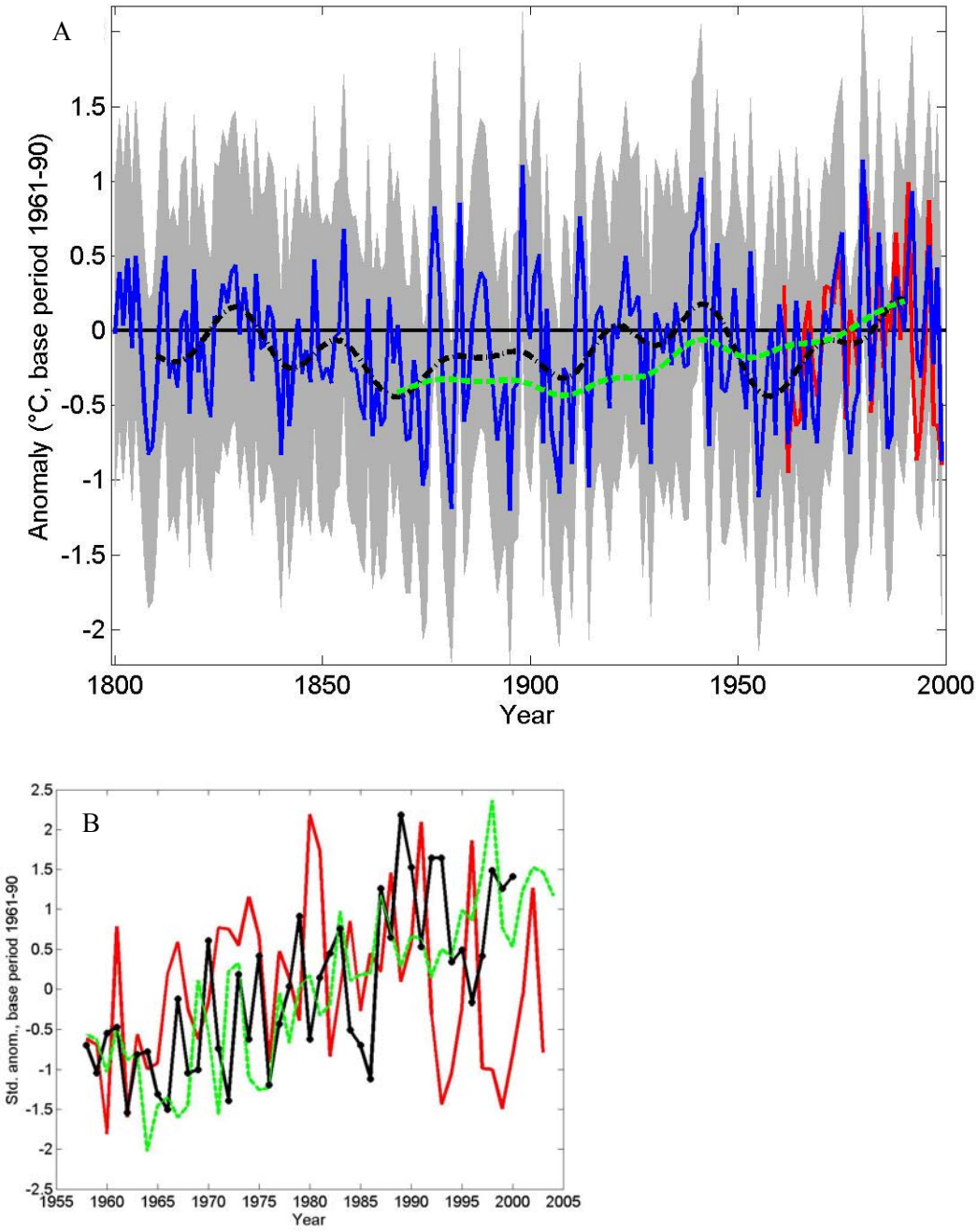

Figure 4.3. Estimates of Antarctic temperature anomalies (excluding the Peninsula), 1800-1999, with a base period of 1961-1990. (a) Blue line, annual resolution ice-core based reconstruction; Red line, instrumental target index, A8; Gray shading, annual resolution 2σ uncertainty estimates; Black dashed line, 20-year low-pass smoothed Antarctic reconstruction, Green dashed line, smoothed instrumental record of SH mean temperature. (b) Red line, normalized values of the annual mean A8 index; Green dashed line, observed SH mean temperature normalized values; Black line with filled circles, CCSM3 ensemble mean 2-m Antarctic temperature anomalies, normalized values.

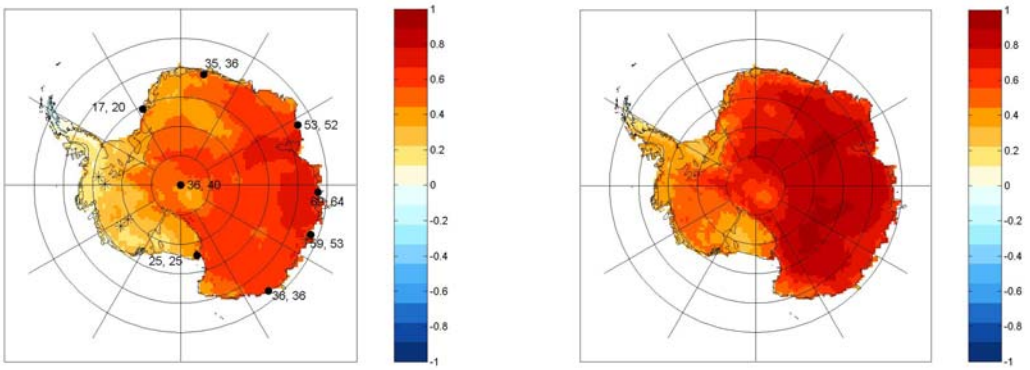

Figure 4.4.S1. Illustration of the spatial representativeness of the A8 target index of the reconstruction. **On left**: Colorscale corresponds to correlation coefficients (r) of the monthly resolution A8 index vs. satellite-derived temperature data *(S3, S4)* for 1982-1999. Correlations across most of the continent are positive. Stations with records used in the A8 index are shown as the dots. The two numbers at each station are the percentage of variance explained in the station's own surface temperature record by the first principal component of all the station records and the amount of variance explained by the mean of all the station records, respectively. **On right**: Colorscale corresponds to correlation coefficients of the monthly resolution first principal component of 1982-1999 satellite data vs. the satellite data field itself, a similar pattern to the first EOF (see Fig. 1a of *4*).

The pattern on the left and the pattern on the right have a spatial correlation of r = 0.90. This demonstrates that the mean or the first principal component of the station observations can estimate well the first-order pattern of temperature variability on the continent.

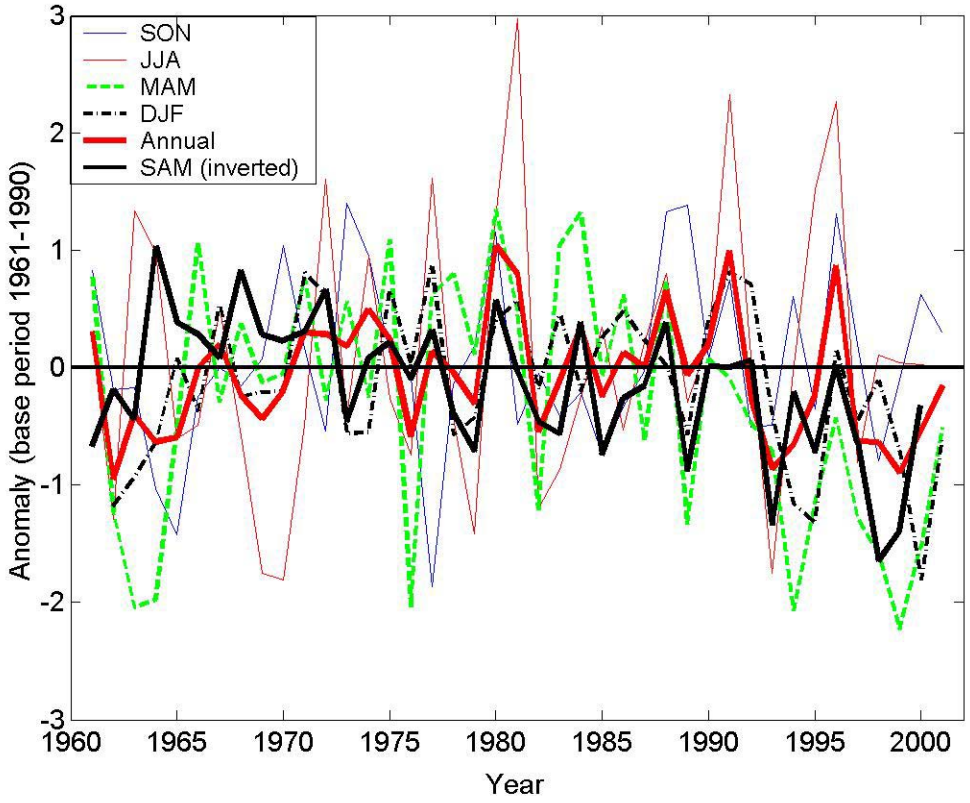

Figure 4.5.S2. Seasonal indices of Antarctic temperatures (from monthly A8 index) compared with the annual A8 index and the SAM. In the legend, SON (spring) is September October November (blue line); JJA (winter) is June July August (thin red line); MAM (fall) is March April May (green dotted line); DJF (summer) is December January February (black dotted line); Annual is A8 (red line); SAM is Southern Annular Mode (black line).

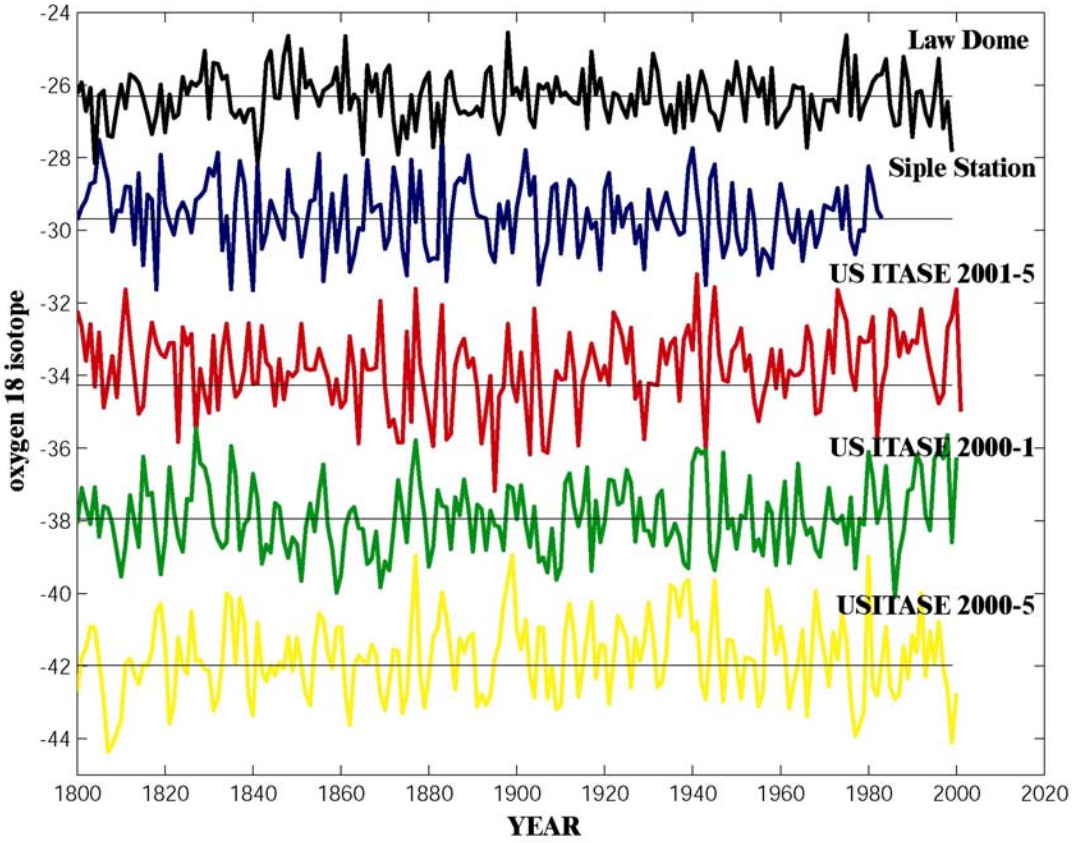

Figure 4.6.S3. The annual mean ice core δ time series used in the reconstruction. Mean values, indicated by the gray lines, have been adjusted for clarity of presentation. US-ITASE 2000-5 record is shown as δD/8, an approximation of the equivalent $\delta^{18}O$ value.

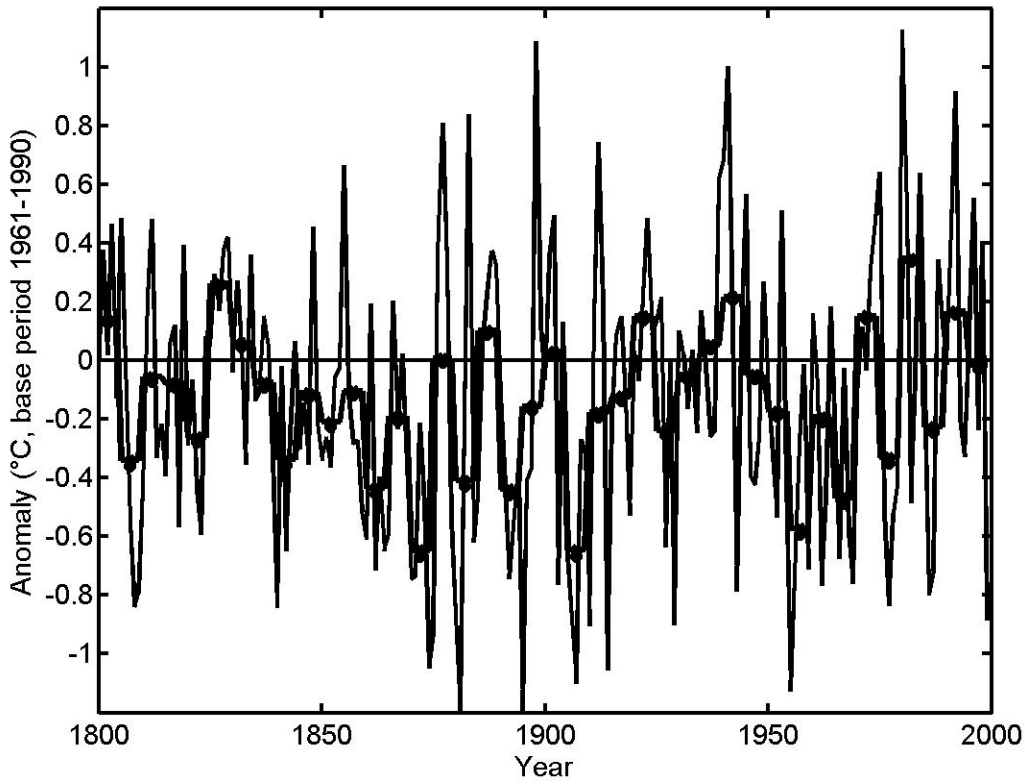

Figure 4.7.S4. The original annual mean reconstruction is shown as the thinner line and its 5-year average values are shown as the heavier line. Reconstruction at 5-yr resolution based on a low-frequency (5-year average) calibration with A8 is shown as the circles.

Notes to Chapter 4

main section

1. D. G. Vaughan *et al*., *Climatic Change* **60**, 243 (2003).

2. J. Turner *et al*., *Int. J. Climatol*. **25**, 279 (2005).

3. D. W. J. Thompson, S. Solomon, S*cience* **296**, 895 (2002).

4. R. Kwok, J. C. Comiso, *Geophys. Res. Lett.* **29**, (2002).

5. D. P. Schneider, E. J. Steig, J. C. Comiso., *J. Climate* **17**, 1569 (2004).

6. G. J. Marshall, *J. Clim.* **16**, 4134 (2003).

7. G. J. Marshall *et al*., *Geophys. Res. Lett*. **31** (2004).

8. D. T. Shindell, G. A. Schmidt, *Geophys. Res. Lett*., **31** (2004).

9. J. C. Comiso, *J. Clim.* **13**, 1674 (2000).

10. P. T. Doran, *et al*., *Nature* **415**, 517 (2002).

11. J. Turner *et al*., *Nature* **418**, 291 (2002).

12. Data sources and methods, including the testing of linear trends and of correlation coefficients for statistical significance are discussed in the supporting text section.

13. N. A. N. Bertler *et al*., *Geophys Res, Lett.* **31** (2004).

14. D. Noone, I. Simmonds, *J. Geophys. Res*. **107**, 4742 (2002).

15. M. Werner, M. Heinmann., *J. Geophys. Res*., **107,** D1 (2002).

16. D. P. Schneider, E. J. Steig, T. van Ommen, *Ann. Glaciol.* **41,** in press.

17. E. J. Steig *et al*., A*nn. Glaciol*. **41,** in press.

18. T. D. van Ommen, V. Morgan, M. A. J. Curran, *Ann. Glaciol*., **39**, 359 (2005).

19. E. Mosley-Thompson, L. G. Thompson, P. M. Grootes, N. Gundestrup, *Ann. Glaciol*. **14**, 199 (1990).

20. P. D. Jones, M. E. Mann, *Rev. Geophys.*, **42,** RG2002 (2004).

21. H. von Storch *et al*., *Science* **306**, 679 (2004).

22. J.L. Kavanaugh, K.M. Cuffey, *Global Biogeochem. Cycles*, **17**, 1 (2003).

23. S. Kaspari *et al*., A*nn. Glaciol*. **39,** 585 (2005).

24. P. A. Mayewski *et al*., A*nn. Glaciol*. **39,** 127 (2005).

25. J.M. Jones *et al*, in preparation, – Seasonal reconstructions of the Antarctic Oscillation

26. J. T. Houghton *et al*., eds., *Climate Change 2001: The Scientific Basis* (Cambridge Univ. Press, Cambridge, 2001).

27. J. M. Jones, M. Widmann, *Nature* **432**, 290 (2004).

28. J. M. Gregory, *Clim. Dynamics*, **16**, 501 (2000).

29. M. M. Holland, C. M. Bitz, *Clim. Dynamics*, **21**, 221 (2003).

30. M. Rauthe, A. Hense, H. Paeth, *Intl. J. Climatol*., **24**, 643 (2004).

31. J. Hansen *et al*., Climate simulations for 1880-2100 with GISS model E, submitted.

supporting text section

S1. J. Turner *et al*., *J. Clim*. **17**, 2890 (2004).

S2. H. von Storch, F.W. Zwiers, *Statistical Analysis in Climate Research* (Cambridge Univ. Press, Cambridge, 2001).

S3. J. C. Comiso, *J. Clim.* **13**, 1674 (2000).

S4. D. P. Schneider, E. J. Steig, J. C. Comiso., *J. Climate* **17**, 1569 (2004).

S5. D. P. Schneider, E. J. Steig, T. van Ommen, *Ann. Glaciol.* **41,** in press.

S6. E. J. Steig *et al*., A*nn. Glaciol*. **41,** in press.

S7. R. W. Jacobel, B.C. Welch, E.J. Steig, D.P. Schneider, *J. Geophys. Res*. **110** (2005).

S8. B. Stenni *et al*., *J. Geophys. Res*. **107** (2002).

S9. W. Graf *et al*., *Ann. Glaciol*. **35**, 195 (2002).

S10. E. M. Thompson, L.G. Thompson, in *Antarctic Peninsula Climate Variability: A Historical and Paleoenvironmental Perspective,* E. Domack *et al*., eds., Antarctic Research Series **79** (American Geophys. Union, Washington, D.C., 2003), pp. 115-127.

S11. R. Mulvaney *et al*., *Ann. Glaciol*. **35**, 45 (2002).

S12. L. G. Thompson *et al*., *Ann. Glaciol*. **20**, 420 (1994).

S13. P. A. Mayewski *et al*., A*nn. Glaciol*. **39,** 127 (2005).

S14. G. J. Marshall, *J. Clim.* **16**, 4134 (2003).

S15. J. T. Kiehl et al., *J. Geophys. Res*. **104**(D24), 31239 (1999).

S16. G. A. Meehl *et al*., *J. Climate*, in press.

S17. 5. J. T. Houghton *et al*., eds., *Climate Change 2001: The Scientific Basis* (Cambridge Univ. Press, Cambridge, 2001).

S18. P.D. Jones *et al*., *J. Geophys. Res*. **106,** 3371 (2001).

S19. P. D. Jones, *Int. J. Climatol*. **11**, 585 (1991)

S20. T. D. van Ommen, V. Morgan, *J. Geophys. Res* **102**(D8), 9351 (1997)

S21. D. G. Vaughan *et al*., *Climatic Change* **60**, 243 (2003).

S22. J. M. Jones, M. Widmann, *J. Clim*. **16**, 3511 (2003).

S23. J. L. Kavanaugh, K.M. Cuffey, *Global Biogeochem. Cycles*, **17**, 1 (2003).

S24. B. D. Santer *et al*., *J. Geophys. Res*. **105**, 7737 (2000).

CHAPTER 5

Spatial covariance of isotopic signals in West Antarctica

5.1 Summary

The stable isotopic concentration of polar snow and ice is commonly interpreted in terms of temperature at the deposition site. Modeling results, however, tend to underscore the importance of moisture source conditions and location, changes in the characteristics of transport processes, and mixing of ambient air, in determining the interannual variance of stable isotope ratios. It follows, then, that modes of atmospheric variability that systematically alter these physical conditions will modulate the isotopic concentration of polar precipitation. Here, new high-resolution data from twelve West Antarctic ice coring sites are used in a compositing analysis to asses whether modes of variability relevant to Antarctic climate (e.g. Southern Annular Mode (SAM), Pacific-South American pattern, etc.) have an expression in the local isotopic composition of the firn. Several locations, mainly within a few hundred km of the West Antarctic Ice Sheet divide (~80°S, 111°W) show a signature of the SAM that is identifiable in nominally monthly resolution data and also preserved in annual mean data. Signs of isotopic anomalies associated with the SAM are consistent with the expectation of positive correlation with the sign of local temperature anomalies. However, the variance and short length of the data is such that only a few statistically significant associations are found, and it is difficult to quantify an exact magnitude of anomaly associated with the SAM itself or its local temperature signature. Other locations, and in particular the higher accumulation (> 30 cm H_2O yr^{-1}) sites to the east (~90°W) do not show a clear SAM signature, but show a weak correspondence with higher-order modes. The location of the strongest SAM anomalies is contrary to the expectation that the largest isotopic anomalies should be found where the largest local temperature anomalies are found and best preserved where the accumulation rate is high. It is argued nonetheless that interpretation in terms of temperature on some regional scale (here, the continent of Antarctica), rather than directly in terms of the SAM, is justified, especially when isotopic records are stacked. These assertions are supported by statistical considerations, but remain to be tested in physical models.

5.2 Introduction

The climate system has a number of internal modes, such as the El Nino-Southern Oscillation (ENSO) and the Northern and Southern annular modes (NAM and SAM,

respectively), which can be empirically described, and have clear physical manifestations. These modes are associated with widespread anomalies in atmospheric parameters, including temperature and precipitation amount. Isotopic tracer modeling studies (e.g. Cole et al., 1999; Noone and Simmonds, 2002a; Werner and Heimann, 2002) demonstrate that these parameters are important in governing isotopic variability, so it seems likely that modes of internal variability may cause systematic shifts in the isotopic composition of precipitation through the modulation of temperature, precipitation, source region conditions and transport pathways. Isotopic ratios are thought traditionally to reflect mainly local temperature, though much more emphasis is now being placed on their role as integrated samples of climate conditions (e.g. White et al., 1997; Cole et al., 1999; Noone, 2001; Noone and Simmonds, 2002a).

In Chapter 1, modes of variability relevant to Antarctica were objectively defined as the leading empirical orthogonal functions (EOFs) of 500-hPa geopotential height anomalies from 20°S-90°S, and were used to explain anomalies in surface temperature across the continent. Until recently, Antarctic ice core records have been too limited to make systematic studies of δ anomalies, and their relationship to temperature and circulation anomalies, feasible. If systematic relationships between modes of the atmospheric circulation and δ anomalies could be identified, it would expand the classical interpretation of ice core δ records in terms of local temperature, as we may consider whether changes in atmospheric circulation may be deduced from δ measurements. Recent general circulation modeling studies using isotopic tracers, focused on the current climate of Antarctica (Noone and Simmonds, 2002b; Werner and Heimann, 2002), provide some theoretical and physical underpinning for the idea that atmospheric circulation reconstruction may be possible from $\delta^{18}O$ and δD records. Here, I use available isotope data from 12 United States International Trans-Antarctic Scientific Expedition (US-ITASE) cores in West Antarctica to develop an empirical basis for linking isotope ratios to the atmospheric circulation.

In previous chapters, stacks of ice cores formed the basis of reconstructing the observed mean Antarctic temperature, which is shown, both by observations and by the reconstruction, to be strongly linked to the SAM. This relationship is further illustrated through regression patterns in 500-hPa geopotential height of the SAM index, the A8 Antarctic temperature index, and the ice core reconstructed A8 index (Figure 5.1). All three regressions show a predominantly annular pattern, with positive anomalies over the Antarctic continent. Anomalies of opposite sign are centered near 50°S. Notably, the ice core reconstruction pattern more closely resembles the A8 temperature pattern than the SAM pattern itself. The A8 and ice core patterns have eastward shifted centers of action in the mid-latitudes compared with the SAM. They also have a relatively

strong positive anomaly in the southwestern Pacific, unlike the SAM pattern. Whatever the cause of the differences, the comparison suggests that the temperature interpretation of stable isotopes may be more fundamental than circulation interpretations, though it still implies that isotope records hold valuable information about the circulation.

The stacked records used in previous chapters do not provide information on the spatial details of Antarctic climate variability. If indeed atmospheric circulation can be reconstructed from ice core records, it would be useful to know *a priori* where to locate an ice core site for the best chance of obtaining a useful record for reconstruction. It has been suggested that temperature anomalies can be a guide to selecting ice core sites (e.g. Jacobel et al, 2005; King and Comiso, 2003), though it has not been made clear that isotope anomalies at the site will bear the same relationship to the atmospheric circulation as do temperature anomalies. In this chapter, I investigate whether such relationships hold by using temperature anomalies from the T_{IR} data set and δ anomalies from the US-ITASE cores to find associations with indices of atmospheric circulation and temperature.

5.3. Data and Methods

Stable isotope measurements (δD and/or $\delta^{18}O$) from twelve US-ITASE ice cores and snow pits have been made at the University of Washington. Records are chosen that span most or all of the era of instrumental climate observations, from 1961 to the present. The cores that also have major ion chemistry measurements, which provide a very reliable dating tool (e.g. Dixon et al., 2005), are considered to be more reliably dated than the cores which have only δ measurements. Where chemistry-based depth-age scales are available, the corresponding δ records are adjusted only so that the isotopic summer maxima are assigned to January 1st, as discussed in previous chapters. Where existing depth-age scales are not available, annual cycles in δ are counted down from the known age of the surface. While the annual δ cycles are fairly robust in these cores (Fig. 5.2), there is still some ambiguity in the annual cycle counting, especially in the upper ~5 m. The identification of absolute age markers, such as the non-sea salt sulfate signature of the 1991 Pinatubo eruption, would clearly help to constrain the timescale, though the required measurements are not yet available for all of the cores discussed here. I use all 12 records for which δ measurements are available in the analyses presented below, though I place greater weight on the results from the cores considered to be well-dated. Table 5.1 lists the cores used, with notes on the depth-age scale and the length of the record; more details about each

of the core sites are given in Table 2.2. Each of the cores has subannual resolution. Once the depths of summer peaks are established, the subannual depth-age scale is derived by linear interpretation between the summer depths. As shown in Chapter 3, this procedure results in a close match of the δ cycle to the temperature cycle at the site. From this depth age-scale, the time scale and the isotope measurements are interpolated to monthly resolution to facilitate comparison with instrumental data.

Instrumentally based indices describing atmospheric circulation and temperature variability are used as the basis for compositing isotopic anomalies. These indices, and their relevance to Antarctic climate, have been discussed in precious chapters. Table 5.2 lists these indices and identifies the relevant data sources. Several of the indices share variance associated with the SAM. This allows the results of the compositing analysis to be verified, as significant anomalies identified in the δ records related to one of the indices should be consistent with anomalies related to another of the indices, if the isotopic anomalies are systematic, rather than random. That is, the somewhat redundant indices provide a reproducibility test on the δ anomalies.

For each of the ice core δ time series, a climatology, or a mean value for each month of the annual cycle, is defined as the average value of all of the months over the length of the record (in most cases, 1961-2000). This cycle is subtracted from the monthly resolution time series, resulting in an anomaly time series. To form annual mean data, the anomalies are averaged over the course of the calendar year. The different resolutions of isotope time series are illustrated by the partitioning of the data from core 2000-3 into monthly, monthly anomaly, annual cycle, and annual mean components (Figure 5.3).

Compositing analysis (e.g. von Storch and Zwiers, 1999) is often used in climate studies to identify signals of certain climate phenomena in other variables. It consists of defining categories or "bins," sorting data into the categories, and computing the means for each category. In this study, the categories are defined on the basis of the climate indices listed in Table 5.2, and the data are the δ anomalies at the 12 ice coring sites. Results are presented for both monthly and annual resolution data. Monthly resolution has the advantage of providing more data points and is the resolution at which climate modes are typically defined. At annual resolution, the ice core time series are smoother, the variance is reduced, and the timescales do not depend on interpolation between annual markers. At the monthly resolution, T_{IR} data are also used for comparison with the isotope means of each category. Composite analysis is preferred over other statistical methods, such as regression, EOF or Maximum Covariance Analysis (MCA), because

it tends to maximize the signal to noise ratio. Also, it makes no assumptions about the relationship of the climate indices to the δ anomalies, and the relationship need not be linear. In both the monthly and annual resolution analyses presented below, the linear trend is removed from each index, and each index is standardized so that it has a standard deviation of one. Two categories are formed from each index, one for index values greater than one standard deviation (1σ), and one for values less than negative one standard deviation (- 1σ). If the indices are normally distributed, then about a third of the data points should fall within one of these two categories, and this is indeed the case with the data used here. To increase the number of samples in the annual analysis, > + 0.5 σ and < -0.5 σ categories are used, increasing the number of values in the categories to roughly two-thirds of the total length of the index time series.

Means for each category are computed, and a difference of means test using the *Students t* statistic is employed to test whether the mean values for +σ and –σ categories are significantly different from each other. Results are labeled as statistically significant when they are significant at the 95% confidence level or above. The 95% confidence intervals on the means are computed as:

$$\text{xbar} - t_{0.025} * s/\sqrt{(n-1)} < \mu < \text{xbar} + t_{0.025} * s/\sqrt{(n-1)} \qquad (5.1)$$

where xbar is the calculated mean for the category, s is the standard deviation of the samples falling within the category, n is the number of samples within the category and μ is the true mean.

5.4. Results

To understand the relationship among the climate indices and among the ice cores, correlation matrices are computed for the two data sets, at monthly resolution for the indices, and at annual resolution for the ice cores (Tables 5.3 and 5.4). As shown in Table 5.3, significant correlations exist among A8, the SAM, Z500-PC1 and T_{IR}-PC1, consistent with interpretations that all reflect the dominant annular variation in the high-latitude Southern Hemisphere atmospheric circulation, as discussed in previous chapters and other studies (e.g. Thompson and Solomon, 2002; Kidson, 1999). The signs of the correlations are arbitrary, but aid in interpreting the results of the composite analysis discussed below. For instance, a positive anomaly when the SAM is greater than one should correspond to a negative anomaly when Z500-PC1 is greater than one, because the SAM and Z500-PC1 are negatively correlated. Similarly, Z500-PC2 has a low

but significant negative correlation with the SOI, and T_{IR}-PC2 has a significant negative correlation with Z500-PC3.

Among the ice cores (Table 5.4), the cores from the years 1999 and 2000 generally have positive correlations with each other, with the exception of 2000-3. The 2000 cores tend to have negative correlations with the 2001 and 2002 cores. Whether this result is a function of a real feature in the climate system, or an artifact of errors in the dating or other aspects of ice core processing, is a point of discussion below.

As discussed above, the monthly ice cores time series are partitioned into climatological variance and monthly anomaly variance. As the annual cycle in δ is an important dating tool but the anomalies are more interesting for interpretation, it is of interest to know what percentage of the total variance can be considered due to the annual cycle, and what percentage is anomaly variance. These statistics are given in Table 5.5. The annual cycle in δ is associated with changes in local temperature, sea ice conditions and seasonal changes in moisture advection, while anomalies are associated with synoptic variability, and by extension, possibly with the modes of atmospheric variability such as the SAM and ENSO (e.g. Noone, 2001). In a statistical sense, as shown by equation 5.1, the amount of anomaly variance (s^2) determines the significance level of the means in each category.

In climate modeling studies focused on the Antarctic domain, Noone and Simmonds (2002b) report that the annual cycle is about half of the total monthly variance of δ. This is remarkably different than the annual cycle of temperature, which on average over Antarctica explains on the order of 90-95% of the total monthly variance of temperature, with lower values in the Peninsula region and near the coasts (Figure 5.3). In each of the cores except for 1999-1, the climatology describes a well-defined annual cycle, with clear winter minima and summer maxima. The values in Table 5.5 seem rather low, with the annual cycle explaining only about 10-40% of the total variance. This further suggests that the modes of atmospheric variability play an important role in determining the isotopic composition of the snow.

Results of monthly resolution compositing analysis are presented in Table 5.6. The T_{IR} anomalies are included as a basis for understanding the spatial structure of the climate signal associated with the indices. With the exceptions of the SOI and Z500-PC2, all of the indices are associated with statistically significant temperature anomalies. Furthermore, each of the categories is associated with T_{IR} anomalies of the same sign across the study area. Therefore, none of the indices by itself shows evidence for a dipole behavior in temperature across the study area. The indices and their relationship to temperature anomalies therefore do not provide a

simple explanation for the negative correlations between the 2000 and 2001 cores. However, the T_{IR} anomalies suggest that the processes associated with T_{IR}-PC2 are more dominant at the 1999 and 2000 sites than those associated with T_{IR}-PC1. For example, at site 1999-1, T_{IR} PC2 > 1σ explains a -2.78°C anomaly, while, T_{IR} PC1 > 1σ explains a comparatively small 1.35°C anomaly. There is a less obvious distinction at the 2001 sites. For example, T_{IR}-PC2 > 1σ at site 2001-5 is associated with a -1.49°C anomaly, while T_{IR}-PC1 > 1σ is associated with a similar 1.27° C anomaly.

Composite analysis of δ anomalies is carried out at both monthly and annual resolution (Tables 5.6 and 5.7). There are only a few δ anomalies significant at the 95% level or above, notably anomalies corresponding to A8 at site 1999-1, to T_{IR}-PC1 at site 2000-1, and to Z500-PC2 at sites 2000-5, 2000-6, and 2001-5. From a rigorous statistical standpoint, these results are problematic, but given the limited number of samples available for each category (especially note that the T_{IR} PCs are quite short) and the high variance of the data, there are other ways to explore whether meaningful relationships exist. For example, the anomalies associated with A8 and anomalies associated with Z500-PC1 should be of the same sign. Likewise, anomalies corresponding to Z500-PC2 should be of opposite sign to those associated with the SOI if the relationships are real. Another important line of comparison is the sign of T_{IR} anomalies at a site compared with the sign of δ anomalies. In the tables, results are typed in bold where the signs are consistent. Finally, signs of annual anomalies can be compared with signs of monthly anomalies. If results are meaningful, then the signs should be the same.

Applying the consistency checks above, some patterns emerge from the data. Anomalies are consistent across the mode 1 categories at sites 1999-1, 2000-1, 2000-4, and 2000-5. These sites have the best-dated, longest δ records of the 2000 cores (see Table 5.1). A few of the 2000 sites have consistent δ-T sign relationships with either the Z500-PC2 or the SOI, but not with both indices. A similar result is found with the Z500-PC3 and the T_{IR}-PC2 indices and the 2000 cores. However, in these categories, the signs of the annual anomalies are not consistent, as they are for the mode 1 categories at the 1999 and 2000 sites.

The 2001 and 2002 cores have fewer significant and/or consistent results than the 1999 and 2000 cores. A clear signal associated with the mode 1 indices does not appear to exist in the 2001 and 2002 records. There is some evidence that cores 2001-3 and 2002-4 may be sensitive to temperature and circulation anomalies associated with Z500-PC3 and T_{IR}-PC2 as the δ anomalies are consistent across the categories and the annual mean. Core 2001-5 is the only record showing

significant anomalies corresponding to the SOI, consistent with its anomalies corresponding to Z500-PC2.

5.5 Discussion

Ice cores acquired as part of the US-ITASE project have presented an opportunity to study the links between modes of atmospheric circulation and anomalies in stable isotope ratios. Recent climate modeling studies (e.g. Noone and Simmonds, 2002b) and empirical results (e.g. Chapters 3,4) have suggested a robust relationship between stable isotope ratios and atmospheric circulation variability, especially associated with the SAM. An important implication is that ice cores may be a rich enough resource to reconstruct not only mean temperature conditions, but also details of the atmospheric circulation.

Here, I have used a compositing analysis to take maximum advantage of the information in each US-ITASE core, using a spatial array of high quality cores and somewhat redundant climate indices to reduce the likelihood that apparently significant relationships arise by chance. In addition to exploring whether there are significant δD and $\delta^{18}O$ anomalies associated with measurements of temperature and circulation variability, I have also addressed the question of whether temperature anomalies can be used as a basis for the identification of potential ice coring sites for the purpose of obtaining proxy records of one of the major modes.

US-ITASE records from cores obtained in central West Antarctica in the years 1999 and 2000 are largely significantly positively correlated with each other. Cores not yet sampled to the starting year of this analysis, 1961, and not yet assigned a timescale based on signals in the major ion chemistry, tend to have some significant correlations with the other cores, though some are inconsistent with expectations. For instance, core 2000-3 has negative correlations with the other 2000 cores. Low correlations are generally found among the 2001 cores, and for unknown reasons, predominantly negative correlations are found between 2001 and 2000 cores.

Results from the compositing analysis are most robust for the 1999 and 2000 cores that are sampled to 1961 and that have ion chemistry based timescales. Specifically, there are very clear δ anomalies in these records corresponding to both phases of the SAM and its related variability patterns (A8, T_{IR}-PC1, etc.). The current results do not demonstrate a large number of statistically significant anomalies. However, the consistency of the sign of anomalies across a large number of related indices and across the well-dated 1999 and 2000 cores strongly suggests that the SAM signal is real. Also, the reconstruction presented in Chapter 4 demonstrates a

statistically significant SAM signal in the stacked ice core record over a much longer period of time than examined in this chapter.

Among the 2001 cores, less clear relationships with any of the indices are found, though some significant anomalies associated with the SOI and the related "Pacific-South America" pattern measured by Z500-PC2 are identified. In other cores, also identified are anomalies consistent with the wavenumber 3 (Z500-PC3) or T_{IR}-PC2 mode. Better dating and cross-dating of some of the 2001 and 2002 cores may help to confirm whether such signals are widespread and robust. In a highly variable climate like West Antarctica, a small error in dating of even ± 1 yr, within the depth-age uncertainty estimated by Steig et al. (in press), could significantly impact the results of a compositing analysis done at high resolution.

The apparent robustness of the SAM-related signal in the 1999 and 2000 cores and the lack of a clear signal in the 2001 cores come as somewhat of a surprise for two reasons. First, mean accumulation rates are about twice as high at the 2001 sites than the 1999 and 2000 sites (Table 2.2), with, for example, 35 cm H_2O yr^{-1} at 2001-3 and 13 cm H_2O yr^{-1}at 2000-5. Thus, one might expect the 2001 cores (especially 2001-2, 2001-3, and 2001-5) to be dated with relative ease, accuracy and precision, and one would also expect climate signals to be well preserved at the high accumulation sites, as the mean temperatures are low and comparable to those at 1999 and 2000 sites.

A second reason that the results of the compositing analysis are somewhat unexpected is by comparison of the isotopic anomalies to the T_{IR} anomalies. The large temperature anomalies (> 2.5°C) associated with T_{IR}-PC2 in central West Antarctica, particularly at the 1999 and 2000 sites, would lead us to believe that this mode is more important locally than the SAM/T_{IR}-PC1. Likewise, using T_{IR} data as a guideline, it would be expected that the SOI and Z500-PC2 have a very weak signature in West Antarctic climate. Nonetheless, a few significant δ anomalies associated with these modes are found. Locally, therefore, the T_{IR} data provide only a rough guideline as to what climate features may be recorded in proxy data from the site. On the other hand, the T_{IR} data set has confirmed independently that the SAM is the most important mode of variability regionally in the Antarctic. Also, the T_{IR} data have shown that the SAM signal is stronger in the area of the 2000 cores than it is in the area of the 2001 cores.

A tentative physical explanation for the varying spatial expression of the SAM in the δ anomalies may be constructed by consideration of the modeling results of Noone and Simmonds (2002b) and the observations of Kaspari et al (2005). Kaspari et al., through studying the spatial expression of US-ITASE accumulation rate records in sea level pressure anomalies, note that the

2001 cores correspond to large near-coastal anomalies, while the 2000 accumulation records show an apparently stronger relationship to sea level pressure anomalies in the mid-latitudes. This suggests that the high accumulation rate 2001 sites are dominated by local, near-coastal moisture sources. According to Noone and Simmonds (2002b), the salient effects of the positive phase of the SAM (when the westerlies and the polar vortex are strong; arguments can be applied in the opposite sense for the negative phase of the SAM) include a southward migration of the circumpolar trough, and a deepening of the cyclones that comprise the trough. Accompanying the associated change in the eddy component of the moisture flux is a reduction in the stationary outflow from the continent. The result is less ambient moisture available near the coast despite the increased cyclone depth. The relative moisture source contribution of the Amundsen and Bellinghausen Seas is reduced. Another feature is that cyclones can transport moisture inland with relative ease, because the critical flow height is reduced. For the 2001 sites with an important local moisture source, many of these changes to the circulation imply an enrichment relative to the mean. The 2000 sites, in contrast, have a more distant moisture source, and the moisture traveling to these sites is more isotopically depleted because it is transported through the near-coastal zone of high moisture convergence, where there is increased rainout. It is this change to the long-range transport, Noone and Simmonds (2002b) argue, that dominates the inland $\delta^{18}O$ anomaly (depletion with positive SAM). Thus, sites which depend more on distant moisture sources would be expected to show a strong depletion anomaly, and this may be what we are observing at the 2000 sites.

The results of the compositing analysis, even those which are consistent as described above, do not lend themselves to obvious linear δ-T or, for example, δ-SAM slopes that could be applied in reconstructions. For instance, at site 1999-1, on the basis of the results in Table 5.6, A8 > 1σ corresponds to a δ-T ratio of 0.59 ‰/°C. SAM > 1 σ and Z500-PC1 > 1σ, which describe essentially the same thing, are associated with ratios of 0.25 ‰/°C and 0.45 ‰/°C, respectively. Likewise, at two West Antarctic sites, 1999-1 and 2000-1, under the same category, Z500-PC1 > 1σ, ratios are 0.45 ‰/°C and 0.30 ‰/°C, respectively. Although these slopes are within 95% confidence intervals, the slope method would yield unsatisfactory errors in the reconstruction of temperature or the SAM from the δ records.

In their general circulation modeling study, Noone and Simmonds (2002b) identify an analogous overall Antarctic δ -T slope associated with the model's Z500-PC1 > 1 σ of 0.49 ‰/°C. Although a SAM signal of consistent sign has now been identified in both model and real-world data, there is no clear linear calibration slope on which to pin reconstructions that is in

agreement among data and models. Future data and model comparison studies will need to consider precipitation timing and post-depositional alterations, which are not accounted for here, as well as raise the possibilities that the model does not accurately resolve all of the relevant physics, or that there is no appropriate linear slope. In the meantime, alternative empirical calibration methods, like that used in the Chapter 4 temperature reconstruction, may be the most viable approach.

In such a reconstruction, it is interesting to ponder whether the isotopic signal is in fact physically controlled by the temperature variations, or if the isotopic records just happen to correlate with a temperature index which covaries with atmospheric circulation features, which are in turn imparting the signal in both δ and temperature. Results presented here and in Chapter 3 show no compelling evidence to limit interpretations of δ anomalies to local temperature. First, correlations of δ with local temperature are no better than correlations with A8 (Tables 3.3 and 3.4). Second, as discussed above, local T_{IR} anomalies at several of the sites are best explained by the variability of T_{IR}-PC2, while corresponding δ anomalies are dominated by the mode 1 variability. Furthermore, the dominant reason for the δ -T correlation is the difference in temperature from vapor source to final condensation and precipitation formation, rather than the local temperature itself, because of the preferential removal of heavy isotopes as condensation proceeds and the air becomes drier with cooler temperatures in poleward moving air masses, as governed by the Clausius-Clapeyron relationship (e.g. Noone, 2001; Cole et al., 1999; Dansgaard, 1964).

Evidence for an interpretation in terms of temperature on a regional scale includes the regression patterns in Figure 5.1, which reveal that the δ pattern in Z500 is more similar to the A8 regression pattern than to the SAM pattern itself. A similar regression pattern using T_{IR}-PC1 instead of A8 is shown in Figure 1.9a. Statistically, it has also been found that the stack of five δ records correlates better with A8 than with the SAM index (see Chapter 3). On the other hand, at individual sites, isotopic anomalies associated with the SAM itself are generally not distinguishable in magnitude from those associated with A8 and T_{IR}-PC1 (Table 5.6). Thus, the argument can be made that it is the SAM which imparts the signal in both A8 temperature anomalies and δ anomalies, so therefore the changes in the atmospheric circulation are first-order. In the Antarctic, it seems, changes in advective processes associated with the SAM act in such a way as to reinforce, rather than erode, temporal δ-T correlations. These are, nonetheless, weaker than spatial or seasonal δ-T correlations, but still of sufficient magnitude to make a reconstruction in terms of temperature compelling, particularly on a continental, rather than local, scale. Despite

the several parameters which influence δ anomalies, Antarctic climate reconstructions are still promising if the SAM systematically modifies the relevant parameters as it oscillates from one phase to the other, rather than the situation in which a shifting combination of controlling factors modifies the δ signal, as suggested by Cole et al. (1999). Results of this compositing analysis suggest that this latter more complicated situation may be relevant to some of the sites, like the 2001 sites, though there are still several possible ways that incorporation of additional influences (like accumulation timing, post-depositional alterations) and improvement of the records (such as better cross-dating) may improve the results. Importantly, this analysis does demonstrate that the SAM signal is robust at several locations.

5.6 Conclusions

Analysis of stable isotope anomalies in US-ITASE ice core records obtained from the West Antarctic Ice Sheet has demonstrated that meaningful isotopic anomalies occur in some areas corresponding to the phase of the SAM. This is consistent with the SAM's dominant role in the observed climate variability of the Antarctic. These results raise the possibility that the SAM can be reconstructed from some combination of these ice core records. Furthermore, these results lend credibility to forward isotopic climate models that depict a strong SAM signature in δ (Noone and Simmonds, 2002b), and suggest that using the model and the data in an inverse reconstruction may be feasible. However, they suggest limitations in obtaining a single δ-T or δ-SAM slope to apply in a reconstruction.

Without the array of US-ITASE cores, it would not be possible to know *a priori*, given current capabilities, where to locate a core for obtaining a record of a climate mode. The T_{IR} data serve as a general basis, but would not obviously lead to the selection of the 1999 and 2000 sites as candidates for reconstructions of the SAM. At these sites, temperature anomalies suggest that locally important patterns of variability, like the wavenumber 3 pattern, would be relatively more important. Clearly, more research is needed as to how to develop a method for selecting candidate sites that incorporates all of the factors (circulation, temperature, accumulation rate, post-depositional change, etc.,) responsible for creating a reliable ice core proxy record. Reconciling model with field data will ultimately lead to the best interpretation and application of isotopic data in paleoclimate reconstructions.

Table 5.1. Ice core records used in this study.

Core Name	Isotope	Depth-age scale notes	Time period
US-ITASE 1999-1	$\delta^{18}O$	Chemistry-based; too low resolution for adjustment based on δ	1961-1999
US-ITASE 2000-1	$\delta^{18}O$	Chemistry-based; δ adjustments made	1961-2000
US-ITASE 2000-2	$\delta^{18}O$	counting of δ cycles	1966-2000
US-ITASE 2000-3	δD	counting of δ cycles	1972-2000
US-ITASE 2000-4	δD	Chemistry-based; δ adjustments made	1961-2000
US-ITASE 2000-5	δD	Chemistry-based; δ adjustments made	1961-2000
US-ITASE 2000-6	$\delta^{18}O$	counting of δ cycles	1978-2000
US-ITASE 2001-1	$\delta^{18}O$	counting of δ cycles	1982-2001
US-ITASE 2001-2	$\delta^{18}O$	Chemistry-based; δ adjustments made	1961-2001
US-ITASE 2001-3	δD	Chemistry-based; δ adjustments made	1961-2001
US-ITASE 2001-5	$\delta^{18}O$	Chemistry-based; δ adjustments made	1961-2001
US-ITASE 2002-4	δD	counting of δ cycles	1961-2002

Table 5.2. Instrumentally based indices used in this study that are relevant to Antarctic climate variability, with brief descriptions and data source identification.

Index	Description	Data source	Time period and resolution
A8	Composite of surface temperature records from 8 Antarctic weather stations	Derived from READER data (Turner et al., 2004); discussed in Chapters 3 and 4	1958-2003; monthly
SAM	Southern Annular Mode station-based index, free of biases in reanalysis data	Marshall (2003)	1958-2000; monthly
Z500-PC1	First principal component of 500-hPa geopotential height, 20°S-90°S	Original data from NCEP-NCAR Reanalysis; derivation discussed in Chapter 1 but extended here to 1961	1961-2003; monthly
Z500-PC2	Second principal component of 500-hPa geopotential height, 20°S-90°S	Original data from NCEP-NCAR Reanalysis; derivation discussed in Chapter 1 but extended here to 1961	1961-2003; monthly
Z500-PC3	Third principal component of 500-hPa geopotential height, 20°S-90°S	Original data from NCEP-NCAR Reanalysis; derivation discussed in Chapter 1 but extended here to 1961	1961-2003; monthly
SOI	Southern Oscillation Index, a measure of the phase and strength of the El Nino-Southern Oscillation	Obtained from NOAA-CIRES Climate Diagnostics Center	1951-2003; monthly
T_{IR}-PC1	First principal component of T_{IR} temperature anomalies over the Antarctic continent	Discussed in Chapter 1	1982-1999; monthly
T_{IR}-PC2	Second principal component of T_{IR} temperature anomalies over the Antarctic continent	Discussed in Chapter 1	1982-1999; monthly

Table 5.3. Correlation matrix of climate indices. Linear trends are removed before computing the correlation. Asterisks (*) indicate the correlation is significant at the 95% level or above.

Index	A8	SAM	Z500-PC1	Z500-PC2	Z500-PC3	SOI	T_{IR}-PC1	T_{IR}-PC2
A8		-0.52*	0.70*	-0.15*	-0.08	0.02	0.72*	-0.02
SAM	-0.52*		-0.73*	-0.01	0.09	0.06	-0.46*	0.11
Z500-PC1	0.70*	-0.73*		0	0	-0.06	0.61*	-0.15*
Z500-PC2	-0.15*	-0.01	0		0	-0.31*	-0.16*	-0.06
Z500-PC3	-0.08	0.09	0	0		-0.04	0.07	-0.49*
SOI	0.02	0.06	-0.06	-0.31	-0.04		0.08	0.04
T_{IR}-PC1	0.72*	-0.46*	0.61*	-0.16*	0.07	0.08		0
T_{IR}-PC2	-0.02	0.11	-0.15*	-0.06	-0.49*	0.04	0	

Table 5.4. Correlation matrix of ice core δ time series. Linear trends are removed before computing the correlation. Asterisks (*) indicate the correlation is significant at the 95% level or above.

Core	1999-1	2000-1	2000-2	2000-3	2000-4	2000-5	2000-6	2001-1	2001-2	2001-3	2001-5	2002-4
99-1		0.39*	0.20	-0.43*	0.26	0.38*	0.34	-0.16	-0.14	-0.42*	-0.02	-0.18
00-1	0.39*		0.17	-0.52*	0.32*	0.39*	0.49*	0.07	-0.22	-0.22	-0.09	-0.19
00-2	0.20	0.17		-0.49*	0.09	0.45	0.69*	-0.15	0.02	-0.09	-0.42*	0.26
00-3	-0.43*	-0.52*	-0.49*		-0.30	-0.59*	-0.43	-0.30	0.11	0.30	0.08	-0.40
00-4	0.26	0.32*	0.09	-0.30		0.52*	0.28	-0.02	-0.19	-0.08	0.10	0.02
00-5	0.38*	0.39*	0.45*	-0.59*	0.52*		0.49	0.01	-0.06	-0.09	-0.10	0.18
00-6	0.34	0.49*	0.69*	-0.43*	0.28	0.49		-0.15	-0.08	-0.54	-0.30	0.01
01-1	-0.16	0.07	-0.15	-0.30	-0.02	0.01	-0.15		0.27	0.13	0.24	0.69*
01-2	-0.14	-0.22	0.02	0.11	-0.19	-0.06	-0.08	0.27		0.06	-0.36*	0.06
01-3	-0.42*	-0.22	-0.09	0.30	-0.08	-0.09	-0.54	0.13	0.06		0.05	0.07
01-5	-0.02	-0.09	-0.42*	0.08	0.10	-0.10	-0.30	0.24	-0.36	0.07		0.00
02-4	-0.18	-0.19	0.26	-0.40	0.02	0.18	0.01	0.69*	0.30	0.05	0.00	

Table 5.5. Variance and standard deviation of ice core δ time series. The percentage of total variance explained by the annual cycle and anomalies may not add up to 100 because of rounding and missing data.

	1999-1	2000-1	2000-2	2000-3	2000-4	2000-5	2000-6	2001-1	2001-2	2001-3	2001-5	2002-4
Isotope	$\delta^{18}O$	$\delta^{18}O$	$\delta^{18}O$	δD	δD	δD	$\delta^{18}O$	$\delta^{18}O$	$\delta^{18}O$	δD	$\delta^{18}O$	δD
Total monthly standard deviation (‰)	2.33	1.77	2.67	17.5	15.5	13.4	1.83	2.26	2.07	16.3	2.19	19.5
Total monthly variance (‰)	5.41	3.12	7.11	306	242	179	3.36	5.09	4.30	264	4.80	381
standard deviation of anomalies (‰)	2.31	1.50	2.15	10.9	13.8	12.8	1.55	1.70	1.66	12.7	1.71	15.9
variance of anomalies (‰)	5.37	2.26	4.62	119	189	163	2.40	2.88	2.77	161	2.94	251
variance of annual cycle (‰)	0.04	0.94	2.71	204	57	17.4	1.03	2.41	1.69	113	2.03	141
Fraction of total variance of anomalies (%)	99	72	65	39	79	91	72	56	64	61	61	66
Fraction of total variance of annual cycle (%)	.8	30	38	67	24	9	31	47	39	43	42	37
standard deviation at annual resolution (‰)	1.97	1.14	1.46	6.57	9.89	9.11	1.24	1.45	0.59	7.7	0.99	11.6
variance at annual resolution (‰)	3.89	1.30	2.12	43.4	97.8	83	1.54	2.11	0.91	59.2	0.98	133

Table 5.6. Results of monthly resolution compositing analysis, showing mean values of δ and TIR anomalies at each ice coring site associated with each category of climate index.
Categories associated with the annular variation of the atmospheric circulation are shown on this page while categories associated with other modes are shown in the continuation of the table on the following page.

Underlined italics: Anomaly significant at 95% level or above.

Bold: TIR anomaly and δ anomaly are of the same sign for the given category.

INDEX / SITE	A8 > 1	A8 < -1	TIRpc1 > 1	TIRpc1 < -1	SAM > 1	SAM < -1	Z500pc1 >1	Z500pc1 < -1
99-1($\delta^{18}O$ ‰)	***0.60***	***-0.55***	**0.01**	**-1.05**	**-0.33**	**0.33**	**0.59**	**-0.37**
99-1 TIR(°C)	***1.01***	***-1.30***	***1.35***	***-1.80***	***-1.33***	***0.66***	***1.30***	***-1.02***
00-1($\delta^{18}O$ ‰)	**0.18**	**-0.24**	***0.64***	***-0.70***	**-0.21**	**0.03**	**0.35**	**-0.15**
00-1 TIR(°C)	***1.05***	***-1.35***	***1.58***	***-1.96***	***-1.53***	***0.54***	***1.17***	***-1.05***
00-2($\delta^{18}O$ ‰)	0.31	0.37	0.53	0.66	**-0.43**	**0.05**	**0.18**	**-0.24**
00-2 TIR(°C)	*1.15*	*-1.54*	*1.65*	*-2.08*	***-1.73***	***0.77***	***1.50***	***-1.16***
00-3 (δD ‰)	-0.08	2.70	1.39	2.92	3.25	-0.20	0.91	0.78
00-3 TIR(°C)	*1.23*	*-1.61*	*1.75*	*-2.07*	*-1.82*	*0.77*	*1.70*	*-1.35*
00-4 (δD ‰)	**1.97**	**-1.80**	**1.47**	**-2.27**	**-2.40**	**0.32**	**2.09**	**-0.54**
00-4 TIR(°C)	***0.98***	***-1.48***	***1.79***	***-2.07***	***-1.32***	***0.92***	***1.58***	***-1.16***
00-5 (δD ‰)	**0.99**	**-3.43**	**1.68**	**-3.90**	**-3.74**	**1.61**	**1.83**	**-3.82**
00-5 TIR(°C)	***0.72***	***-1.08***	***1.42***	***-1.93***	**-0.77**	**0.94**	***1.21***	***-0.85***
00-6($\delta^{18}O$ ‰)	**0.15**	**-0.20**	-0.23	-0.28	**-0.36**	**0.07**	0.06	0.04
00-6 TIR(°C)	***0.96***	***-1.37***	*1.56*	*-1.88*	***-0.98***	***0.80***	*1.32*	*-1.06*
01-1($\delta^{18}O$ ‰)	-0.37	-0.30	**0.38**	**-0.23**	0.25	-0.35	-0.11	0.03
01-1 TIR(°C)	*1.13*	*-1.08*	***1.77***	***-2.12***	*-1.61*	*0.63*	*1.12*	*-0.91*
01-2($\delta^{18}O$ ‰)	-0.26	0.08	-0.08	0.45	-0.08	-0.14	-0.22	-0.06
01-2 TIR(°C)	*1.07*	*-0.84*	1.56	-1.85	*-1.63*	*0.41*	*0.95*	*-0.80*
01-3 (δD ‰)	-1.36	0.62	1.74	4.33	2.07	-0.43	-0.75	-0.39
01-3 TIR(°C)	*1.00*	*-0.68*	*1.60*	*-1.89*	*-1.51*	*0.42*	*0.78*	*-0.64*
01-5($\delta^{18}O$ ‰)	0.00	-0.35	-0.15	0.01	0.10	-0.33	-0.08	0.04
O1-5 TIR(°C)	*1.07*	*-0.64*	*1.27*	*-1.86*	-1.08	0.24	0.51	-0.47
02-4 (δD ‰)	-3.28	-0.56	1.10	4.19	1.16	-3.43	-2.58	4.18
02-4 TIR(°C)	*1.51*	*-1.28*	*2.10*	*-1.98*	-1.53	1.01	1.19	-1.01

(Table 5.6 continued)
Categories are grouped - Correlated (see Table 5.3) indices Z500PC-2 and SOI, and indices Z500-PC3 and TIR-PC2 are adjacent to each other.

Z500pc2 > 1	Z500pc2 < -1	SOI > 1	SOI < -1	Z500pc3 > 1	Z500pc3 < -1	TIRpc2 > 1	TIRpc2 < -1	
								SITE
0.36	-0.33	-0.05	-0.14	0.67	0.15	-0.73	-0.83	99-1(δ^{18}O ‰)
0.01	0.22	0.17	0.42	*1.76*	*-1.36*	*-2.78*	*2.84*	99-1 TIR(°C)
-0.14	**0.09**	0.11	-0.32	**0.20**	**-0.10**	0.05	0.16	00-1(δ^{18}O ‰)
-0.58	**0.84**	-0.12	-0.07	***1.10***	***-0.74***	*-2.59*	*2.15*	00-1 TIR(°C)
0.19	-0.34	-0.77	0.03	-0.06	0.36	-0.42	-0.21	00-2(δ^{18}O ‰)
-0.42	0.87	-0.16	-0.13	0.86	-0.52	*-2.43*	*2.18*	00-2 TIR(°C)
-1.71	**1.37**	0.77	1.84	**0.58**	**-1.43**	6.84	0.99	00-3 (δD ‰)
-0.18	**0.72**	-0.34	-0.07	***1.13***	***-0.78***	*-2.63*	*2.35*	00-3 TIR(°C)
4.23	-2.19	-0.53	-1.20	-0.62	-2.68	**-0.79**	**2.83**	00-4 (δD ‰)
0.05	0.23	-0.27	-0.07	*1.70*	*-1.28*	***-2.98***	***2.78***	00-4 TIR(°C)
4.01	***-0.78***	-3.08	-0.31	-1.03	1.13	-2.69	-0.23	00-5 (δD ‰)
0.12	**-0.13**	-0.03	0.18	*1.66*	*-1.43*	*-2.50*	*2.52*	00-5 TIR(°C)
0.35	*-0.65*	-0.19	0.13	-0.19	0.29	0.12	0.13	00-6(δ^{18}O ‰)
0.08	0.00	0.04	0.27	*1.60*	*-1.37*	*-2.76*	*2.56*	00-6 TIR(°C)
-0.30	-0.41	0.39	-0.03	0.63	0.20	0.12	0.42	01-1(δ^{18}O ‰)
-0.75	0.73	-0.10	-0.22	0.73	-0.29	*-1.78*	*1.51*	01-1 TIR(°C)
-0.15	**0.15**	-0.10	0.17	0.21	0.18	**-0.02**	**0.40**	01-2(δ^{18}O ‰)
-0.76	**0.53**	0.10	-0.29	0.58	-0.18	***-1.58***	***1.44***	01-2 TIR(°C)
0.07	0.18	-0.03	0.28	**1.43**	**-2.90**	**-0.46**	**7.01**	01-3 (δD ‰)
-0.60	0.42	0.03	-0.31	**0.72**	**-0.41**	***-1.65***	***1.52***	01-3 TIR(°C)
-0.61	***0.51***	***0.81***	***-0.48***	0.00	-0.61	-0.20	-0.13	01-5(δ^{18}O ‰)
-0.68	**0.37**	**0.00**	**-0.16**	*1.02*	*-0.57*	*-1.49*	*1.40*	O1-5 TIR(°C)
1.38	0.24	1.73	5.16	*4.74*	*-3.30*	**-0.24**	**9.13**	02-4 (δD ‰)
-1.00	0.72	-0.54	-0.34	0.31	0.14	***-1.14***	***0.62***	02-4 TIR(°C)

Table 5.7. Results of annual resolution compositing analysis, showing mean values of δ anomalies at each ice coring site associated with each category of climate index. Categories associated with the annular variation of the atmospheric circulation are shown on this page while categories associated with other modes are shown in the continuation of the table on the following page.

Underlined bold: Anomaly significant at 95% level or above.

Italics: Sign of annual anomaly contradicts sign of monthly anomaly.

INDEX	A8 > 0.5	A8 < -0.5	TIRpc1 > 0.5	TIRpc1 < -0.5	SAM > 0.5	SAM < -0.5	Z500pc1 > 0.5	Z500pc1 < -0.5
SITE								
99-1($\delta^{18}O$ ‰)	0.93	-0.34	0.50	-1.43	-1.20	0.63	0.76	-0.63
00-1($\delta^{18}O$ ‰)	0.37	-0.04	0.98	-0.47	-0.23	0.38	0.26	-0.12
00-2($\delta^{18}O$ ‰)	*-0.20*	*0.09*	0.56	0.13	-0.40	0.44	0.53	-0.22
00-3(δD ‰)	-4.20	2.93	*-0.67*	4.62	2.00	-2.77	*-2.95*	0.92
00-4(δD ‰)	3.24	-1.26	3.01	*0.58*	-3.75	1.17	1.39	-1.15
00-5(δD ‰)	5.20	-3.32	3.69	-3.94	**-5.94**	**5.77**	5.19	-2.97
00-6($\delta^{18}O$ ‰)	*-0.01*	-0.47	*0.44*	-0.08	-0.22	*-0.02*	0.09	0.05
01-1($\delta^{18}O$ ‰)	*0.94*	0.10	*-0.01*	-0.02	-0.24	-0.07	*0.79*	-0.11
01-2($\delta^{18}O$ ‰)	*-0.59*	0.24	-0.49	0.69	*0.30*	*0.03*	*0.26*	*0.43*
01-3(δD ‰)	-3.00	1.10	3.96	3.65	0.55	*1.59*	*0.03*	*0.58*
01-5($\delta^{18}O$ ‰)	0.16	-0.27	-0.42	0.06	0.08	-0.05	-0.06	*-0.04*
02-4(δD ‰)	-2.38	1.16	*-1.41*	6.02	2.86	-0.60	-3.58	4.99

(Table 5.7 continued)
Categories are grouped - Correlated (see Table 5.3) indices Z500PC-2 and SOI, and indices Z500-PC3 and TIR-PC2 are adjacent to each other.

Z500pc2 > 0.5	Z500pc2 < -0.5	SOI > 0.5	SOI < -0.5	Z500pc3 > 0.5	Z500pc3 < -0.5	TIRpc2 > 0.5	TIRpc2 < -0.5	SITE
0.35	-0.27	*0.26*	-0.09	0.56	*-0.28*	*0.28*	-1.08	99-1(δ^{18}O ‰)
0.02	0.34	0.37	-0.27	0.25	*0.02*	*-0.15*	*-0.12*	00-1(δ^{18}O ‰)
0.37	*-0.04*	*0.19*	0.25	*0.24*	0.51	*0.01*	*0.37*	00-2(δ^{18}O ‰)
-2.05	3.43	2.96	-0.25	*-0.52*	-0.47	*1.70*	*-0.37*	00-3(δD ‰)
3.34	*0.42*	*3.55*	-0.45	-0.05	*1.52*	-2.98	2.74	00-4(δD ‰)
1.71	-1.22	*1.06*	*0.03*	*1.91*	*-1.31*	-1.79	*4.03*	00-5(δD ‰)
0.30	*0.03*	*0.27*	*0.03*	-0.22	0.77	0.26	*-0.18*	00-6(δ^{18}O ‰)
0.31	*0.11*	-0.08	*-0.41*	*-0.05*	-0.66	*-0.67*	0.23	01-1(δ^{18}O ‰)
-0.13	*-0.37*	-0.14	0.15	-0.08	0.17	*0.19*	0.22	01-2(δ^{18}O ‰)
-0.30	1.21	-0.19	1.25	2.07	-1.36	-1.17	4.59	01-3(δD ‰)
-0.13	0.40	0.45	-0.39	0.08	-0.23	*0.19*	*0.28*	01-5(δ^{18}O ‰)
1.27	1.40	*-0.84*	0.47	4.69	-3.17	-0.06	10.00	02-4(δD ‰)

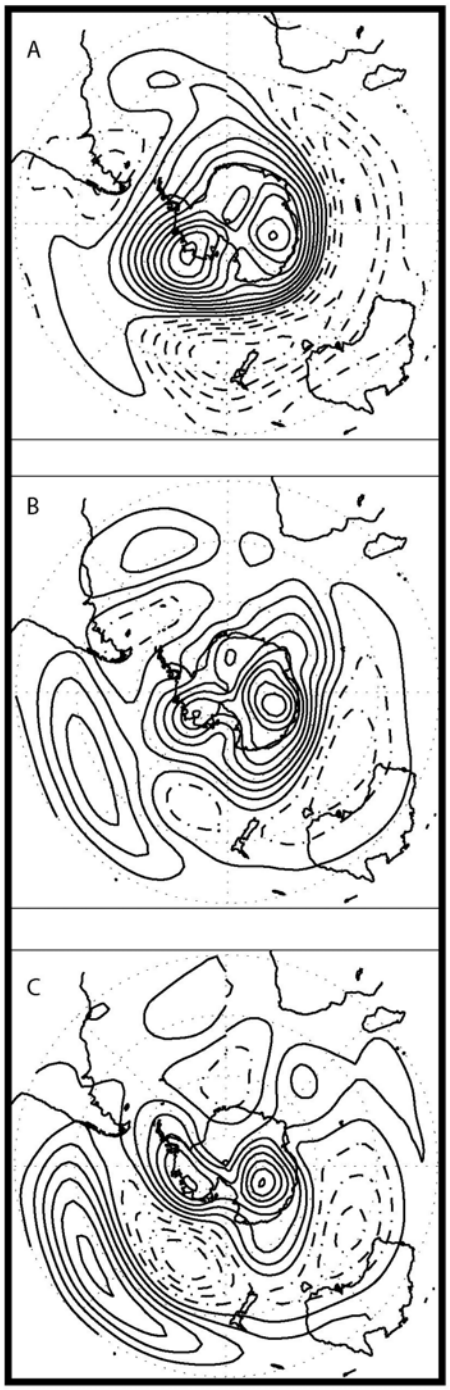

Figure 5.1. Regression patterns in annual 500-hPa geopotential height anomalies. Units are in m, contour interval is 2 m. Positive values are shown as solid lines and negative values as dashed lines. (a) Marshall's (2003) SAM index used as the base time series; (b) Antarctic A8 temperature index used as the base time series; (c) Calibrated (as in Chapter 4) ice-core based temperature index used as the base time series of the regression.

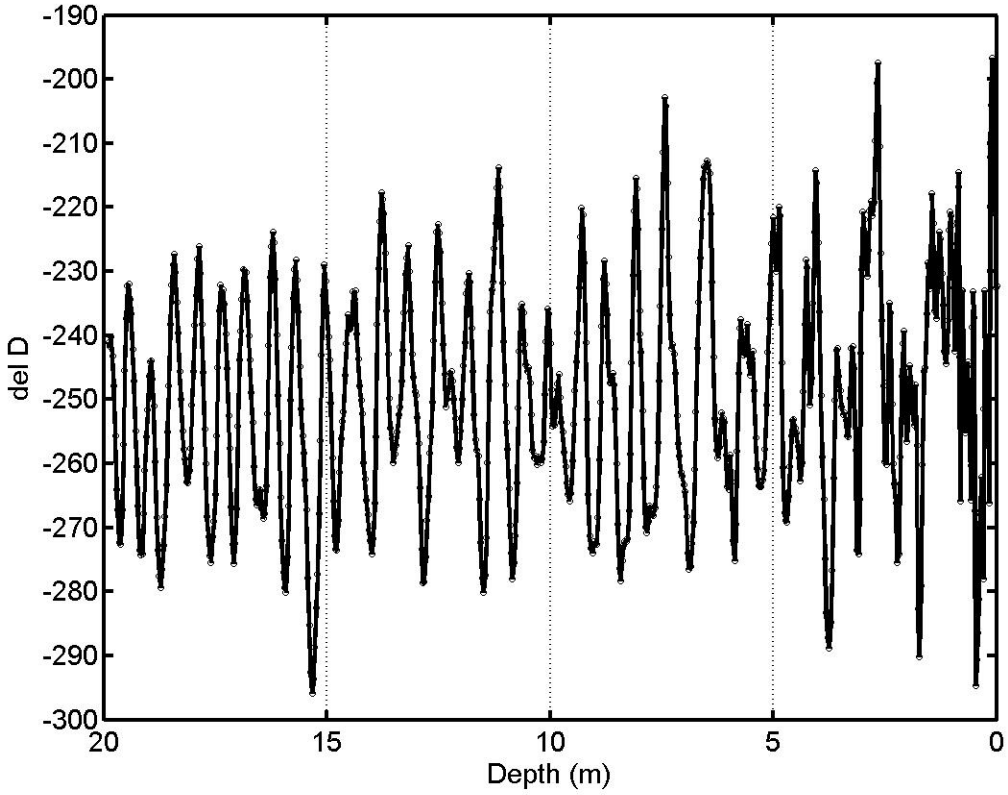

Figure 5.2. Isotope data versus depth at the sampling resolution from core US-ITASE 2000-3. The predominant fluctuation of ~50‰ is attributed to the annual cycle, with more negative values interpreted as representing cold, winter conditions.

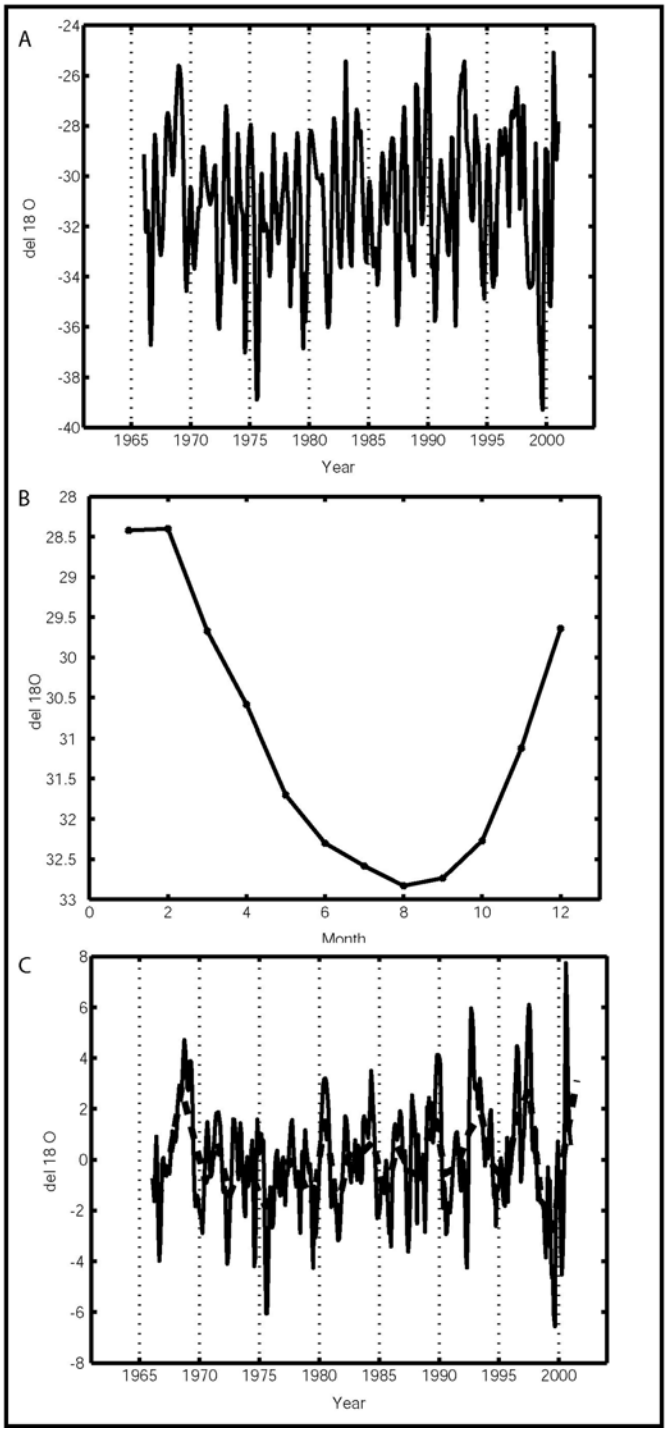

Figure 5.3. Oxygen isotope data from core US-ITASE 2000-2. (a) Monthly resolution data showing the full range of variability; (b) The climatological monthly values removed from the monthly time series; (c) Monthly anomaly time series shown as the solid line, with annual values shown as the thicker dashed line.

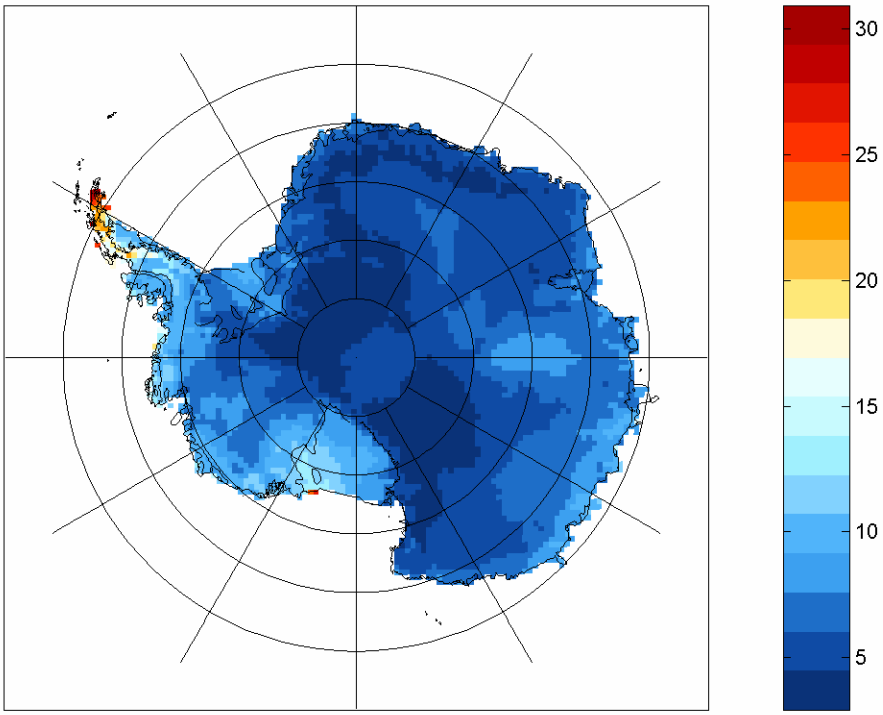

Figure 5.4. Percent of total monthly variance explained by anomalies of T_{IR}. The remaining percent is explained by the annual cycle.

CHAPTER 6

Conclusions and future outlook

In this dissertation I have focused on understanding Antarctic climate variability and change via investigations of meteorological observations and ice core records. The past six years has been an exciting and quickly advancing time to be working in this field. As I look over my bibliography, it appears that the majority of cited papers have appeared since I began as a graduate student. Two papers in particular, Thompson and Solomon (2002) and Doran et al. (2002), have focused almost as much attention on Antarctic climate change as the dramatic ice shelf collapses in the Antarctic Peninsula region. Their work and that of countless others have reinforced conclusions which now seem obvious: Antarctic climate is highly variable, warming and cooling trends are difficult to identify but not impossible to reconcile and disaster could happen (e.g. West Antarctic Ice Sheet collapse) if current hard-to-decipher trends continue. The important role of a paleoclimatologist is to place the warming and cooling trends into a long-term context so that we may understand the workings of the climate system and how current trends are likely to play out in the future, especially in light of human influences on climate and the potential for climate variability and change to have large societal impacts.

The work I have presented can be grouped into two broad themes, modern Antarctic climate variability and reconstruction of Antarctic climate using ice core records. A brief summary of findings from each chapter, organized by the two themes, follows.

Modern Antarctic climate variability

Although we have a good understanding of monthly to yearly climate variations in many parts of the world, in Antarctica our understanding is just beginning. Records of meteorological observations from a limited number of research stations are barely long enough to produce a baseline climatology. In Chapter 1, I addressed the problem of having only a limited number of weather stations through investigations into the variance and covariance of two satellite data sets. From a maximum covariance analysis, two main results emerged. One, the passive microwave data and infrared data share significant covariance, underscoring their usefulness as indicators of the spatial structure of Antarctic climate variability. Eventually, this may also give us more information about the ice sheet itself (e.g. Winebrenner et al., 2005). Second, it became evident from the analysis in Chapter 1 that the temperature anomalies across the ice sheet are

interpretable in terms of the well-known modes of the Southern Hemisphere atmospheric circulation.

Other Chapters were less explicitly focused on modern variability, but some relevant results were discussed. In Chapter 3, a simple average of several weather station temperature records proved to be a good indicator of Antarctic climate variability, and a possible target for reconstruction. Called A8, this record serves as a surrogate for the first mode of satellite temperatures (T_{IR}-PC1) which is too short itself to be of much use for ice core calibration. The T_{IR} modes will be extended in a future study, but the first mode will largely take the form of A8 because the underlying weather station data are the same. Chapter 4 used an updated A8 index as a baseline for an ice core reconstruction. The A8 index itself proved to be interesting. It shows the same cooling of Antarctica from 1966-2000 and 1982-1999 that Doran et al. (2002) and Comiso (2000) highlighted, respectively, using more spatially representative data and more sophisticated (or complicated) methods. But it also made it clear, that, at least since sufficient observations began, Antarctica has experienced a warming trend. In addition, A8 is significantly correlated with the Southern Annular Mode. In Chapter 5, I presented and briefly summarized most of the indices relevant to modern Antarctic climate variability, because we may eventually be able to reconstruct not only A8, but also other climate indicators.

Antarctic ice core records

Somewhat surprisingly, Antarctic ice cores have been used to infer more about the Last Glacial Maximum and the Antarctic Cold Reversal than about the era of Scott, Shakleton and Mawson at the turn of the last century. The very long (now up to 800,000 years (e.g. EPICA members, 2004)) records have been highly valuable, but nonetheless do not reveal much about natural Antarctic climate variability in today's climate state. In this dissertation, motivated by the vision of the International Trans Antarctic Scientific Expedition, I have investigated how the short recent meteorological records could be extended with data from ice cores.

In Chapter 2, I showed that, as a result of field work and lab analysis by many people, we now have extensive ice core data that are of high quality and fit the basic premise of stable isotopic ratios of water as proxies for temperature. In Chapter 3, I showed the clear seasonal cycles in the isotopic ratios that could be used as a dating tool and possibly as a means of δ-T calibration. Comparison to interannual temperature anomalies, however, proved that such a calibration is of questionable applicability. As an alternative focus, I introduced the A8 index,

showing that it has as much meaning and as much or more potential for skillful reconstruction as does local temperature.

Chapter 4 compiled the best-dated, highest resolution ice core records for reconstruction of A8 back to 1800. An effort was made to address scaling issues arising from the unknown δ-T relationship across a spectrum of frequencies as well as potential biases in the records (especially seasonality, accumulation and moisture source trends). In comparison with global warming trends, the reconstruction indicates that Antarctic warming has been only modest. Using the long Orcadas records and the SAM reconstruction from Jones, I showed that much Antarctic temperature variability can be linked to the SAM. Climate models, by contrast, show more warming over Antarctica than in the global or SH mean and less of a link to the SAM. In comparison with the observed SH mean temperature record, it is interesting that only the 1990s stand out as a time when the SH warmed and Antarctica did not.

Finally, in Chapter 5, the spatial variation of isotopic anomalies in West Antarctica was related to several climate indices. Results of compositing analysis showed that several locations have anomalies with temporal variability consistent with variations in the SAM. The results raised larger issues in paleoclimatology and ice coring, such as the assumption of maximum correlation with local temperature anomalies. Certain regional scale temperature indices, like A8, nonetheless suggest a physical connection with the proxy. The one published general circulation modeling study of the isotopic signature of the SAM (Noone and Simmonds, 2002b) appears to have qualitative agreement with observations made from ITASE data.

Future Outlook

There are several ways in which the results and methods of this dissertation could be extended and/or combined with the ideas of other investigators. The intersection of high-resolution ice core studies with isotopic tracers in general circulation models is a promising area for future research. This could lead to more complete physical descriptions of the ice core record that will aid in reconstructions of the SAM and other modes of atmospheric circulation. Quantitative reconstructions that are more spatially resolved than the one presented in this thesis are needed, as are reconstructions longer than the 200-year time period examined here.

BIBLIOGRAPHY

Abdalati, W., Steffen, K., Otto, C., and K.C. Jezek, 1995: Comparison of brightness temperatures from SSMI instruments on the DMSP F8 and F11 satellites for Antarctica and the Greenland ice sheet, *International Journal of Remote Sensing*, ***16*** (7), 1223-1229.

Angelis, H.D., and P. Skvarca, 2003: Glacier surge after ice shelf collapse, *Science*, **299**, 1560-1562.

Armstrong, R.L., A. Chang, A. Rango, and E. Josberger, 1993: Snow depths and grain-size relationships with relevance for passive microwave studies, *Annals of Glaciology*, **17**, 171-176.

Barbraud, C., and H. Weimerskirch, 2001: Emperor penguins and climate change, *Nature*, **411**, 183-186.

Bertler, N.A.N., P.J. Barrett, P.A. Mayewski, R.L. Fogt, K.J. Kreutz, and J. Schulmeister, 2004: El Nino suppresses Antarctic warming, *Geophys. Res. Lett*, **31**.

Bindschadler, R., 1998: Future of the West Antarctic Ice Sheet, *Science*, **282**, 428-429.

Bradley, R.S. 1999. *Paleoclimatology: Reconstructing Climates of the Quaternary* (2nd edition), Academic Press, 610 pp.

Bretherton, C.S., C. Smith, and J.M. Wallace, 1992: An Intercomparison of Methods for Finding Coupled Patterns in Climate Data, *J. Climate*, **5**, 541-560.

Bretherton, C.S., M. Widmann, V.P. Dymnikov, J.M. Wallace, and I. Blade. 1999. The effective number of spatial degrees of freedom in a time-varying field. *J. Climate*, **12**, 1990-2009.

Bromwich, D.H., 1989: Satellite analyses of Antarctic katabatic wind behavior, *Bulletin of the American Meteorological Society*, **70** (7), 738-748.

Bromwich, D.H., A.N. Rogers, P. Kallberg, R.J. Cullather, J.W.C. White, and K.J. Kretz, 2000: ECMWF analyses and reanalysis depiction of ENSO signal in Antarctic precipitation, *Journal of Climate*, **13**, 1406-1420.

Bromwich, D. H. and A. N. Rogers, 2001: The El Niño-Southern Oscillation modulation of West Antarctic precipitation. *Ant. Res. Ser.,* **77**, 91-104.

Bromwich, D.H., A.J. Monaghan, and Z. Guo, 2004: Modeling the ENSO modulation of Antarctic climate in the late 1990s with Polar MM5, *J. Climate,* **17** (1), 109-132.

Bromwich, D.H., Z. Guo, L. Bai, and Q. Chen, 2004: Modeled Antarctic precipitation, Part I: Spatial and temporal variability, *J. Climate*, **17**, 427-447.

Cai, W., and I.G. Watterson, 2002: Modes of interannual variability of the southern hemisphere circulation simulated by the CSIRO climate model*, J. Climate,* **15**, 1159-1174.

Carleton, A.M., John, G., and R. Welsch, 1988: Interannual variations and regionality of Antarctic sea-ice-temperature associations, *Annals of Glaciology*, **27**, 403-408.

Carleton, A.M., 2003: Atmospheric teleconnections involving the Southern Ocean, *J. Geophys. Res*., **108**(C4), 8080.

Cavalieri, D.J., 1991: NASA Sea Ice Validation Program for the DMSP SSM/I, *Journal of Geophysical Research*, **96** (C12), 21,969-21,970.

Chang, T.C., P. Gloersen, T. Schmugge, T.T. Wilheit, and H.J. Zwally, 1976: Microwave emission from snow and glacier ice, *Journal of Glaciology*, **16** (74), 23-39

Cole, J.E., D. Rind, R.S. Webb, J. Jouzel, and R. Healy, 1999: Climatic controls on interannual variability of precipitation $\delta^{18}O$: Simulated influence of temperature, precipitation amount, and vapor source region. *J. Geophys. Res*., **104**(D12), 14,223-14,235.

Comiso, J.C., 1994: Surface temperatures in the polar regions from Nimbus 7 temperature humidity infrared radiometer, *Journal of Geophysical Research*, **99** (C3), 5181-5200.

Comiso, J. C., 2000: Variability and trends in Antarctic surface temperatures from in situ and satellite infrared measurements, *J. Climate*, **13**, 1674-1696.

Criss, R.E., 1999: *Principles of Stable Isotope Distribution*. Oxford University Press, 254 pp.

Cuffey, K.M., and E.J. Steig, 2002: Isotopic diffusion in polar firn: implications for interpretation of seasonal climate parameters in ice-core records, with emphasis on central Greenland, *J Glaciol.,* **44**(117), 273-283.

Dansgaard, W., 1964: Stable isotopes in precipitation, *Tellus* **XVI** (4).

Dixon, D., Mayewski, P.A., S. Sneed, M. Handley, 2005: A 200-year sub-annual record of sulfate in West Antarctica, from 16 ice cores. *Ann. Glaciol*., **39**, 545-556.

Doran, P.T., and Coauthors, 2002: Antarctic climate cooling and terrestrial ecosystem response, *Nature*, **415**, 517-520.

Enomoto, H., and Coauthors, 1998: Winter warming over Dome Fuji, East Antarctica, and the semiannual oscillation in the atmospheric circulation, *J. Geophys. Res.,* **103**, D18, 23,103-23,111.

EPICA Community Members, 2004: Eight glacial cycles from an Antarctic ice core, *Nature* **429**, 623-626.

Epstein, S., and T. Mayeda, 1953: Variaiton of $\delta^{18}O$ content of waters from natural sources, *Geochimica et Cosmochimica Acta*, **4** (5), 213-224.

Fischer, H., F. Traufetter, H. Oerter, R. Weller, and H. Miller, 2004: Prevalence of the Antarctic circumpolar wave over the last two millennia recorded in Dronning Maud Land ice, *Geophys. Res. Lett*., **31**.

Garreaud, R. D., and D.S. Battisti, 1999: Interannual (ENSO) and interdecadal (ENSO-like) variability in the Southern Hemisphere tropospheric circulation, *J. Climate*, **12**, 2113-2123.

Ghil, M., and R. Vautard, 1991: Interdecadal oscillations and the warming trend in global temperature time series, *Nature*, **350**, 324-327.

Gillett, N.P., and D.W.J. Thompson, 2003: Simulation of recent Southern Hemisphere climate change, *Science,* **203***,* 273-275.

Gloersen, P., 1987: In-orbit calibration adjustment of the Nimbus-7 SMMR, NASA Tech Memo #100678, 39 pp., Washington, D.C.

Gloersen, P., D. Cavalieri, W. J Campbell, and J. Zwally, 1990: Nimbus-7 SMMR polar radiances and Arctic and Antarctic sea-ice concentrations on CD-ROM, National Snow and Ice Data Center, Boulder, CO.

Gloersen, P., and W.B. White, 2001: Reestablishing the circumpolar wave in sea ice around Antarctica from one winter to the next, *Journal of Geophysical Research*, **106** (C3), 4391-4395.

Gong, D., and S. Wang, 1999: Definition of Antarctic Oscillation Index, *Geophys. Res. Lett.*, **26** (4), 459-462.

Goodwin, I.D., T.D. van Ommen, M.A.J. Curran, P.A. Mayewski, 2004: Mid latitude winter climate variability in the Southern Indian and Southwest Pacific regions since 1300 AD, *Climate Dynamics*, **22** (8), 783-794.

Gow, A.J., 1969: On the rates of growth of grains and crystals in south polar firn, *Journal of Glaciology*, **8** (53), 241-252.

Graf, W., Oerter, H., Reinwarth, O., Stichler, W., Wilhelms, F., Miller, H., Mulvaney, R., 2002: Stable isotope records from Dronning Maud Land, Antarctica, *Ann. Glaciol*., **35**, 195-201.

Gregory, J.M., 2000: Vertical heat transports in the ocean and their effect on time-dependent climate change, *Clim. Dynamics*, **16**, 501-515.

Hartmann, D.L., 1994: *Global Physical Climatology*, Academic Press, 411 pp.

Hines, K.M., D.H. Bromwich, and G.J. Marshall, 2000: Artificial surface pressure trends in the NCEP-NCAR Reanalysis over the Southern Ocean and Antarctica, *J. Climate*, **13**, 3940-3952.

Hirasawa, N., H. Nakamura, and T. Yamanouchi, 2000: Abrupt changes in meteorological conditions observed at an inland Antarctic station in association with wintertime blocking, *Geophys. Res. Lett.,* **27** (13)*,* 1911-1914.

Holland, M.M., C.M. Bitz, 2003: Polar amplification of climate change in coupled models, *Clim. Dynamics*, **21**, 221-232.

Hollinger, J.P., Pierce, J.L., and G.A. Poe, SSSM/I instrument evaluation, *IEEE Transactions Geoscience Remote Sensing*, **28**, 781-790, 1990.

Houghton, J.T. and others, eds.. 2001. *Climate Change 2001: The Scientific Basis.* Cambridge University Press, 881 pp.

Ichiyanagi, K., Numaguti, A., and K. Kata, 2002: Interannual variation in stable isotopes in Antarctic precipitation in response to El Niño -Southern Oscillation, *Geophys. Res. Lett.*, **29**(1).

Isaksson, E., and K. Melvold, 2002: Trends and patterns in the recent accumulation and oxygen isotopes in coastal Dronning Maud Land, Antarctica: interpretations from shallow ice cores, *Ann. Glaciol*., **35**, 175-180.

Jacobel, R., B. Welch, E.J. Steig, and D.P. Schneider, 2005: Hercules Dome, Antarctica: A Possible Site for deep ice core drilling, *Journal of Geophysical Research*, **110**.

Jezek, K.C., D.J. Cavalieri, and A. Hogan, 1990: Antarctic ice sheet brightness temperature variations, *CRREL Monographs*, **90** (1), 217-223.

Jezek, K.C., C.J. Merry, and D.J. Cavalieri, 1993: Comparison of SSMR and SSM/I passive microwave data collected over Antarctica, *Annals of Glaciology*, **17**, 131-136.

Johannessen, O.M., E.V. Shalina, and M.W. Miles, 1999: Satellite evidence for an Arctic sea ice cover in transformation, *Science*, **286**, 1937-1940.

Johnsen, S.J., H.B. Clausen, K M Cuffey, G. Hoffmann, J. Schwander, and T. Creyts, 2000: Diffusion of stable isotopes in polar firn and ice: the isotope effect in firn diffusion. In *Physics of Ice Core Records (*ed. T Hondoh), pp 121-140. Hokkaido University Press.

Jones, J., and M. Widmann, 2003: Instrument and tree ring based estimates of the Antarctic Oscillation, *J. Climate*, **16**(21), 3511-3524.

Jones, J.M., and M. Widmann, 2004: Early peak in Antarctic Oscillation Index, *Nature* **432**, 290-291.

Jones, P.D., 1991: Southern Hemisphere sea level pressure data – an analysis and reconstructions back to 1951 and 1911, *Int. J. Climatol*., **11**(6), 585-607.

Jones, P.D., 1995: Recent variations in mean temperature and the diurnal temperature range in Antarctica, *Geophysical Research Letters*, **22** (11), 1345-1348.

Jones, P.D., T.J. Osborn, K.R. Briffa, C.K. Folland, E.B. Horton, L.V. Alexander, D.E. Parker, N.A. Rayner, 2001: Adjusting for sampling density in grid box land and ocean surface temperature time series, *J. Geophys. Res*., **106**(D4), 3371-3380.

Jones, P.D., Mann, M.E., 2004: Climate over past millennia, *Rev. Geophys*., **42**.

Jouzel, J., R.B. Alley, K.M. Cuffey, W. Dansgaard, P. Grootes, G. Hoffmann, S.J. Johnsen, R.D. Koster, D. Peel, C.A. Shuman, M. Stievenard, M. Stuiver, and J. White, 1997: Validity of the temperature reconstruction from water isotopes in ice cores. *J. Geophys. Res*., **102**(C12), 26,471-26,487.

Jouzel, J., F. Vimeux, N. Caillon, G. Delaygue, G. Hoffmann, V. Masson-Delmotte, and F. Parrenin, 2003: Magnitude of isotope/temperature scaling for interpretation of central Antarctic ice cores, *J. Geophys. Res*., **108**(D12), 4361.

Kalnay, E., and Coauthors, 1996: The NCEP/NCAR 40-Year Reanalysis Project, *Bull. Amer. Metero. Soc*., **77**, 437-472.

Karl, T.R., and K.E. Trenberth, 2003. Modern global climate change. *Science* **302**, 1719-1723.

Kaspari, S., P.A. Mayewski, D.A. Dixon, V.B. Spikes, S.B. Sneed, M.J. Handley, G.S. Hamilton, 2005: Climate variability in West Antarctica derived from annual accumulation rate records from ITASE firn/ice cores, *Ann. Glaciol*, **39**, 545-594.

Kavenaugh, J.L. and K.M. Cuffey, 2003: Space and time variation of $\delta^{18}O$ and δD in Antarctic Snow revisited, *Global Biogeochem. Cyc*., **17**(1).

Kidson, J.W., 1988: Interannual variations in the Southern Hemisphere circulation, *J. Climate*, **1**, 1177-1198.

Kidson, J.W., 1999: Principal modes of Southern Hemisphere low-frequency variability obtained from the NCEP-NCAR reanalyses, *J. Climate*, **12**, 2808-2830.

Kidson, J.W., and J.A. Renwick, 2002: The Southern Hemisphere evolution of ENSO during 1981-1999, *J. Climate*, **15**, 847-863.

Kiehl, J.T., T.L. Schneider, R.W. Portmann, S. Solomon, 1999: Climate forcing due to tropospheric and stratospheric ozone, *J. Geophys., Res*., **104**(D24), 31239-31254.

King, J.C., 1994: Recent climate variability in the vicinity of the Antarctic Peninsula, *Int. J. Climatol*., **14**, 357-369.

King, J.C., and J. Turner, 1997: *Antarctic Meteorology and Climatology*, Cambridge University Press, 409pp.

King, J.C., and S.C. Harangozo, 1988: Climate change in the western Antarctic peninsula since 1945: Observations and possible causes, *Annals of Glaciology*, **27**, 571-575.

King, J.C., and J.C. Comiso, 2003: The spatial coherence of interannual temperature variances in the Antarctic Peninsula, *Geophys. Res. Lett*., **30**(2).

Kistler, R., and Coauthors, 2001: The NCEP-NCAR 50-Year Reanalysis: Monthly means CD-ROMS and Documentation, *Bull. Amer. Metero. Soc.,* **82**, 247-268.

Kreutz, K.J., P.A. Mayewski, I.I. Pittalwala, L.D. Meeker, M.S. Twickler, and S.I. Whitlow, 2000: Sea level pressure variability in the Amundsen Sea region inferred from a West Antarctic glaciochemical record, *J. Geophys. Res*., **105**(D3), 4047-4059.

Kuhn, M.H., A.J. Riordan, and I.A., Wagner, 1973: The Climate of Plateau Station, in *Climate of the Arctic*, Geophysical Institute, University of Alaska, pp. 255

Kwok, R, and J.C. Comiso, 2002: Spatial patterns of temperature variability in Antarctic surface temperature: Connections to the Southern Hemisphere Annular Mode and Southern Oscillation. *Geophys. Res. Lett*., **29**, 1705.

Laurmann, J.A., and W.L. Gates, 1977: Statistical considerations in the evaluation of climatic experiments with atmospheric general circulation models, *Journal of the Atmospheric Sciences*, **34**, 1187-1199.

Liu, H., K.C. Jezek, and B. Li, 1999: Development of an Antarctic digital elevation model by integrating cartographic and remotely sensed data: A Geographic Information System based approach, *Journal of Geophysical research*, **104** (B10), 23,199-23,213.

Mann, M.E., Bradley, R.S., and M.K. Hughes, 1998: Global-scale temperature patterns and climate forcing over the past six centuries, *Nature*, **392**, 779-787.

Mann, M.E., Bradley, R.S., and M.K. Hughes, 1999: Northern Hemisphere temperatures during the past millennium: Inferences, uncertainties, and limitations, *Geophysical Research Letters*, **26** (6), 759-762.

Mann, M.E., R.S. Bradley, and M.K. Hughes, 2000: Long-Term variability in the El Nino/Southern Oscillation and associated teleconnections, in *El Nino and the Southern Oscillation: Multiscale Variability and its Impacts on Natural Ecosystems and Society*, edited by H.F. Diaz, and Markgraf, K., pp. 357-412, Cambridge University Press.

Mann, M.E., and P.D. Jones, 2003: Global surface temperatures over the past two millennia, *Geophys. Res. Lett*., **30**(15).

Marshall, G.J., 2002a: Analysis of recent circulation and thermal advection change in the northern Antarctic Peninsula, *Int. J. Climatol*., **22**, 1557-1567.

Marshall, G.J., 2002b: Trends in Antarctic geopotential height and temperature: A comparison between NCEP-NCAR and radiosonde data, *J. Climate*., **15**, 659-674.

Marshall, G.J., 2003: Trends in the Southern Annular Mode from observations and reanalysis, *J. Clim.*, **16**, 4134-4143.

Marshall, G,J., P.A. Stott, J. Turner, W.M. Connolley, J.C. King, and T.A. Lachlan-Cope, 2004: Causes of exceptional atmospheric circulation changes in the Southern Hemisphere, *Geophys. Res. Lett*., **31**.

Maslanik, J. and J. Stroeve, 1990-2001: DMSP SSM/I daily polar gridded brightness temperatures on CD-ROM, National Snow and Ice Data Center, Boulder, CO.

Masson, V., F. Vimeux, J. Jouzel, V. Morgan, M. Delmotte, P. Ciais, C. Hammer, S. Johnsen, V. Lipenkov, E. Mosley-Thompson, J. Petit, E.J. Steig, M. Stievenard, and R. Vaikmae, 2000: Holocene climate variability in Antarctica based on 11 ice-core isotopic records, *Quaternary Research*, **54**, 348-358.

Masson-Delmotte, V., M. Delmotte, V. Morgan, D. Etheridge, T. van Ommen, S. Tartarin, and G. Hoffmann, 2003: Recent southern Indian Ocean climate variability inferred from a Law Dome ice core: new insights for the interpretation of coastal Antarctic isotopic records, *Climate Dynamics,* **21** (2), 153-156..

Mayewski, P.A., and I.D. Goodwin, 1996: International Trans-Antarctic Scientific Expedition (ITASE), "200 years of past Antarctic climate and environmental change," Science and Implementation Plan, PAGES Workshop Report, Series 97-1, 48 pp.

Mayewski, P., and Coauthors, 2003: Antarctic oversnow traverse-based Southern Hemisphere climate reconstruction, *EOS Transactions American Geophysical Union*, **84**(22), 205,210.

Mayewski, P.A., K.A. Maasch, J.W.C. White, E.J. Steig, E. Meyerson, I. Goodwin, V. Morgan, T.D. van Ommen, M.A.J. Curran, J. Souney, and K. Kreutz, 2005: A 700-year record of southern hemisphere extratropical climate variability. *Ann. Glaciol*., **39,** 127-132.

Meehl, G.A., W. M. Washington, B.D. Santer, W.D. Collins, J.M. Arblaster, A. Hu, D.M. Lawrence, H. Teng, L.E. Buja, W.G. Strand, in press, Climate change in the 20th and 21st centuries and climate change commitment in the CCSM3, *J. Climate*.

Meese, D.A., A.J. Gow, R.B. Alley, G.A. Zielinski, P.M. Grootes, M. Ram, K.C. Taylor, P.A. Mayewski, J.F. Bolzan, 1997: The Greenland Ice Sheet Project 2 depth-age scale: methods and results, *J. Geophys Res*., **C12**, 26, 411-26,423.

Mo, K.C., and G.H. White, 1985: Teleconnections in the Southern Hemisphere, *Mon. Wea. Rev*., **113**, 22-37.

Mo, K.C., and R.W. Higgins, 1998: The Pacific South American modes and tropical convection during the Southern Hemisphere winter, *Mon. Weather. Rev*., **126**, 1581-1596.

Mo, K.C., 2000: Relationships between low-frequency variability in the Southern Hemisphere and sea surface temperature anomalies, *J. Climate*, **13**, 3599-3610.

Morgan, V., M. Delmotte, T. van Ommen, J. Jouzel, J. Chappellaz, S. Woon, V. Masson-Delmotte, and D. Raynaud, 2002: Relative timing of delglacial and climate events in Antarctica and Greenland, *Science*, **297**, 1862-1864.

Morse, D.L., D.D. Blakenship, E.D. Waddington, T.A. Neuman, 2002: A site for deep ice coring in West Antarctica: Results from aerogeophysical surveys and thermo-kinematic modeling, *Ann. Glaciol*., **35**, 36-44.

Mosley-Thompson, E. and L. G. Thompson, 2003: Ice core paleoclimate histories from the Antarctic Peninsula: Where do we go from here? In: Antarctic Peninsula Climate Variability: A Historical and Paleoenvironmental Perspective, edited by E. Domack *et al*., *Antarctic Research Series*, Vol. 79, 115-127, AGU, Washington, D.C.).

Mote, T.L., Anderson, M.R., Kuivinen, K.C. and C.M. Rowe, 1993: Passive microwave-derived spatial and temporal variations of summer melt on the Greenland ice sheet, *Annals of Glaciology*, **17**, 233-238.

Mulvaney, R., H. Oerter, D.A. Peel, W. Graf, C. Arrowsmith, E.C. Pasteur, B. Knight, G.C. Littot, W.D. Miners, 2002: 1000 year ice-core records from Berkner Island, Antarctica, *Ann. Glaciol*., **35**, 45-51.

Neumann, T.A., 2003: Effects of firn ventilation on geochemistry of polar snow, Ph.D. Thesis, University of Washington, Seattle, WA, USA.

Noone, D.C., 2001: A physical assessment of variability and climate signals in Antarctic precipitation and the stable water isotope record. Ph.D. Thesis., University of Melbourne, Australia, 404 pp.

Noone, D.C., and I. Simmonds, 2002a: Associations between $\delta^{18}O$ of water and climate parameters in a simulation of atmospheric circulation for 1979-1995. *J. Climate*, **15**, 3150-3169.

Noone, D.C., and Simmonds, I., 2002b: Annular variations in moisture transport mechanisms and the abundance of $\delta^{18}O$ in Antarctic Snow, *J. Geophys. Res*., **107**(D24).

North, G.R., T.L. Bell and R.F. Cahalan, 1982: Sampling errors in the estimation of empirical orthogonal functions, *Mon. Weather Rev.*, **110**, 699-706.

Oppenheimer, M., 1998: Global warming and the stability of the West Antarctic Ice Sheet, *Nature*, **393**, 325-332.

Palmer, A.S., T.D. van Ommen, M.A.J. Curran, and V. Morgan, 2001: Ice core evidence for a small solar source of Antarctic nitrate, *Geophys. Res. Let*., **28**(10), 1953-1956.

Peterson, R.G., and W.B. White, 1998: Slow oceanic teleconnections linking the Antarctic Circumpolar Wave with the tropical El Niño-Southern Oscillation, *Journal of Geophysical Research*, **103** (C11), 24,573-24,583.

Petit, J.R., J. Jouzel, D. Raynaud, M.I. Barkov, J.M. Barnola, I. Basile, M. Benders, J. Chappellaz, M. Davis, G. Delaygue, M. Delmotte, V.M. Kotlyakov, M. Legrand, V.Y. Lipenkov, C. Lorius, L. Pepin, C. Ritz, E, Saltzman and M. Stievenard, 1999: Climate and

atmospheric history of the past 420,000 years from the Vostok ice core, Antarctica, *Nature*, *399*, 429-436.

Rauthe, M., A. Hense, H. Paeth, A model intercomparison study of climate change signals in the extratropical circulation, *Int. J. Climatol*., **24**, 643-662.

Renwick, J.A., and M.J. Revell, 1999: Blocking over the south Pacific and Rossby wave propagation, *Mon. Weather Rev*., **127**, 2233-2247.

Ribera, P., and M.E. Mann, 2003: ENSO-related variability in the Southern Hemisphere, 1948-2000, *Geophys Res. Lett.,* **30**(1).

Rick, U., and M. Albert, 2005: Relationships between snow microstructure and permeability near a potential deep-drilling site in West Antarctica, *Ann. Glaciol*., **39**, 62-66.

Ridley, J., 1993: Surface melting on Antarctic peninsula ice shelves detected by passive microwave remote sensors, *Geophysical Research Letters*, **20** (23), 2639-2642.

Rogers, J.C., 1983: Spatial variability of Antarctic temperature anomalies and their association with the Southern Hemisphere circulation, *Annals of the Association of American Geographers*, **73** (4), 502-518.

Samsom, J., 1989: Antarctic surface temperature time series, *Journal of Climate*, **2**, 1164-1172.

Santer, B.D., T.M.L. Wigley, J.S. Boyle, D.J. Gaffen, J.J. Hnilo, D. Nychka, D.E. Parker, K.E. Taylor, 2000: Statistical significance of trends and trend differences in layer-average atmospheric temperature time series, *J. Geophys. Res*., **105**(D6), 7337-7356.

Scambos TA, C. Hulbe C, M. Fahnestock, J. Bohlander, 2000: The link between climate warming and break-up of ice shelves in the Antarctic Peninsula, *J. Glaciol*., **46**, 516-530.

Schneider, D.P., and E.J. Steig, 2002: Spatial and temporal variability of Antarctic ice sheet microwave brightness temperatures, *Geophys. Res. Lett*., **29**(20).

*Schneider, D.P., E.J. Steig, and J.C. Comiso, 2004: Recent climate variability in Antarctica from satellite-derived temperature data. *J. Climate*, **17**, 1569-1583.

*Schneider, D.P., E.J. Steig, and T. van Ommen, in press: High-resolution ice core stable isotopic records from Antarctica: towards interannual climate reconstruction, *Annals of Glaciology,* **41**.

*Schneider, D.P., E.J. Steig, C. Bitz, D. Dixon, P.A. Mayewski, T. van Ommen and J. Jones: Ice core evidence for Antarctic climate change, in preparation.

Schoeller, D.A., A.S. Colligan, T. Shriver, H. Avak, C. Bartok-Olson, 2000: Use of an automated chromium reduction system for hydrogen isotope ratio analysis of physiological fluids applied to doubly labeled water analysis, *J. Mass Spectrometry*, **35**(9), 1128-1132.

Shepherd, A., D. Wingham, E. Rignot, 2004: Warm ocean is eroding West Antarctic Ice Sheet, *Geophys. Res. Lett.*, **31**.

Shindell, D.T., and Schmidt, G.A., 2004: Southern hemisphere climate response to ozone changes and greenhouse gas increases, *Geophys. Res. Lett.*, **31**.

Shuman, C.A., R.B. Alley, S. Anandakrishnan and C.R. Stearns, 1995: An empirical technique for estimating near-surface air temperature trends in central Greenland from SSM/I brightness temperatures, *Remote Sensing Environment*, **51** (245-252), 245-252.

Shuman, C.A., and Stearns, C.R., 2001: Decadal length composite inland West Antarctic temperature records, *J. Climate*, **14**, 1977-1988.

Shuman, C.A., and J.C. Comiso, 2002: In situ and satellite surface temperature records in Antarctica. *Ann. Glaciol.*, **34**, 113-120.

Smith, S.R., and C.R. Stearns, 1993: Antarctic climate anomalies surrounding the minimum in the Southern Oscillation Index, in *Antarctic Meteorology and Climatology: Studies Based on Automatic Weather Stations*, edited by D.H. Bromwich, and Stearns, C.R., pp. 149-174, American Geophysical Union.

Solomon, S., 2001: *The Coldest March*. Yale University Press, 383 pp.

Stark, P., 1994: Climatic warming in the central Antarctic peninsula area, *Weather*, **49**, 215-220.

Stearns, C.R., L.M. Keller, G.A. Weidner, and M. Sievers, 1993: Monthly mean climatic data for Antarctic Automatic Weather Stations, in *Antarctic Meteorology and Climatology: Studies based on Automatic Weather Stations*, edited by D.H. Bromwich, and C.R. Stearns, pp. 1-21, American Geophysical Union.

Steffen, K., W. Abdalati, and J. Stroeve, 1993: Climate sensitivity studies of the Greenland ice sheet using satellite AVHRR, SMMR, SSM/I and in situ data, *Meteorology and Atmospheric Physics*, **51**, 239-258.

Steig, E.J., D.L. Morse, E.D. Waddington, M. Stuiver, P.M. Grootes, P.A. Mayewski, S.L Whitlow, and M.S. Twickler, 2000: Wisconsinan and Holocene climate history from an ice core at Taylor Dome, western Ross Embayment, Antarctica. *Geograf. Annal.* **82**A, 213-235.

Steig, E.J., P.A. Mayewski, D. Dixon, S. Kaspari, M. Frey, D.P. Schneider, S.A. Arcone, G.S. Hamilton, V.B. Spikes, M. Albert, D. Meese, A. Gow, C.A. Shuman, J.W.C. White, S. Sneed, J. Flaherty, and M. Wumkes, High-resolution ice cores from US-ITASE (West Antarctica): development and validation of chronologies and determination of precision and accuracy, *Annals of Glaciology*, **41**, in press.

Stenni, B., M. Proposito, R. Grognani, O. Flora, J. Jouzel, S. Falourd, and M. Frezotti. 2002. Eight centuries of volcanic signal and climate change at Talos Dome (East Antarctica). *J. Geophys. Res.,* **107**(D9), 10.129/2000JD000317.

Stroeve, J., J. Maslanik and L. Xiaoming, 1998: An intercomparison of DMSP F11- and F13-derived sea ice products, *Remote Sensing Environment*, **64**, 132-152.

Summerhayes, C., 2004: Antarctica and Climate Change, *Geoscientist*, **15**(2), 6-7.

Surdyk, S., 2002: Using microwave brightness temperature to detect short-term surface air temperature changes in Antarctica: An analytical approach, *Remote Sens. Environ*. **80**, 256-271.

Thomson, D.J., 1982: Spectrum estimation and harmonic analysis, *Procedings IEEE*, **70**, 1055-1096.

Thompson, D.W.J. and J.M. Wallace, 1998: The Arctic Oscillation in the wintertime geopotential height and temperature fields, *Geophysical Research Letters*, **25** (9), 1297-1300.

Thompson, D.W.J., and J.M. Wallace, 2000a: Annular modes in extratropical circulation, Part 1: Month-to-month variability. *J. Climate*, **13**, 1000-1016.

Thompson, D.W.J., and J.M. Wallace, 2000b: Annular modes in the extratropical circulation. Part II: Trends, *Journal of Climate*, **13**, 1018-1036.

Thompson, D.W.J., and S. Solomon, 2002: Interpretation of recent southern hemisphere climate change, S*cience,* **296**, 895-899.

Thompson, E.M., L.G. Thompson, P.M. Grootes, and N. Gunderstrup. 1990. Little Ice Age (Neoglacial) paleoenvironmental conditions at Siple Station, Antarctica. *Ann. Glaciol.,* **14**, 199-204.

Thompson, L.G., D.A. Peel, E. Mosley-Thompson, R. Mulvaney, J. Dai, P.N. Lin, M.E. Davis and C.F. Raymond, 1994: Climate since A.D. 1510 on Dyer Plateau, Antarctic Peninsula: Evidence for recent climate change. *Annals of Glaciology*, **20**, 420-426.

Turner, J., J.C. King, T.A. Lachlan-Cope, and P.D. Jones, 2002: Recent temperature trends in the Antarctic, *Nature* **418**, 291-292.

Turner, J, 2004: The El Nino-Southern Oscillation and Antarctica, *Int. J. Climatol*., **24**, 1-31.

Turner, J., S.R. Colwell, G.J. Marshall, T.A. Lachlan-Cope, A.M. Carleton, P.D. Jones, V. Lagun, P. A. Reid, and S. I agovkina, 2004: The SCAR READER Project: Toward a high-quality database of mean Antarctic meteorological observations, *J. Climate*, **17**, 2890- 2898.

Turner, J., S.R. Colwell, G.J. Marshall, T.A. Lachlan-Cope, A.M. Carleton, P.D. Jones, V. Lagun, P. A. Reid, and S. I agovkina, 2005: Antarctic climate change during the last 50 years, *Int. J. Climatol*., **25**, 279-294.

van den Broeke, M., 1998: The semiannual oscillation and Antarctic climate, part I: Influence on near-surface temperatures (1957-1979), *Antarctic Science*, **10** (2), 175-183.

van den Broeke, M., 2000: On the interpretation of Antarctic temperature trends*, J. Climate*, **13**, 3885-3889.

van den Broeke, M., 2000: The semiannual oscillation and Antarctic climate. Part 3: The role of near-surface wind speed and cloudiness, *International Journal of Climatology*, **20**, 117-130.

van den Broeke, M., 2000: The semiannual oscillation and Antarctic climate, part 5: Impact on the annual temperature cycle as derived from the NCEP/NCAR reanalysis, *Climate Dyn.*, **16**, 369-377.

van den Broeke M, C. Reijmer C, and R. van de Wal, 2004: Surface radiation balance in Antarctica as measured with automatic weather stations, *J. Geophys. Res. Atmos*., **109**(D9), 1-16.

van der Veen, C.J., and K.C. Jezek, 1993: Seasonal variations in brightness temperature for central Antarctica, *Annals of Glaciology*, **17**, 300-306.

van Lipzig, N.V.M., E. van Meijaard, and J. Oerlemans, 2002: The effect of temporal variations in the surface mass balance and temperature inversion strength on the interpretation of ice core signals, *J. Glaciol.*, **48**(163), 611-621.

van Loon, H., 1967: The half-yearly oscillations in middle and high southern latitudes and the coreless winter, *Journal of the Atmospheric Sciences*, **24**, 472-486.

van Ommen, T.D., and V. Morgan, 1997: Calibrating the ice core paleothermometer using seasonality. *J. Geophys. Res*., **102**(D8), 9351-9357.

van Ommen, T.D., V. Morgan, and M.A.J. Curran, 2005: Deglacial and Holocence changes in accumulation at Law Dome, *Ann. Glaciol*, **39**, 359-365.

Vaughan, D.G., and C.S.M. Doake, 1996: Recent atmospheric warming and retreat of ice shelves on the Antarctic peninsula, *Nature*, **379**, 328-331.

Vaughan, D.G., J.L. Bamber, M. Giovinetto, J. Russell, and A.P.R. Cooper, 1999, Reassessment of net surface mass balance in Antarctica, *J. Climate*, **12**, 933-946.

Vaughan, D.G., G.J. Marshall, W.M. Connolley, J.C. King, and R. Mulvaney, 2001: Devil in the detail, *Science*, **293**, 1777-1779.

Vaughan, D.G., G.J. Marshall, W. M. Connolley, C. Parkinson, R. Mulvaney, D.A. Hodgson, J.C. King, C. J. Pudsey, and J.C. Turner, 2003: Recent Rapid Regional Climate Warming on the Antarctic Peninsula, *Climatic Change* **60**, 243-274.

Venegas, S.A., 2003: The Antarctic Circumpolar Wave: A combination of two signals?, *J. Climate*, **16**(15), 2509-2525.

von Storch, H., 1995: Spatial patterns: EOFs and CCA, in *Analysis of Climate Variability*, edited by H. Von Storch, and Navarra, A., pp. 227-253, Springer.

von Storch, H., F.W. Zwiers, 2001: *Statistical Analysis in Climate Research*, Cambridge Univ. Press, 484 pp.

von Storch, H., E. Zorita, J.M. Jones, Y. Dimitriev, F. Gonzalez-Rouco, S.B. Tett, 2004: Reconstructing past climate from noisy data, *Science*, **306**, 679-682..

Wallace, J.M., Smith, C., and C.S. Bretherton, 1992: Singular Value Decomposition of Wintertime Sea Surface Temperature and 500-mb Height Anomalies, *J. Climate*, **5**, 561-576.

Wallace, J.M. and P.V. Hobbs, 1977: *Atmospheric Science: An Introductory Survey*. Academic Press, 467 pp.

Walland, D., and I. Simmonds, 1999: Baroclinicity, meridional temperature gradients, and the Southern semiannual oscillation, *Journal of Climate*, **12**, 3376-3382.

Warren, S.G., 1996: Antarctica, in *Encyclopedia of Climate and Weather*, Oxford University Press, 32-39.

Watanabe, O., J. Jouzel, S. Johnsen, F. Parrenin, H. Shoji, and N. Yoshida, 2003: Homogeneous climate variability across East Antarctica over the past few glacial cycles, *Nature*, **422**, 509-512.

Wendler, G., and Y. Kodama, 1993: The kernlose winter in Adelie Coast, in *Antarctic Meteorology and Climatology: Studies based on Automatic Weather Stations*, edited by D.H. Bromwich, and C.R. Stearns, pp. 139-147, American Geophysical Union.

Werner, M., and M. Heimann, 2002: Modelling the interannual variability of water isotopes in Greenland and Antarctica, *J. Geophys. Res*., **107**(D1).

White, W.B., and P.G. Peterson, 1996: An Antarctic circumpolar wave in surface pressure, wind, temperature, and sea-ice extent, *Nature*, **380**, 699-702.

White, J.W.C., L.K. Barlow, D. Fisher, P. Grootes, J. Jouzel, S.J. Johnsen, M. Stuiver, and H. Clausen, 1997: The climate signal in the stable isotopes of snow from Summit, Greenland: Results of comparisons with modern climate observations, *J. Geophys. Res*., **102**(C12), 26,425-26,439.

White, J.W.C., E.J. Steig, J. Cole, E.R. Cook and S.J. Johnsen, 1999: Recent, annually resolved climate as recorded in stable isotope ratios in ice cores from Greenland and Antarctica. *Amer. Met. Soc. Sym. Glob. Clim. Change Stud.:* **10**, 300-302.

Wilks, D.S. 1995. *Statistical methods in the Atmospheric Sciences*, Academic Press, 467pp.

Wilson, J.D., and K.C. Jezek, 1993: Co-registration of an Antarctic digital elevation model with SSM/I brightness temperatures, *Annals of Glaciology*, **17,** 93-97.

Yuan, X., and D.G. Martinson, 2000: Antarctic sea ice extent variability and its global connectivity, *Journal of Climate*, **13**, 1697-1717.

Zwally, H.J., 1977: Microwave emissivity and the accumulation rate of polar firn, *J. Glaciol.*, **18**, 195-215.

Zwally, H. J. and S. Fiegles, 1994: Extent and duration of Antarctic surface melting, *J. Glaciol.*, **40** (136), 463-476.

Zwally H.J., M. Giovinetto, M. Craven, V. Morgan, and I. Goodwin, 1998: Areal distribution of the oxygen-isotope ratio in Antarctica: comparison of results based on field and remotely sensed data. *Ann. Glaciol*, **27**, 583-590.

*contained within this dissertation

Vita

David P. Schneider

Education

University of Washington, Seattle, WA

2005 Ph.D, Department of Earth and Space Sciences. Dissertation (with advisor Eric Steig and committee members John M. Wallace, Stephen Warren, and Dale Winebrenner): *Antarctic climate of the past 200 years from an integration of instrumental, satellite, and ice core proxy data*

University of Pennsylvania, Philadelphia, PA

2001 M.S., Earth and Environmental Science. Thesis (with advisor Eric Steig): *Recent spatial and temporal climate variability in Antarctica: Insights from passive microwave brightness temperature data*

Carleton College, Northfield, MN

1999 B.A. *cum laude*. Geology major with minor in Environmental and Technology Studies. Senior thesis (with advisor David Bice): *Signs of stress under pressure: The stress and strain significance of syntectonic quartz veins in the Maverick Shale, Mazatzal Mountains, Arizona and their structural and Proterozoic tectonic context*

Research Interests

Interpretation of paleoclimate records; Polar meteorology and climatology; Stable isotope geochemistry; Remote sensing of polar regions; Science and public policy

Technical Research Experience

Field:

United States International Trans-Antarctic Scientific Expedition (ITASE): Worked two field seasons (2000 and 2001) in West Antarctica on an ice-core drilling traverse under the direction of principal investigator Eric Steig and field leader/principal investigator Paul Mayewski. Obtained snow and ice samples for stable isotope analysis, performed density measurements and stratigraphy observations, made weather observations, assisted in ice core drilling and other scientific projects.

Summit, Greenland: Field assistant in 2000 season for Eric Steig on real-time stable isotope monitoring and ice core drilling projects.

Keck Geology Consortium Mazatzal Mountains Project, Arizona: Conducted field work in summer 1998 gathering and mapping structural geology data for my senior undergraduate thesis.

Skatafell, Iceland: Field assistant in summer 1997 for a senior's thesis work. Mapped surface features on a glacial outwash plain, measured clast sizes.

Laboratory:

National Ice Core Laboratory, Denver, CO. Participated in four core processing lines (2000 Siple Dome, 2000-2002 ITASE), prepared ice core samples for stable isotope analysis.

Stable Isotope Lab, Quaternary Research Center, University of Washington. Knowledgeable in operation of ThermoFinnegan and Micromass gas isotope ratio mass spectrometers.

Teaching Experience

Teaching Assistant, Spring 2003 and Spring 2002, University of Washington: Taught laboratory sections for Introduction to Geology, led field trips, wrote quizzes, graded assignments.

Teaching Assistant, Fall 1999, University of Pennsylvania: Taught laboratory sections for Introduction to Geology, wrote lab exercises, graded exams and assignments.

Laboratory Assistant, Department of Geology, Carleton College: Assisted in lab and field trip sessions for several courses, including: Introduction to Geology, Sedimentary Geology, and Paleobiology.

Substitute teacher, Farmington Municipal Schools, Farmington, NM, winter 1998: Taught and supervised students in all subjects, elementary and middle school levels.

Awards and Honors

American Meteorological Society Summer Policy Colloquium graduate student fellow, 2005
Bjerknes Conference (Norway) travel grant, 2004
Scientific Committee on Antarctic Research conference (Germany) travel grant, 2004
Nominated to Sigma Xi, 1999
Nominated to Mortar Board Society, 1999
Keck Foundation fellowship, 1998
Danish International Studies Scholarship, 1997
Carleton College Dean's List, 1996, 1997
Lutheran Brotherhood scholarship, 1995-1999

Affiliations and Service

- Member: American Geophysical Union, American Meteorological Society, Geological Society of America, National Association of Science Writers, Sigma Xi
- Reviewer: *Annals of Glaciology*, *Antarctic Science*, *Journal of Climate,* National Science Foundation
- Senator, Graduate and Professional Student Senate, University of Washington, 2002-2004
- Trip leader, volunteer, Sierra Club Inner City Outings program, Seattle, WA, 2003-present

Publications

Peer-reviewed papers:

Schneider, D.P., and E.J. Steig, 2002: Spatial and temporal variability of Antarctic ice sheet microwave brightness temperatures, *Geophysical Research Letters,* **29,** 25.1-25.4.

Schneider, D.P., E.J. Steig, and J.C. Comiso, 2004: Recent climate variability in Antarctica from satellite-derived temperature data, *Journal of Climate*, **17**, 1569-1583.

Schneider, D.P., E.J. Steig, and T. van Ommen: High-resolution ice core stable isotopic records from Antarctica: towards interannual climate reconstruction, *Annals of Glaciology,* **41**, in press.

Schneider, D.P., E.J. Steig, C. Bitz, D. Dixon, P.A. Mayewski, T. van Ommen and J. Jones: Ice core evidence for Antarctic climate change, in preparation.

Jacobel, R., B. Welch, E.J. Steig, and D.P. Schneider, 2005: Hercules Dome, Antarctica: A Possible Site for deep ice core drilling, *Journal of Geophysical Research*, **110**, F01015.

Steig, E.J., P.A. Mayewski, D. Dixon, S. Kaspari, M. Frey, D.P. Schneider, S.A. Arcone, G.S. Hamilton, V.B. Spikes, M. Albert, D. Meese, A. Gow, C.A. Shuman, J.W.C. White, S. Sneed, J. Flaherty, and M. Wumkes, High-resolution ice cores from US-ITASE (West Antarctica): development and validation of chronologies and determination of precision and accuracy, *Annals of Glaciology*, **41**, in press.

Winebrenner, D.P., E.J. Steig, and D.P. Schneider, 2005:: Temporal covariation of surface and microwave brightness temperatures in Antarctica, with implications for the observation of surface temperature variability using satellite data, *Annals of Glaciology*, **39**, 346-350.

Abstracts:

Steig, E.J., and D.P. Schneider, 2002: Interannual to millennial-scale variability of Antarctic ice sheet climate, *Eos Trans. AGU*, **83**(19), Spring Meet. Suppl., Abstract A41A-12.

Schneider, D.P., and E.J. Steig, 2002: The Southern Annular Mode and ENSO Signals in Antarctic Surface Temperatures & Implications for Ice Core Paleoclimate Reconstructions, *First Joint EPICA/ITASE Workshop*, Potsdam, Germany, 18-20 September.

Steig, E.J., and D.P. Schneider, 2002: Spatial patterns of low-frequency climate variability in Antarctica, *First Joint EPICA/ITASE Workshop*, Potsdam, Germany, 18-20 September.

Schneider, D.P., E.J. Steig, and J.C. Comiso, 2002: Influences of the Southern Annular Mode and the El-Nino Southern Oscillation on Antarctic climate and their expression in remotely-sensed climate data, *Eos Trans. AGU*, **83**(47), Fall Meet. Suppl., Abstract C51A-0931.

Schneider, D.P., and E.J. Steig, 2003: Characteristics of Isotopic records in US-ITASE Cores, *Tenth Annual WAIS Workshop*, 17-20 September, Sterling, VA.

Schneider, D.P., E.J. Steig, and J.C. Comiso, 2004: Recent climate variability in Antarctica from satellite-derived temperature data, *15th Symposium on Global Change and Climate Variations*, Seattle, WA, American Meteorological Society Annual Meeting, Abstract J6.5.

Schneider, D.P., E.J. Steig, and T. van Ommen, 2004: Interpretation of high-resolution stable isotopic ice core records from the US-ITASE traverse and other recent Antarctic drilling

projects, *Symposium on ITASE*, Scientific Committee on Antarctic Research 28th meeting and Open Science Conference, Bremen, Germany, 26-28 July.

Schneider, D.P., E.J. Steig, J.M. Jones, T. van Ommen, and D. Dixon, 2004: Ice core evidence of Antarctic climate change and its connections with the Southern Annular Mode, Bjerknes Centenary 2004: Climate Change in High Latitudes, 1-3 September, Bergen, Norway.

Steig, E.J., D.P. Schneider, M.E. Mann, S.D. Rutherford, T. van Ommen, C.A. Shuman, D. Dixon, P.A. Mayewski, and J.W.C. White, 2004: Antarctic temperatures since 1856, *Eleventh Annual WAIS Workshop*, 29 September-2 October, Sterling, VA.

Popular science writing articles (all appearing in Northwest Science and Technology magazine)**:**

UW's Kirsten Wind Tunnel Keeps the Northwest Flying (Autumn 2003)
Secrets to Superbug's Resistance Revealed (Autumn 2003)
Vancouver, City on the Edge [book review] (Winter 2004)
Peak Performance: Doctors scale mountains to research the body's response to high altitudes (Winter 2005)
Avalanches in the Northwest (Winter 2005)